Journal of
Composites Science

MDPI

Review

Polymer–Metal Composite Healthcare Materials: From Nano to Device Scale

Wai-Ki Wong [1,†], Chun-Him (Nathanael) Lai [2,*,†], Wai-Yin Cheng [3], Lok-Him Tung [2], Chuen-Chung (Raymond) Chang [3,4] and King-Chi (Franco) Leung [5]

[1] Department of Bioengineering, Imperial College London, London SW7 2AZ, UK; wai.wong20@imperial.ac.uk
[2] Department of Biomedical Engineering, The Chinese University of Hong Kong, Hong Kong SAR 518172, China; tunglokhim@gmail.com
[3] Laboratory of Neurodegenerative Diseases, School of Biomedical Sciences, LKS Faculty of Medicine, The University of Hong Kong, Hong Kong SAR 999077, China; nanocwy@connect.hku.hk (W.-Y.C.); rccchang@hku.hk (C.-C.C.)
[4] State Key Laboratory of Brain and Cognitive Sciences, The University of Hong Kong, Hong Kong SAR 999077, China
[5] State Key Laboratory for Chemical Biology and Drug Discovery, Department of Applied Biology and Chemical Technology, The Hong Kong Polytechnic University, Kowloon, Hong Kong SAR 999077, China; kingchifranco.leung@polyu.edu.hk
* Correspondence: nathanlch@link.cuhk.edu.hk
† These authors contributed equally to this work.

Abstract: Metals have been investigated as biomaterials for a wide range of medical applications. At nanoscale, some metals, such as gold nanoparticles, exhibit plasmonics, which have motivated researchers' focus on biosensor development. At the device level, some metals, such as titanium, exhibit good physical properties, which could allow them to act as biomedical implants for physical support. Despite these attractive features, the non-specific delivery of metallic nanoparticles and poor tissue–device compatibility have greatly limited their performance. This review aims to illustrate the interplay between polymers and metals, and to highlight the pivotal role of polymer–metal composite/nanocomposite healthcare materials in different biomedical applications. Here, we revisit the recent plasmonic engineered platforms for biomolecules detection in cell-free samples and highlight updated nanocomposite design for (1) intracellular RNA detection, (2) photothermal therapy, and (3) nanomedicine for neurodegenerative diseases, as selected significant live cell–interactive biomedical applications. At the device scale, the rational design of polymer–metallic medical devices is of importance for dental and cardiovascular implantation to overcome the poor physical load transfer between tissues and devices, as well as implant compatibility under a dynamic fluidic environment, respectively. Finally, we conclude the treatment of these innovative polymer–metal biomedical composite designs and provide a future perspective on the aforementioned research areas.

Keywords: polymer–metal composites; healthcare materials; biomolecules detection; intracellular RNA detection; photothermal therapy; neurodegenerative diseases; dental implants; cardiovascular stents

Citation: Wong, W.-K.; Lai, C.-H.; Cheng, W.-Y.; Tung, L.-H.; Chang, C.-C.; Leung, K.-C. Polymer–Metal Composite Healthcare Materials: From Nano to Device Scale. *J. Compos. Sci.* **2022**, *6*, 218. https://doi.org/10.3390/jcs6080218

Academic Editor: Francesco Tornabene

Received: 28 June 2022
Accepted: 22 July 2022
Published: 26 July 2022

1. Introduction

A composite is defined as the combination of two or more materials with different physical and chemical properties, thereby creating new materials with advanced structural properties and functionalities [1]. Polymer–metal composites offer tunable properties of materials in both the nanoscale and the bulk scale [2,3]. From the nanoscale to the device level, the tunable properties of polymer–metal composite materials are crucial to the design of healthcare materials for diagnostics, therapeutic, antibacterial, and bio-substitute applications. The selection of polymers and metallic materials render complementary effects upon each other, and therefore the rational design of polymer–metal composites creates combined materials with finely adjusted material properties. The advantages of polymer–metal

composite materials are more than retain the advantages of both polymer and metallic materials. There are various types of interactions that occur between polymers and metallic materials, including electrostatic forces, metal–ligand interactions, gold–thiol bond, and condensation reactions, which can be considered as synthetic strategies that change the material hierarchy (two dimensions into three dimensions structures, layered structures, highly-organized assemble) and thereby create new structures, such as nanoassemblies, nanocomposite hydrogels, nanodisk composites. These structures are valuable platforms to leverage the inherit properties of polymer–metal composites and serve different purposes (Figure 1). For example, the surface of the polydimethylsiloxane (PDMS) substrate can be modified with silver film via wavy patterning to give a transparent stretchable electronic that is useful for human-health monitoring devices [4]. The surface modification of metallic nanoparticles (e.g., gold nanoparticles, iron nanoparticles) with polyethylene glycol (PEG) creates passivated surfaces that the reduce aggregation of nanoparticles, interactions with non-targeted serum and tissue proteins, and further reduce uptake by the reticuloendothelial system (RES), thereby collectively improving the biocompatibility of nanoparticles and the circulation time of nanomedicine [5]. The incorporation of magnetic nanoparticles/microstructures in hydrogels can give metal composite hydrogels with magnetic stimulations that promote the healing of different tissues [6]. Polymers can be composited with metal ion (iron ion) or metal oxide (e.g., titanium oxide) to improve adhesiveness [7], or to enhance the mechanical performance and biointegration of healthcare implants [8]. Natural macromolecules such as DNA can be used to link gold nanoparticles with different sizes and form highly organized chiral nanoassemblies by tailoring the design of DNA chains. Such chiral nanoassemblies respond to circularly polarized light and stimulate the differentiation of neural stem cells into neuronal phenotypes [9].

Plasmonic particles are characterized by localized surface plasmon resonance (LSPR). Briefly, the electrons in nanoparticles vibrate under electromagnetic waves. The colloidal materials thereby oscillate and scatter light [10,11]. For example, small gold nanoparticles (<10 nm in diameter) exhibit the representative red color due to a high absorption band across visible light spectrum, except wavelengths of 600–700 nm [12]. Therefore, the sizes of gold nanoparticle dispersions can be analyzed from the absorption spectrum [13]. Indeed, colloidal gold nanoparticles are a common carrier agent in lateral flow tests, where a red line is observed in the test strip due to the immobilization and accumulation of gold nanoparticles [14]. The aggregation of gold nanoparticles, such as salt induced aggregation and biomolecule conjugate linkages, would cause the significant change in absorption spectra [15,16]. Such size dependent optical properties are highly attractive in developing biosensors for rapid diagnosis. In the context of cell interactive biomedical applications, such as drug delivery and bio-imaging, the precise delivery of nanoparticles to target cells is crucial. For example, plasmonic particles, which also feature high photothermal conversion efficiency, could be delivered to tumor tissues for photothermal therapy [17]. Nonetheless, off-target delivery may harm healthy tissues during photothermal therapy. Biomolecules, such as peptides and antibodies, are often decorated on the particle surface to achieve precise delivery, or to avoid the leakage of nanomaterials to non-targeted tissues [18]. Due to the excellent fluorescence quenching properties on plasmonic surfaces, biomolecule–plasmonic particle conjugates often act as bio-imaging reporters upon dissociation from plasmonic particles [19]. The cellular uptake of such biomolecule–plasmonic nanocomposites provides great potential in live cell imaging. Furthermore, nanoparticles, such as superparamagnetic iron oxide nanoparticles (SPIONs), are excellent contrast agents for magnetic resonance imaging (MRI) and are often modified with biomolecules and polymers to achieve precise delivery. For example, SPIONs modified with cell surface receptor targeting peptides and neurotoxin targeting peptides can serve as a theranostic agent that penetrates the blood–brain barrier (BBB) and targets neurotoxins for the (1) alleviation of neurodegenerative diseases symptoms as well as (2) MRI monitoring [20].

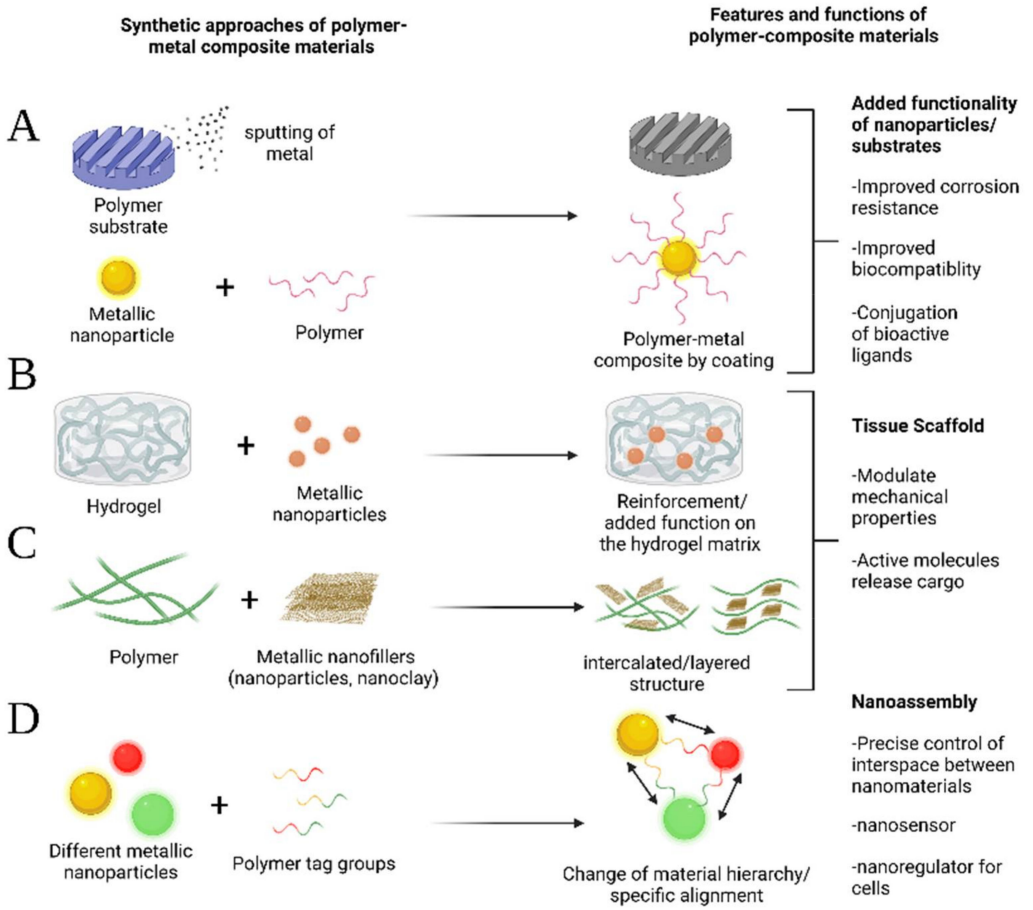

Figure 1. Synthetic approaches, features, and functions of polymer-metal composite materials. (**A**) Surface modification approach; (**B**) Built-in approach; (**C**) Intercalation approach; (**D**) Multi-crosslinking approach.

At the tissue level, cells are harbored in an extracellular matrix (ECM) comprising glycosaminoglycans, proteoglycans, and glycoproteins. Indeed, a cell adheres to such a complex extracellular environment and acquires both biochemical and mechanical signals. Disrupting the interactions between cell and ECM, such as focal adhesion, would severely affect cell motility [21,22]. Without proper tissue–implant integration, the implants might be recognized as foreign materials and trigger undesired foreign body reaction, including sustained fibrosis and the formation of scar tissues, which lead to chronic inflammation. Therefore, cell-surface interactions become a critical concern in medical implants design [23,24]. Herein, we focus on the polymer–metal composite dental implants, which mediate physical load, to emphasize the importance of good tissue–device integration (osseointegration) upon implant maintenance in vivo. Besides, biomedical devices might be exposed to dynamic biofluids. For example, cardiovascular stents continuously interact with both blood plasma and surrounding endothelial cells. Nonetheless, the vascular narrowing due to neointima formation after percutaneous coronary intervention, also known as in stent restenosis, remains a major challenge [25,26]. The first major breakthrough in terms of cardiovascular stents was the invention of drug-eluting stents, a class of polymer-metal cardiovascular stent. Such metallic-based stents are coated with polymers for effective drug loading and drug release, which inhibit platelets activation and vascular smooth muscle cells hyperproliferation, thus preventing in-stent restenosis [27]. The polymer metal cardiovascular stents have demonstrated better clinical performances over bare metal implants and serve as one of the major devices for cardiovascular diseases treatment. Based on the foundation of drug-eluting stents, in the subsequent discussion,

we also include the recent development of polymer metal cardiovascular stents, which can withstand complicated and dynamic fluidic environments.

The present review highlights the pivotal role of polymer–metal composite materials in the field of healthcare materials from the nanoscale to device level. We first discuss the recent advancements of biomolecule detection in cell free samples as benefited by plasmonic biotechnology. We subsequently highlight updated polymer–metal nanocomposites design covering intracellular RNA detection, photothermal therapy, and nanomedicine for neurodegenerative diseases as selected significant live cell interactive biomedical applications. At the device level, the interactions between biomaterials and surrounding tissues are critical to healthcare devices design. We revisit the current challenges on dental implants and cardiovascular implants and further discuss the merits of polymer–metal composites in respective areas. Finally, we provide the future perspective of polymer–metal composites design in the mentioned research areas.

2. Plasmonic Biotechnology for Diverse Biomedical Applications

Plasmonic metallic nanoparticles can interact with electromagnetic radiation. The absorption and scattering of the light of plasmonic particles are geometry and size dependent. The surface modification of plasmonic particles by target specific biomolecules (e.g., antibody, nucleic acid) confers biosensing applications. These features have motivated researchers to develop new biomolecule detection platforms in recent years, with the aim of improving sensitivity, automation, and throughput scale [28,29]. Conventional research biomolecules analysis tools present time consumption issues. For example, the conventional quantitative polymerase chain reaction (qPCR) requires multiple amplification cycles of target sequences. Immunoblotting also requires lengthy procedures in respect of electrophoresis and antibody detection. The inconvenient procedures are highly undesired for scalable diagnosis in routine clinical settings. In this section, we review recent plasmonic biotechnology examples advancing disease diagnosis and biomolecule detection in cell free samples such as serum. Besides, cells could interact and internalize surrounding nanomaterials [30,31]. Herein, we include three popular research areas in our discussion: intracellular RNA detection, photothermal therapy, and nanomedicine for neurodegenerative diseases, which together cover the diagnostic and therapeutic application examples of live cell targeting polymer–metal composite nanoparticles.

2.1. Plasmonic Biosensor Platforms for Cost-Effective, Rapid, High Throughput Diagnosis

2.1.1. High Sensitivity Plasmonic Assisted Immunosorbent Assay

In the fluorescence-linked immunosorbent assay (FLISA), targets captured by immobilized antibodies would be further recognized by fluorescently tagged antibodies. Compared to a glass substrate, according to an early report by Tabakman et al. [32], gold/silver plasmonic chips improved the signal-to-noise ratio and extended the detection range to femtomolar range in near-infrared regime (Figure 2a). Plasmonic nano-surfaces can couple with fluorophores (5–90 nm distance) to amplify fluorescence, known as plasmonic enhanced fluorescence [33,34]. The plasmonic gold chip also outperformed a glass substrate due to fluorescence enhancement. However, continuous gold film instead quenched fluorescence and was thereby not considered suitable for FLISA [35,36] (Figure 2b). Recently, Luan et al. [37] designed an "add on plasmonic-fluor label" to replace a single fluorophore tag on an antibody (Figure 2c) and it showed excellent sensitivity. The add-on construct comprised multiple fluorophores (>200) and elicited the plasmon enhanced fluorescence based on the gold nanorod core. According to the example provided, labeling human IL-6 with a plasmonic fluorophore improved the limit of detection down to 20 fg/mL (Figure 2d), in contrast to conventional FLISA with a limit of detection of 95 pg/mL. FLISA with improved sensitivity provides a possibility to detect low abundance biomarkers, such as IL-6 for early cancer diagnosis [38].

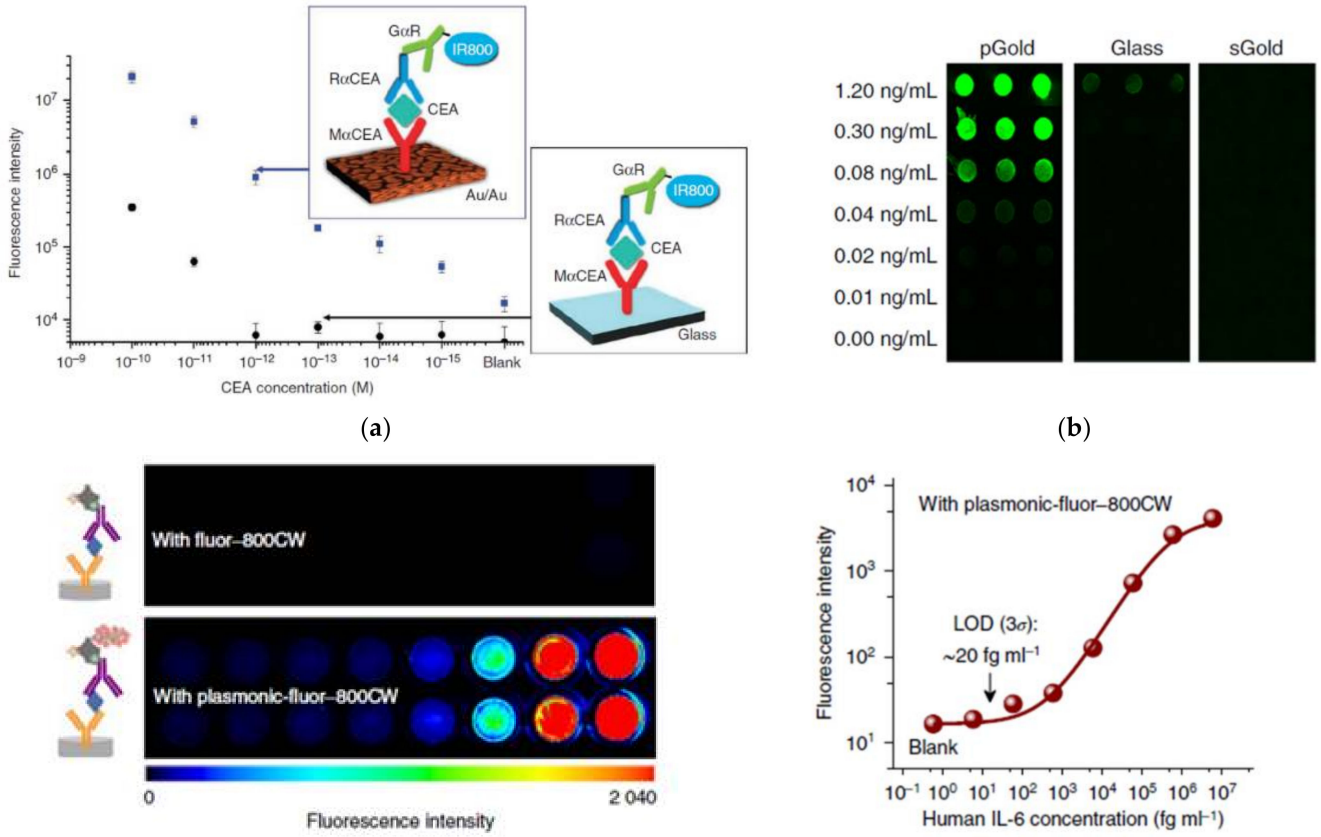

(**a**) (**b**)

(**c**) (**d**)

Figure 2. Plasmonic assisted Fluorescence-linked immunosorbent assay. (**a**) Fluorescence intensity-Carcinoembryonic antigen concentration calibration performed by gold/silver plasmonic chip and glass (Figure reprinted with permission from Ref. [32] Copyright Springer Nature); (**b**) Fluorescence map showing the performance of plasmonic gold chip (left), glass (middle) and sputtered gold chip (right) in different concentration of cardiac troponin I (Figure reprinted with permission from Ref. [36] Copyright Springer Nature); (**c**) Fluorescence map and (**d**) Fluorescence quantification of conventional FLISA and plasmonic FLISA in detection of human IL-6 across serial dilution (6 fg/mL to 6 ng/mL) respectively (Figure 2c,d are reprinted with permission from Ref. [37] Copyright Springer Nature).

2.1.2. Plasmonic Nanoparticles Mediated Timely Detection of Nucleic Acid

The polymer chain reaction assay is a common nucleic acid detection tool in laboratory settings. However, lengthy operations could hinder the research progress or medical diagnosis. Improving the simplicity and efficiency of nucleic acid analysis assay would benefit both research and clinical settings. For example, in the context of the current coronavirus pandemic (COVID-19), the PCR test has been a globally common diagnostic strategy. Timely report of test results is critical to COVID-19 monitoring. To elicit the optical feature of plasmonic nanoparticles on nucleic acid detection, Moitra et al. [39] proposed the use of antisense oligonucleotide modified gold nanoparticles for SARS-CoV-2 RNA detection. Briefly, the SARS-CoV-2 RNA sequence binded to antisense oligonucleotide on gold nanoparticles, and AuNPs subsequently aggregated in a few minutes. This change in surface plasmon resonance was visible and immediate. Therefore, such a simple operation might enable self-diagnostic potential by the layman, thereby reducing the cost of labor resources in a scalable test centre. Although the limit of detection (0.18 ng/μL) is not comparable to conventional qPCR (2.0 copies/μL), these naked eye observable results bypass the necessity of conventional PCR computed detection machinery [39,40]. Recently, Cheong et al. [41] developed a nanoPCR system, which adopted the high photothermal

conversion efficiency and magnetic sensitivity of $Zn_{0.4}Fe_{2.6}O_4$@Au nanoparticles to respectively assist the thermocycling process (Figure 3a) and fluorescence detection (Figure 3b). The system could complete a PCR process in less than 17 min with a limit of detection of 3.2 copies/μL. Conventional RT-qPCR procedures require around 2 h, which is lengthy. These immediate, simplified diagnosis strategies are presently subject to massive demand from society.

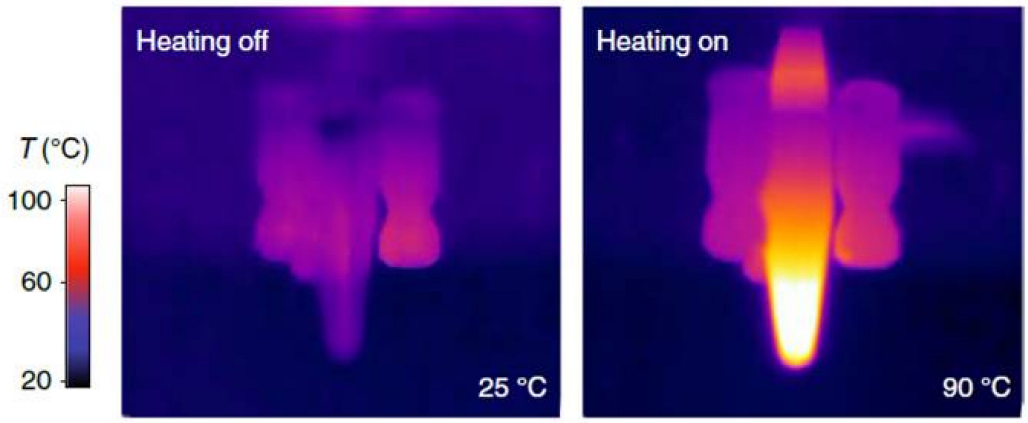

(**a**)

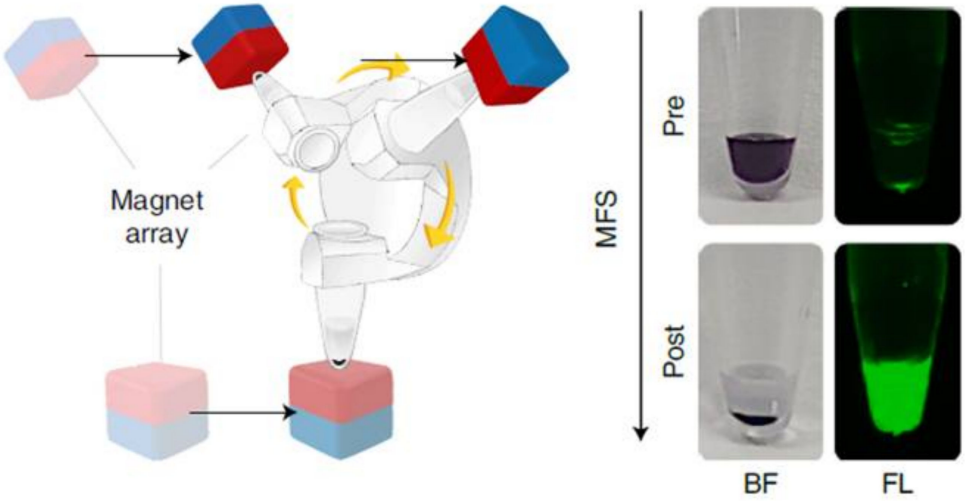

(**b**)

Figure 3. Plasmonic nanoparticles mediated detection of nucleic acid. (**a**) Thermal image of $Zn_{0.4}Fe_{2.6}O_4$@Au nanoparticle solution during 532 nm light source off (**left**) and on (**right**). (**b**) Fluorescence reporter from target nucleic acid was quenched due to proximity to gold nanoshell (**left**). Magnet field sedimented nanoparticles and recovered fluorescence in the fluorescence reporter containing supernatant (**right**) Figure 3a,b are reprinted with permission from Ref. [41] Copyright Springer Nature.

2.1.3. Gold Nanoparticle Assisted Multiplexed Exosome Profiling

Exosomes are nanoscale, lipid bilayer extracellular vesicles for biomolecule (e.g., nucleic acid, protein) transportation between cells and they expresses multiple proteins on their surface [42]. The altered exosome acts as a potential biomarker in disease diagnosis, including in the case of kidney disorders (e.g., acute kidney injury, diabetic nephropathy) [43], cardiovascular diseases (e.g., acute myocardial infarction, acute coronary syndromes), [44] osteoarthritis [45], and cancers [46]. Jiang et al. [47] reported an aptamer/gold nanoparticle (AuNP) biosensor colorimetric assay. Notably, AuNP was modified by a target protein

specific aptamer, which prevented the aggregation of AuNP in salty solution. Upon recognizing the target protein, the AuNP bound aptamer dissociates and binds to the exosome surface. The immediate aggregation of AuNPs leads to an increased absorbance ratio (A650/A520), which could quantify the target protein expressing exosome. Besides, Liang et al. [48] developed a nanoplasmon-enhanced scattering (nPES) assay, which elicits the light scattering using a gold nanosphere and gold nanorod (Figure 4a). Of importance, the gold nanosphere and gold nanorod show distinct scattering spectrums, which allows multiplexed immuno-labelling of the target under dark field microscopy. To distinguish free protein and exosomes of different size, Wu et al. [49] reported templated plasmonics for exosomes (TPES) platform, which highlighted the in situ growth of gold nanoshells (Figure 4b). More importantly, the absorption spectrum of the resultant exosome-templated gold nanostructure relies on the size of both exosome and gold nano-seed. Further addition of the aptamer-fluorescent probe targeting exosomal protein would be quenched by a gold nano-shell, which therefore enables the detection of target surface proteins.

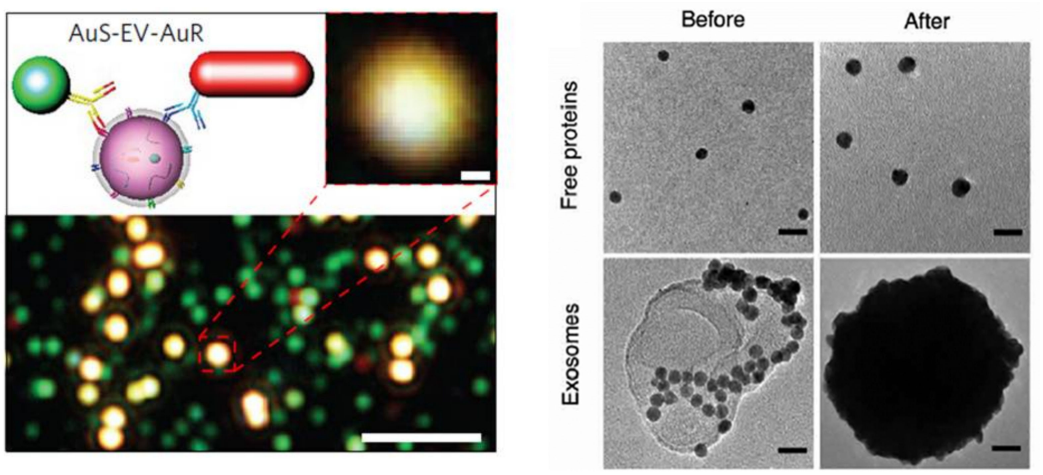

(**a**) (**b**)

Figure 4. Recent examples on advanced nano-plasmonic exosome sensors. (**a**) Nanoplasmon-enhanced scattering (nPES) assay. Antibody bearing gold nanosphere and gold nanorod are used to label different protein on the exosome surface under dark field microscopy (scale bar: 2 μm and 100 nm in main image and magnified image respectively) (Figure reprinted with permission from Ref. [48] Copyright Springer Nature). (**b**) Transmission electron microscopy showing in situ growth of gold nanoshell on exosome, leading to the formation of exosome@gold nano-structure (Figure reprinted with permission from Ref. [49] Copyright American Association for the Advancement of Science).

2.2. Intracellular RNA Detection

Metallic nanoparticles, such as gold and silver, can quench fluorescence on their surfaces when the fluorophore is close enough to the plasmonic surface (<5 nm) [19,50,51]. This feature has attracted researchers to design fluorophore-plasmonic nano-complexes for bioimaging applications. The nanoflare system (or commercially named SmartFlare^{TM}) is a derivative of spherical nucleic acid to detect intracellular RNA targets under fluorescence microscopy [52,53]. A nanoflare is modified by hybridized ssDNA complexes containing a (1) recognition sequence and (2) fluorescence tagged reporter sequence. Upon cellular uptake, fluorescence recovers when target RNA replaces a reporter sequence. The release of the fluorescence tagged reporter sequence contributes to fluorescence signal distribution over the imaged cell. The nanoflare has covered popular biomedical research areas such as human tumor cell isolation [54] and drug toxicity testing [55]. Besides, nanoflares could be internalized by exosomes to detect microRNA targets, thus offering a convenient tool for exosome-based diagnosis strategies [56]. Oligonucleotide modified gold nanoparticles are less vulnerable to intracellular degradation [57], so the application of intracellular RNA nanoprobe could be further expanded to gene delivery. Zhang et al. [58] conjugated

siSOX9 (i.e., a small interfering RNA against SOX9) on a Tubb3 and Fox3 targeting multiplexed nanoprobe. Silencing SOX9 could induce neural stem cell differentiation while the expression of related markers Tubb3 and Fox3 could be monitored by a nanoprobe. Kyriazi et al. [59] designed a nano-dimer for both drug delivery and mRNA detection. The nano-dimer links two DNA-gold nanoprobes. Each nanoprobe targets different intracellular mRNA and respectively encapsulates drugs, doxorubicin (DOX) and mitoxantrone (MTX), within the flare-recognizer DNA duplex. Upon the binding of a target sequence and release of the flare-sequence, the respective intercalated drug would be released (Figure 5). In this case, the drug acts as both chemotherapeutic agent and fluorescent reporter of the existence of target mRNA.

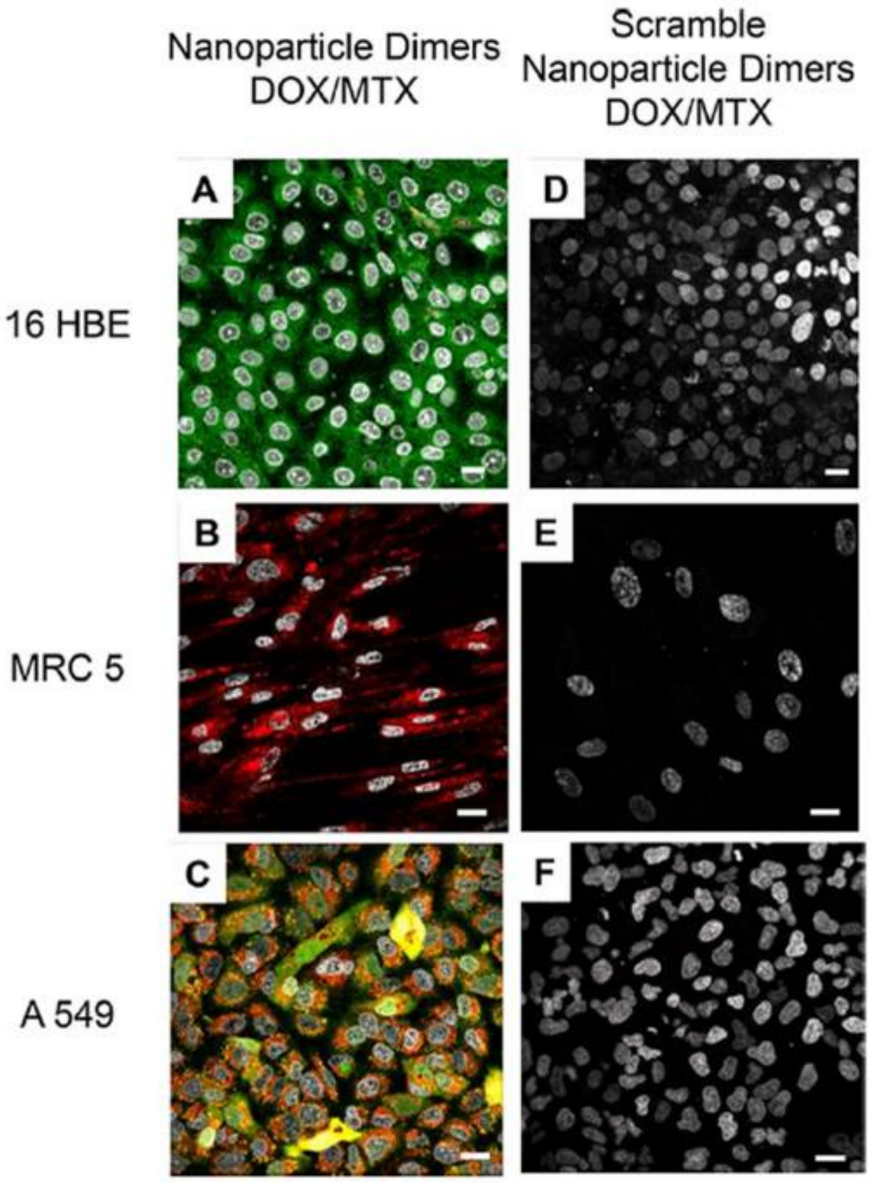

Figure 5. Confocal microscopy showing release of fluorescent drug from DNA-gold nano-dimer upon recognition of target intracellular mRNA sequence in vitro. DOX and MTX were intercalated in keratin 8 mRNA targeting DNA duplex and vimentin mRNA targeting DNA duplex respectively. (**A**) 16 HBE and A 549 cells expressed keratin 8. The release of DOX from gold nanoprobe recovered the quenched fluorescence of DOX. (**B**) MRC 5 and (**C**) A549 cells expressed vimentin. The release of MTX from gold nanoprobe recovered the quenched fluorescence of MTX. (**D**–**F**) No fluorescence detected from non-targeting scramble nano-dimer, suggesting the release of drug was target specific (Figure reprinted with permission from Ref. [59] Copyright American Chemical Society).

The use of hairpin DNA could group recognition domain and reporter domain into one oligonucleotide sequence, which could simplify the detection system. An early report by Jayagopal et al. [60] developed a hairpin DNA-modified gold nanoparticle for intracellular RNA detection. Upon recognition of the target sequence, unfolding of the hairpin displaces the fluorophore from the gold nanoparticle surface, thus leading to the recovery of detectable fluorescence. Besides, the hairpin sequence could be conjugated on nanoparticles in a dissociable form, which would allow the distribution of the fluorophore over the imaged cell [61–63]. Briefly, the fluorescent hairpin DNA probes were immobilized on polydopamine shells through a π–π interaction. The quenched fluorescence recovers upon recognition of the mRNA target and the release of DNA probe from the nanocomplex. Furthermore, Choi et al. [62] showed that the single administration of hairpin DNA immobilized polydopamine coated gold nanoparticles could achieve longer term intracellular micro-RNA (detectable on day 5) imaging compared to SmartFlare^{TM}.

2.3. Photothermal Therapy

Photothermal therapy (PTT) elicits the photothermal conversion of nanomaterials for cancer cell killing. Briefly, near-infrared (NIR) light energy is converted to heat by PTT responsive nanomaterials, and the tumor is then regressed through necrosis or apoptosis [17,64,65]. Several metallic nanomaterials have been frequently investigated for PTT application such as: gold nanoparticles [66] and iron oxide nanoparticles [67]. Photothermal nano-agents are often modified by ligands, such as arginine-glycine-aspartic acid (RGD) peptide motif (targeting αVβ3 integrin) [68,69] and folic acid (targeting folate receptor) [70], to maximize the cellular uptake and enhance the destructive effect. At the intracellular level, mitochondria are well known to regulate cell function through mediating important metabolic activities, such as generating ATP, coordinating redox and calcium level [71,72]. Mitochondrial activity is also critical to tumor growth and metastasis [71]. Thus, targeting mitochondria might further enhance PTT antitumor outcomes via mitochondria destruction [73].

The systemic distribution of colloidal nanomaterials could lead to the inefficient uptake of PTT responsive nanomaterials by solid tumorigenic tissues. In recent years, the delivery of PTT nanomaterials via tissue adhesive hydrogels is an emerging strategy to restrict the loss of PTT responsive nanomaterials to neighboring healthy tissues or circulation [74–77]. For example, Xing et al. [76] reported an injectable collagen hydrogel for the delivery of the gold nanoparticle and photodynamic agent, meso-tetra (N-methyl-4-pyridyl) porphine tetrachloride (TMPyP) to intratumoral region. The combinatorial photothermal and photodynamic therapy benefited by multiple irradiation cycles over time with one injection of hydrogel (Figure 6). A single or double irradiation treatment did not inhibit tumor growth effectively, however multiple irradiation treatments achieved significant tumor suppression. A successful therapeutic outcome would likely be attributed to the precise delivery and retention of gold nanoparticles and TMPyP, which enable subsequent future treatment. Furthermore, a biocompatible hydrogel could promote tissue regeneration. Recently, Liao et al. [77] reported a gold nanorod and hydroxyapatite nanoparticle laden gelatin/chondroitin hydrogel for both the postoperative photothermal effect and bone regeneration. After surgical removal of bone cancerous tissue, photothermal therapy at resection lesions could eradicate residual tumor cells, thereby preventing tumor recurrence. The hydrogel also promoted bone repair after surgery. Therefore, hydrogels might act as a tissue substitute and promote resected lesion regeneration besides the retention of PTT nanomaterial. In comparison with solid tumors, nanomaterials could be modified with the Sgc8 aptamer to target protein tyrosine kinase-7 (PTK7) expressed in leukemia [78–80]. However, treating leukemia by PTT might be challenging in vivo due to its circulating feature. More investigations are desired for exploring the possibility of treating leukemia via PTT.

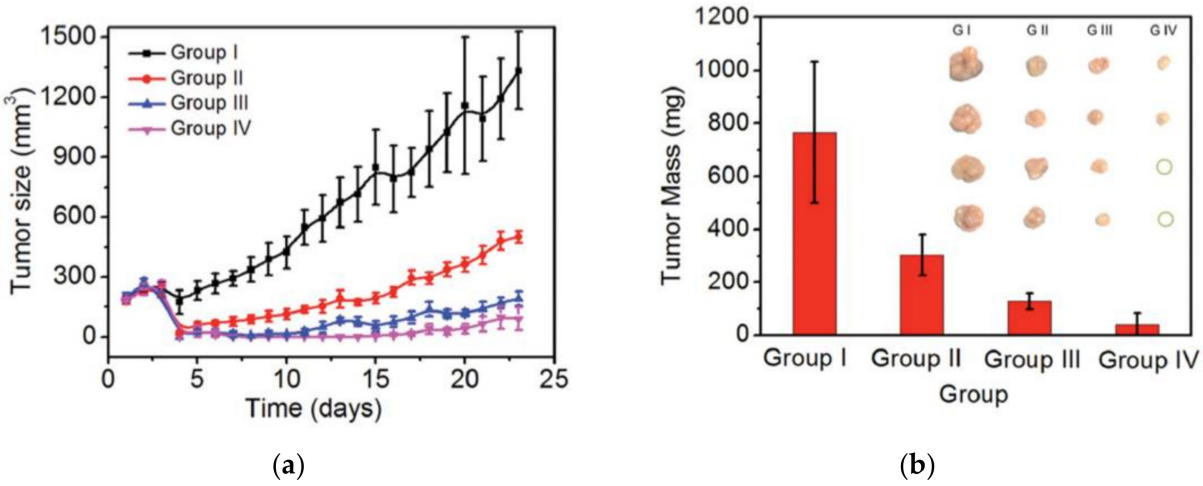

(**a**) (**b**)

Figure 6. Hydrogel delivered a photothermal agent gold nanoparticle, and photodynamic agent TMPyP enabled multiple treatments. Group I to IV represented 1, 2, 4, 5 times of irradiation received over different time points (12 h, 24 h, 48 h, 96 h, 120 h after intratumoral injection of hydrogel). (**a**) Tumor size was monitored over time. (**b**) Tumor weight was recorded after 23 d of treatment (Figure reprinted with permission from Ref. [76] Copyright John Wiley & Sons).

2.4. Polymer-Metal Nanocomposites for Detection and Treatment of Aging-Related Neurodegenerative Disease

Aging is the main risk factor for various neurodegenerative diseases, such as Alzheimer's disease (AD) and Parkinson's disease (PD). One in ten individuals aged ≥65 years suffers from AD and its prevalence increases with age [81]. There are also other factors that can aggravate the pathogenesis of aging-related neurodegenerative diseases, such as systemic inflammation [82], mental stress [83], environmental pollutants [84], and disrupted circadian rhythms [85]. Currently, there are no effective treatments available for curing aging-related neurodegenerative diseases, which tend to progress in an irreversible manner and become an inevitable medical cost to society. Conventional therapies for neurodegenerative disease treatments, such as cholinesterase inhibitors for AD or Levodopa for PD, are inadequate to cure AD and PD, presumably due to two reasons, namely (1) multiple pathological mechanisms of AD and PD and (2) multiple membrane barriers, including the blood–brain barrier (BBB), that hinder drug delivery [86,87]. Polymer–metal nanocomposites have been a powerful tool to deliver drugs or bioactive molecules to specific tissues by tuning the surface properties and functionalities of the nano-cargo, such as surface modification with different ligands (antibodies, aptamers, and polymers), the introduction of surface chemistry (reactive groups, surface charge, and hydrophobicity), and physical properties (cargo shape, rigidity, surface roughness, and porosity) [88–90]. With the advancement of pathological studies on aging-related neurodegenerative diseases, polymer–metal nanocomposites-based nano-cargos serve an important role for the detection and treatment of aging-related neurodegenerative diseases.

2.4.1. Polymer–Metal Nanocomposites for Treatment of Alzheimer's Disease

The neuropathological hallmarks of AD are the formation of β-amyloid (Aβ)/neuritic plaques and the formation of neurofibrillary tangles. Although the exact underlying mechanisms of such Alzheimer type neuropathologic changes remain elusive, there are several risk factors and microscopic features that have been extensively studied [91], including the accumulation of beta-amyloid peptide, intracellular accumulation of hyperphosphorylated tau protein, diminished level of acetylcholine, dysfunctional mitochondria, and neuroinflammation. There are several FDA-approved drugs, e.g., Aducanumab, Donepezil, Memantine, and Galantamine, that can treat only the symptoms of AD with limited ability to cross the BBB [92]. Currently, polymer–metal nanocomposites are considered a promising

class of drug-delivery nano-cargo that can improve BBB penetration and contain ligands for target-specific drug delivery. Gold nanoparticle-based nanocomposites can easily penetrate the BBB and have been extensively used as a nano-cargo. Giralt et al. [93] have reported peptide conjugated AuNPs with the transferrin receptor-targeted peptide sequence THRPPMWSPVWP and an Aβ-targeted peptide sequence, LPFFD. The THRPPMWSPVWP sequence can interact with transferrin receptors that are present in the microvascular endothelial cells of the BBB, and triggers transport across the BBB. The LPFFD sequence can recognize Aβ toxic protein aggregates and destroy them via microwave irradiation both in vitro and in vivo (Sprague–Dawley rats). AuNPs can also be coated with poly(ethylene glycol) (PEG) to improve biocompatibility. The PEG-coated-AuNPs conjugated with anthocyanin have shown enhanced neuroprotection in an AD mice model [94]. In the last decade, drug-delivery nanocomposite cargo for AD has overcome the limitation of bioinert metallic nanoparticles, but also with the use of bioactive metallic nanoparticles. Selenium is an essential micronutrient for the brain and also involved in neutralization of reactive oxygen species (ROS) in the brain [95]. These properties render selenium nanoparticles (SeNPs) a potent component of nano-cargo to treat AD. Liu et al. [96] have shown that SeNPs conjugated with epigallocatechin-3-gallate and a neuron targeted Tet-1 peptide can effectively inhibit Aβ fibrillation and elicit neuroprotection. Aβ-targeted peptide sequence LPFFD together with a BBB penetrating TGN peptide can also be conjugated to the SeNPs and inhibit βA aggregation [97]. Zhang et al. [98] have reported SeNP encapsulated poly(lactic-co-glycolic acid) (PLGA) nanospheres with curcumin molecules that can achieve a sustained release of curcumin, thereby effectively eliciting neuroprotection to the transgenic 5XFAD mice via its anti-oxidant, anti-inflammatory, anti-amyloid, and anti-Tau hyperphosphorylation activities. Cerium nanoparticles (CeO_2) are well known to function as a recyclable ROS scavenger by shuttling between Ce^{3+} and Ce^{4+} forms. Mook-Jung et al. [99] reported a triphenylphosphonium(TPP)-PEG conjugated CeO_2 with small core size (3 and 10 nm) that can be delivered into the mitochondria efficiently, thereby eliciting neuroprotective effects by ROS consumption. Although TPP-PEG-CeO_2 cannot penetrate the BBB and can only be stereotactically injected into the 5XFAD mice, the mitochondria targeting nanocomposite with ROS scavenging properties open up a new strategy to treat AD.

Currently, the clinical trials consider AD are mainly focused on amyloid plaques. There is emerging evidence indicating the importance of β-Amyloid oligomers (AβOs), the major component of amyloid plaque found in AD [100,101]. Recent studies have shown that the AβOs are found in the early stage of pathogenesis and may serve as a potential biomarker for early diagnosis and as a new target for therapy [102,103]. One way to detect AβOs is to collect cerebrospinal fluid (CSF) from a patient and then perform an enzyme-linked immunosorbent assay (ELISA) [103]. Lee et al. [104] reported a AuNPs based electrochemical impedance sensor that can detect subfemtomolar levels of the AβOs. The AuNPs were embedded with a thin layer of highly conductive poly (3,4-ethylene dioxythiophene) (PEDOT), followed by an intermediate layer of poly(thiophene-3-acetic acid) (PTAA), which can be used for the immobilization of cellular prion protein receptor (PrPC), a AβOs specific receptor [105]. The binding between AβOs and PrPC creates an extremely small change in the electrochemical signal which is transferred and amplified by the electrical impedance. The AuNPs−PEDOT−PTAA/PrPC sensor exhibited a wide detection range from 10^{-8} to 10^{-4} nM and were able to test with 5xFAD AD and WT C57BL/6J mouse models. Magnetic resonance imaging (MRI) is the most widely used imaging technique that can be utilized for brain disease diagnostics, presumably due to its high spatial and temporal resolution with minimal invasiveness. However, MRI often requires the aid of a targeted contrast agent to improve the sensitivity in the area of interest [106]. Recently, there are several studies reporting polymer metal nanocomposite to serve as an AD biomarker specific MRI contrast agent. Superparamagnetic iron oxide nanoparticles (SPIONs) have been widely used as contrast agents because of their superparamagnetic properties. SPIONs-coated with AβOs specific scFv antibody W20 and class A scavenger receptor activator XD4 peptide (W20/XD4-SPIONs) have demonstrated good

BBB penetration, followed by the selective binding of the AβOs. The W20/XD4-SPIONs provide a pronounced MR signal in the AD mice, while no MR signal in the PD mice, the Huntington's disease mice, and the WT mice [107]. The gadolinium-based contrast agent is one of the paramagnetic agents used for MRI in clinical settings. Wong et al. [108] have reported a core-shell $NaGdF_4$:Yb^{3+},Tm^{3+}@$NaGdF_4$ nanoparticle that serves as both an MRI contrast agent and a near-infrared (NIR) fluorescent probe, thereby achieving dual modality imaging. Such core-shell nanoparticles were then coated with biocompatible mesoporous silica and incorporated with a AβOs selective cyanine dye, F-SLOH, for BBB penetration. The NP@SiO_2@F-SLOH was administered via tail vein and has shown higher upconversion fluorescence signal in APP/PS1 transgenic mice than in their WT counterpart at 30 min postinjection. MR image of 2 h postinjection indicated a stronger MR signal in the transgenic mice than that of WT mice. Moreover, the NP@SiO_2@F-SLOH has shown the suppression of various Aβ species, including AβOs and monomers, which may be due to the ROS scavenging properties of the nanocomposite.

2.4.2. Polymer–Metal Nanocomposites for Treatment of Parkinson's Disease

Similar to Alzheimer's disease, Parkinson's disease (PD) is a multifactorial neurodegenerative disease characterized by tremor, rigidity, and bradykinesia [109]. The neuropathological hallmarks of PD are the formation of Lewy bodies and Lewy neurites, which are closely associated with the accumulation of α-synuclein (α-Syn), TAR DNA-binding protein 43 (TDP-43), and pathological tau aggregation [110–112]. Studies have shown that α-synuclein correlated with the loss of dopaminergic neurons in both in vivo (e.g., A53T transgenic mouse model) and PD patients [113–115], which leads to diminished levels of dopamine (DA). Levodopa, a precursor of DA, is one of the major treatments for PD that can effectively ameliorate PD symptoms. However, long-term administration of Levodopa can lead to complications such as drug-induced dyskinesia and somnolence [116]. Ruiz-Molina et al. [117] reported a neuromelanin (NM) inspired coordination metal–polymer nanocomposite as a theranostic agent. A NM inspired nanocomposite was prepared via a reversible self-assembly of $Fe(AcO)_2$, dopamine, and the ditopic ligand 1,4-bis(imidazol-1-ylmethyl)benzene BIX to give DA nanoscale coordination polymers (DA-NCPs). The DA-NCPs have shown enhanced uptake by BE(2)-M17 cells in comparison with free DA, as well as slower metabolism kinetics than that of the free DA. The biodistribution analysis indicated that the intranasal administered DA-NCPs enter the dopaminergic neurons via the nigrostriatal pathway, leading to an increase in striatal and substantia nigra pars compacta (SNPC) DA levels. Moreover, the presence of iron ions in DA-NCPs facilitates the track of nanoparticles by MRI imaging.

Studies have shown the involvement of ROS-mediated mitochondrial dysfunction in the pathogenesis of Parkinson's disease [118]. Thus, the delivery of ROS-scavenging nanocargos to dysfunctional mitochondria is one way to ameliorate PD. Li et al. [119] reported biomimetic ultrasmall nanoparticles that can elicit ROS scavenging and promote the anti-inflammatory properties of microglia. Ultrasmall Cu_2-xSe nanoparticles (~3 nm) were selected and first modified with poly(vinylpyrrolidone) (PSP), followed by coordination with a flavonoid derivative, quercetin (Qe), to give the CSPQ nanoparticles. Ultrasmall size nanoparticles have been demonstrated with better ultrasound-aided BBB penetration in comparison with their larger counterpart, while the Cu^{2+}-Qe complex possessed better enzymatic properties and stability [120]. The CSPQ nanoparticles were then modified with the neuronal cell membrane (CE, i.e., MES23.5 cells) as a camouflage that could interact with microglia via its surface α4β1 integrin and VCAM-1 expressed on the cell membrane, as shown in the immunofluorescence staining. The CSPQ-CM nanoparticles elicit multienzyme properties for ROS scavenging in the PD mice model, and simultaneously promote both the expression of anti-inflammatory cytokines interleukin-10 (IL-10) and biomarker CD206 of microglia, as well as inhibit the expression of pro-inflammatory interleukin-6 (IL-6). Notably, such CSPQ-CM np can be traced by photoacoustic imaging and significantly improve the PD symptoms, as evidenced by the recovery of the DA levels in CSF of

mice. Zhang et al. [121] reported a self-oriented nanocarrier that can achieve effective drug delivery by virtue of its exosomal structure. In this work, a mesenchymal stem cell-derived exosome was modified with a neuroprotective miRNAs miR-133b and an acetylcholine receptor-targeted peptide SA-RVG29 to give a PR-EXO. Such PR-EXO was then mixed with PP@Cur, a micellar core constituted of a ROS-responsive polymer, SPIONs, and curcumin. Unlike conventional nanocarriers that can be trapped by endosome/lysosome after cell entry, the resulting PR-EXO/PP@Cur is an engineered exosome that avoids endosome/lysosome formation via membrane fusion with SH-SY5Y cells, thus leading to the enhanced accumulation of drugs in the action site. The PR-EXO/PP@Cur nanocarriers can be traced by T2 MRI images and a reduction of α-Syn aggregation, increased expression of IL-10, and reduced expression of IL-6, IL-1β, and TNF-α in microglia have been shown. The behavioral test indicated that the MPTP-induced PD model mice improved their movement and coordination ability significantly after the treatment with PR-EXO/PP@Cur.

The emergence of microbiota–gut–brain-axis research has led to a potent therapy for neurodegenerative diseases via the modulation of gut microbiota [122]. Wang et al. [123] recently developed an upconversion optogenetic micro-nano-system encapsulated with engineered *Lactococcus* lactis (*L.* lactis) that can achieve gut–brain axis regulation (Figure 7). A sodium alginate microsphere was used and modified with chitosan and small-intestine targeting antibody proton-dependent transporter 1 (PepT1) to achieve a small-intestine targeting and pH responsive cargo that can effectively deliver and release *L.* lactis. The sodium alginate microsphere was then encapsulated with three engineered *L.* lactis strains that produce brain health-related probiotics, namely gamma-aminobutyric acid (GABA), granulocyte-colony stimulating factor (GCSF), or glucagon-like peptide-1 (GLP1), upon blue light exposure. On the other hand, a biocompatible upconversion microsphere (UCM) was prepared from thulium (Tm)−coped−rod-shape and PEG prepolymer. MPTP induced PD mice model that administered with *L.* lactis encapsulated sodium alginate microsphere and UCM could relieve PD symptoms after NIR irradiation, as evidenced by reduced expression of tyrosine hydroxylase (TH), αSyn, AIF1 protein, IL-2, IL-6, and TNF-α in the mice brain. Interestingly, the electrophysiological recordings suggested that the GLP1 expressed by *L.* lactis in the gut together with the treatment of UCM and NIR irradiation could excite the neurons in nucleus of the solitary tract (NTS), suggesting that the peripheral nervous system can elicit short-term effects to the central nervous system.

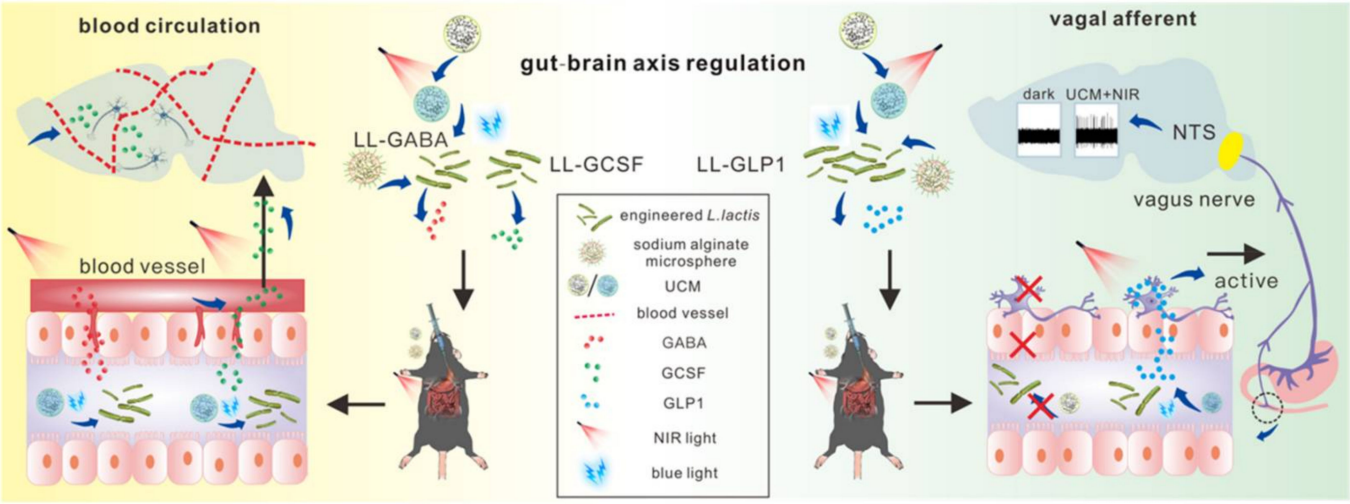

Figure 7. Schematic diagram of gut-brain axis regulation via the upconversion optogenetic micro−nano system. The upconversion induced blue light activates three plasmid engineered L lactis to mitigate PD symptoms via the gut-brain axis. Figure reprinted with permission from Ref. [123] Copyright American Chemical Society.

3. Polymer–Metal Composites Materials for Healthcare Device

Medical and surgical approaches are regarded as two major branches in medical practice. There are diseases or injuries that require localized intervention, such as cardiovascular disease, bone fracture, and tooth loss. Healthcare devices serve a crucial role in surgical treatment by replacing or supporting damaged tissues. At the device level, bulk properties of materials, such as elastic modulus, tensile strength, shear strength, radial strength, yield strength, fatigue strength, ductility, corrosion resistance, and biocompatibility, are closely related to the longevity and the performance of healthcare devices [124,125]. Especially, for implants as their primitive function is designed to provide long lasting, good mechanical support to tissues in realizing long-term tissue healing [126]. Furthermore, the material-cell interactions in the implant-tissue interface modulate cell behaviors such as cell adhesion, proliferation, and differentiation, therefore, the microscopic properties of implant such as surface topology, surface roughness, surface wettability, and degradation kinetics are pivotal to match in scale to regulate cell behaviors and improve tissue healing [127]. An ideal medical implant requires optimized properties in both bulk and microscopic scale that can hardly be accomplished by using a single material. Metallic implants such as titanium-based implants possess excellent mechanical properties in general but suffer from corrosion [128,129]; polymeric implants can be multifunctional and biodegradable, however, difficult to provide some crucial mechanical properties like ductility [125]. With the advance of polymer science and metallurgy, the polymer–metal composite materials serve as an emerging class of healthcare device with optimized bulk and microscopic properties, such polymer–metal composite devices provide good mechanical support, good bio-integration, good hygiene and minimized bacterial infection, and reduced hypersensitivity reactions (Figure 8).

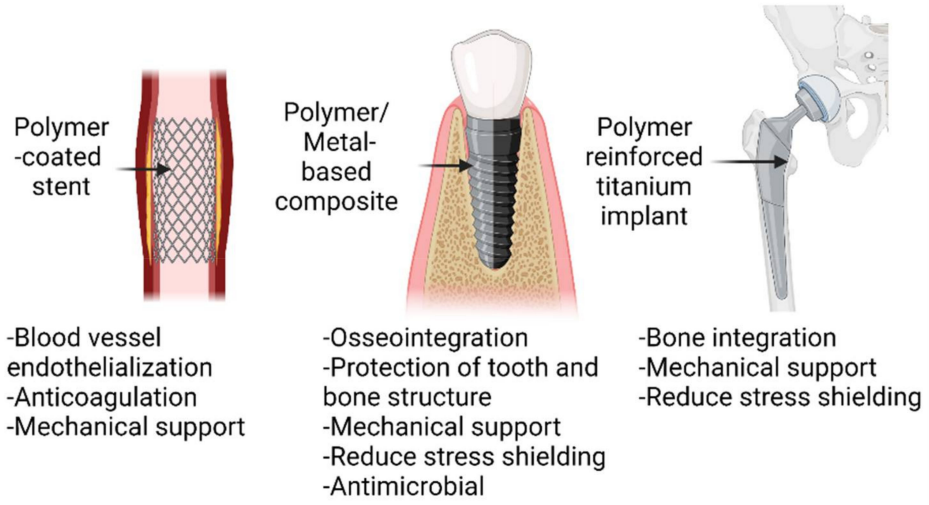

Figure 8. Polymer–metal composite materials as cardiovascular stents, dental implants, and orthopedic implants.

3.1. Polymer–Metal Composite Materials for Dental Implant

Dental implant is one of the most common dental treatments to replace missing teeth. The primarily function of a dental implant is restoring the patient to a normal profile regardless of the status of the stomatognathic system [130,131]. Similar to the orthopedic implants, conventional dental implant relies on titanium as implant materials to fulfill several requirements: (1) good fatigue strength and wear resistance to withstand cyclic occlusal load (axial bite force: 500 N–800 N) [132–134], (2) good corrosion resistance to withstand different types of corrosions that take place in the oral cavity (galvanic, pitting, stress, and microbial corrosion) [128,135], and (3) bioinert to body environment and good biocompatibility [136]. In bulk scale, titanium alone is insufficient to fabricate dental implant for osseointegration (i.e., bone ingrowth into implant), presumably due

to huge difference of elastic modulus (i.e., stiffness) between metal/metal alloy-based dental implant (titanium: 110 GPa, Zirconia: 210 GPa, Cobalt-Chromium: 180–210 GPa) and surrounding bond tissues (cortical bone: 13.8 GPa, spongy bone: 1.38 GPa) [137–139], such difference in elastic modulus creates risk of mechanical overloading of bone (namely stress-shielding), leading to bone damage and bone resorption [140–142]. In nanoscale, reported studies have shown that the immune reactions and bacterial infections may be the underlying mechanism of marginal bone lost and peri-implantitis [23,143–149]; on the other hand, bone healing and bone remodeling after dental implant treatment is determined by osseointegration, peri-implant osteogenesis (i.e., distant osteogenesis and contact osteogenesis), and osteoclastogenesis [137,150–155]. Incorporation of polymers into titanium dental implants via coating or polymer composite materials endow the dental implants with proper load transfer and distribution, enhanced bone healing, minimized immune reactions, and antimicrobial properties [156,157].

3.1.1. Polymer–Metal Composite Dental Implant with Improved Load Transfer, Osseointegration, and Osteogenesis

Polyetheretherketone (PEEK) is FDA approved, a dominant member of Polyaryletherketone (PAEK) family which has been extensively used in dental implant due to their compatible elastic modulus (PEEK: 4 GPa, carbon-nanofibre-reinforced PEEK: 18 GPa) [158,159], high flexural strength (140–170 MPa), radiolucent, highly biocompatible and bio-stable [160–162]. Lee et al. [163] has demonstrated that PEEK-coated titanium/zirconia dental implants exert lower levels of von-Mises stress to the bone in comparison with metal-based implants. The major limitations of PEEK-based dental implants are their limited osteoconductivity and lack of bioactivity which may trigger implantitis and implant failure [164]. Inspired by the good osseointegration properties of titanium, metallic materials (metallic complex, metallic nanoparticles) may serve as a potential additives to endow PEEK bioactivity and make PEEK-based dental implant possible. As such there are different metallic materials being used to modify PEEK, such as titanium [165], titanium dioxide [166–169], and strontium based materials [170,171], by either surface modification or melt-blending [172,173]. Strontium based materials such as strontium ranelate coated PEEK can strengthen the osteoblast adhesion, increase the alkaline phosphatase activity, increase collagen secretion and ECM mineralization deposition [170]. Titanium-coated PEEK has shown improved proliferation of osteoblast and higher percentage of bone-to-implant contact [165]; while titanium oxide coating has also shown beneficial effects on the osseointegration [166–169,174,175]. Bone remodeling comprise different levels of hierarchical structural changes at macro (e.g., cortical bone, spongy bone), micro (osteons, trabeculae), and nanoscale (collagen I and hydroxyapatite composited ceramic-interspersed collagen fibril) [176,177]. However, the surface properties of PEEK do not favor osseointegration due to its inherent hydrophobicity and bioinert. It is well known that hydrophilic implants favor plasma proteins and cells adhesion, and one way to increase surface wettability is to control the surface roughness of materials [178]. Metallic materials are useful tools to introduce micro and nanofeatures to implant surfaces, and endow new functionalities, such as rough surface (i.e., increase surface roughness), thereby promoting osteogenesis and osseointegration.

Elawardly et al. [179] has demonstrated that both the ceramic-filled PEEK and the carbon fiber-reinforced PEEK discs shown significantly improved wettability after sand-blasted treated with 50/110 microns of aluminum oxide particles, in compared with untreated group; such PEEK-based materials show good wettability when the surface average roughness (Ra) value was either <1.0 or >1.7 μm. Interestingly, in comparison with microscale surface roughness, implants with nanoscale surface roughness introduced have better osseointegration [176]. Some reported studies have shown that introduction of titanium-based nanofeatures on implant surface, such as TiO_2 nanonodule [180], TiO_2 nanotube [181], and TiO_2 nanopores [169] can further improve the osseointegration via several effects: (1) improved cell adhesion, cell spreading, and therefore, bone-implant integration, (2) improved ALP levels, and (3) promote the formation of hydroxyapatite (HA).

The functions of nanoporous titanium implant surface has been recently shown that such nanofeature can promote osteogenesis by inhibiting the differentiation of macrophages into osteoclast (i.e., osteoclastogenesis) by blocking integrin mediated FAK phosphorylation and downstream MAPK pathway, and elicit a prohealing cytokines secretion profile [168]. The titanium nanofeatures increase the hydrophilicity of PEEK dental implant, which has shown to facilitate immobilization and delivery of bone morphogenetic protein-2 (BMP-2), thereby significantly enhancing the osseoconductivity of PEEK implant [167]. With the cytotoxicity concern on TiO_2 nanoparticle leaching from TiO_2 coating, Wu et al. [167] has developed a titanium oxide nanoparticle/PEEK composite with rough surface that increase the growth rate of osteoblast and higher bone volume/tissue volume (Figure 9). The interplay between the titanium and PEEK as a polymer–metal composite material has significantly improved the performance of dental implants in both nano scale and device scale. In nano scale, the titanium–based nanofeatures improve the bioactivity of the implant surface, thus improved osseointegration; in device scale, the PEEK-based implant becomes compatible with the stiffness of surrounding bone, which ensures proper load transfer upon occlusion force.

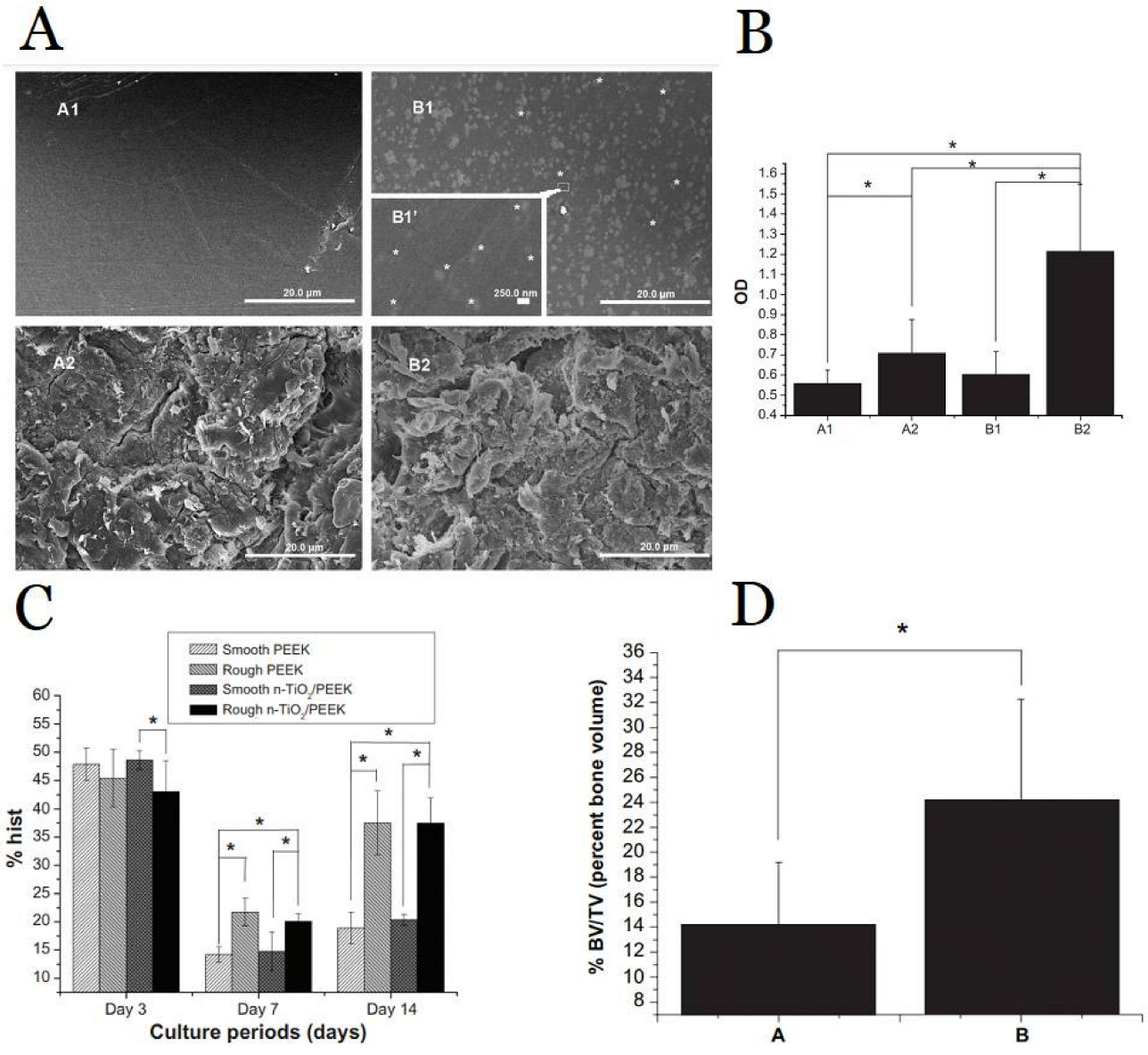

Figure 9. (**A**) Scanning electron microscopy images of PEEK and TiO_2 nanoparticle/PEEK composite (n-TiO_2/PEEK) before and after blasted treatment (A1 smooth PEEK; A2 rough PEEK; B1 smooth

n-TiO_2/PEEK; B2 rough n-TiO_2/PEEK; (**B**) Cell attachment testing indicates significantly improved osteoblast cells adhesion in B2 rough n-TiO_2/PEEK than the other groups (A1, A2, B1); (**C**) Flow cytometric analysis indicates rough implant surface promote cell proliferation (both PEEK and n-TiO_2/PEEK); (**D**) Microcomputed tomography indicates significant increase in bone volume/tissue volume in n-TiO_2/PEEK than PEEK implant. Note: * $p < 0.05$ Figure reprinted with permission from Ref. [167] Copyright Dovepress.

3.1.2. Antimicrobial Polymer-Metal Composite Dental Implant

Periodontal disease is the main cause of tooth loss which is considered as a huge threat to oral health [182]. The onset of periodontal disease is well known to be the collective outcome of bacterial infection and inflammatory responses [183]. It is noteworthy that the periodontal tissue is continuously exposed to oral microbiota during mastication and respiration [184]. In the healthy state, localized bacterial challenge and host immune response is balanced. However, the colonization of "keystone" pathogens (change of microbiota constituent and their total counts) increase the pathogenicity of local microbiota and over activate immune response [185,186]. For example, the bacterial infection triggers the generation of specialized T_H17 cells, namely "bone-damaging T cells", to fight against bacteria by concurrently initiating mucosal immune responses and inducing bone loss to inhibit infection [187]. The dental implant confronts the same challenge after implantation when bacterial infection takes place, from both the implant-associated infection, daily mastication, and respiration which eventually lead to the peri-implantitis [188]. Therefore, developing an antimicrobial dental implant can greatly reduce the major cause of periodontal disease by inhibiting bacterial growth and bacterial biofilm formation, thereby improving the oral health and the longevity of the dental implant.

Typical dental implant contaminations involve the polymicrobial biofilm formation, which can be suppressed using antibiotics. Therefore, antibiotics coated/encapsulated dental implants have been demonstrated as one of the major approaches to fight against bacterial infection [189]. Polymer-based coatings are advantageous for antibiotics delivery due to its high antibiotics upload capacity, controlled release of therapeutic concentration of antibiotics in proximity to infected area, biocompatible, and biodegradable; many antibiotic-encapsulated polymer/biopolymer coatings have been developed in the last two decades [189,190]. The early stage of polymer-coating development employed polymers such as poly(D,L-lactide) [191,192], poly-L-lactide [193], due to their excellent biodegradability. Recently, several new coating strategies have been developed with mild processing conditions (low temperature, organic solvent free, radiation free) used in titanium implants, such as polydopamine coating, surface controlled free radical polymerization, azide-alkyne click reaction, salinization, polyelectrolytes deposition, electrophoretic deposition (EPD), and dynamic covalent chemistry, which allow more bioactive polymers employed as an antibiotics cargo with improved antimicrobial outcomes [194–199]. Namely, chitosan can improve drug residence time at mucosal surface [200]; polymethacrylate grafted with functionalized poly(ethylene glycol) (PEG) improve conjugation of antibiotics thereby increase antibiotics loading [194]; PEG dimethacrylate hydrogel functionalized with oligonucleotide enhanced stability to human serum [195]; and PEG-poly(propylene sulfide) enable oxidation responsive (i.e., hyperinflammatory environment) release of antibiotics [201,202]. Interestingly, studies have shown that antibiotics-loaded with nanostructured titanium implants (pillar-type and pocket-type nanostructure) have better anti-biofilm performance [203,204]. However, systematic study on the effect of nanofeatures on the polymeric coated titanium dental implants has remained unexplored.

One of the major concerns of antibiotic release dental implants is the associated risks of bacterial resistance [205], and therefore, various antimicrobial materials have developed to serve as an alternative to antibiotics. Chitosan-based coating is a promising antimicrobial biopolymer for dental implants, as chitosan elicits excellent antimicrobial properties towards both Gram-positive and Gram-negative bacteria via disruption of their mem-

brane functions [206]. Other attributes of chitosan such as anti-inflammatory properties, non-toxic, and biocompatible render chitosan-based dental implants worthy for clinical studies [207]. Chitosan combined with other bioactive materials like hydroxyapatite and graphene have been demonstrated in promoting osteoblast proliferation and inhibiting microbial growth [208,209]. Antimicrobial polypeptides (AMPs) is another class of antimicrobial materials with amphipathic properties and notable anti-adhesive properties [210]. Such extra anti-adhesive properties render AMP-coated dental implants extra protection against the formation of biofilm and subsequent implant contamination [211–214]. It is noteworthy that different antimicrobial dental implants using antibiotics or AMPs generally suffered from gradual depletion of the antimicrobial properties, presumably due to lack of renewable properties. Recently, Wu et al. [215] have developed a long-lasting antibacterial porous polymeric coatings with self-renewal properties using N-halamine polymer (Figure 10), which is prepared from surface pore-making of titanium implant, followed by surface grafting of polyacrylic acid (PAA), and reacted with ethylenediamine and sodium hypochlorite to give the chlorinated N-halamine surface (Ti-PAA-NCl). The amide N-halamine group possesses moderate transfer rate of oxidative Cl+, which is able to kill bacteria through both contact killing and release killing. Ti-PAA-NCl retains its antibacterial properties (68% against *P*. gingivalis) after 20th cyclic antibacterial test and after stored in PBS for 4 weeks (89%) and 12 weeks (79%), which is durable enough to cover the period of osseointegration (at least 4 weeks after implantation, 3 months to complete) [216]. Notably, Ti-PAA-NCl can replenish its antibacterial property by simply peri-implant irrigation.

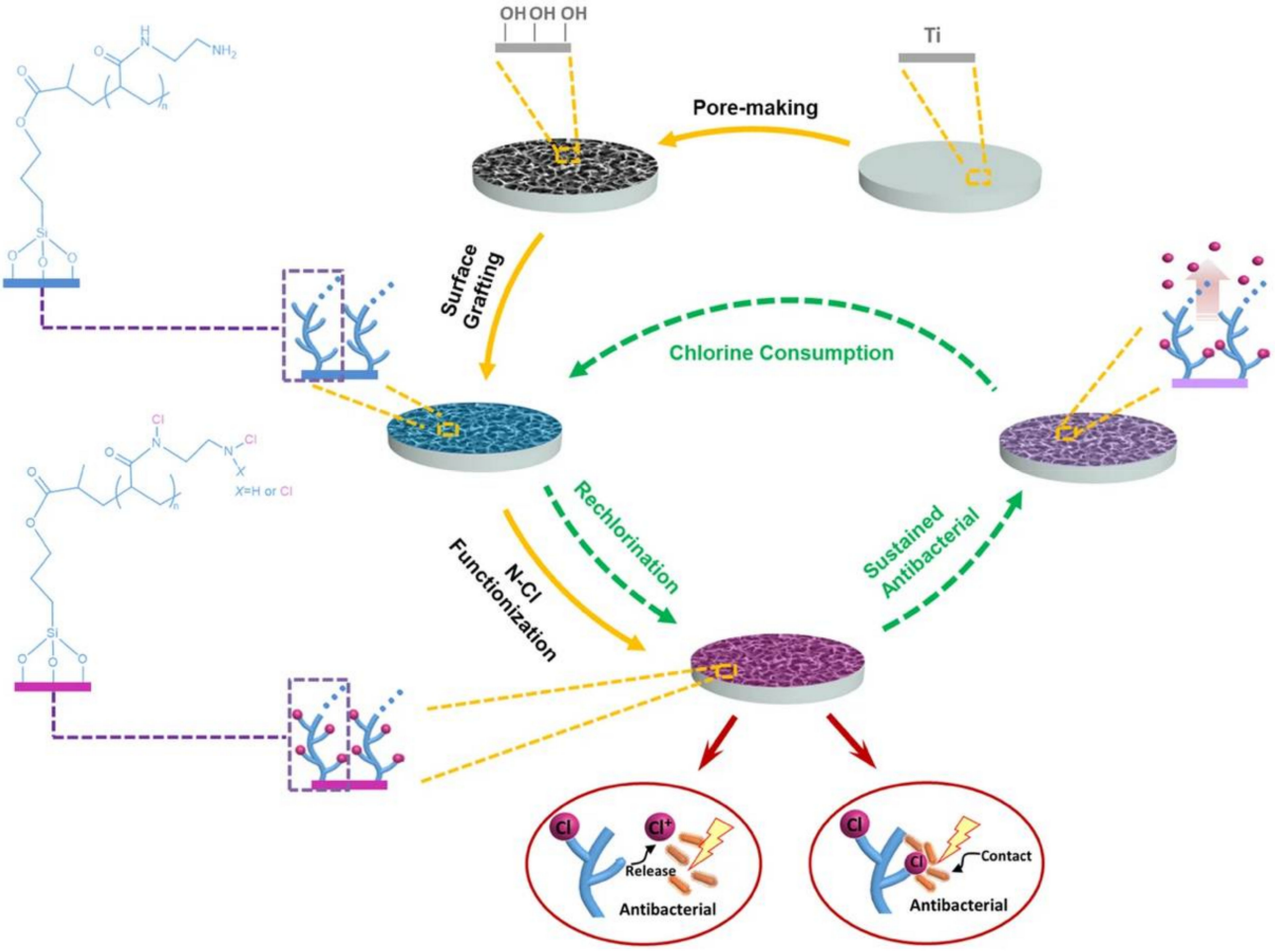

Figure 10. Preparation, mechanism of antibacterial property, and regeneration of antibacterial property of the porous N-halamine polymeric coated titanium. Antibacterial property replenished by

simply peri-implant irrigation using 5% NaOCl solution for 15 min. Figure reprinted with permission from Ref. [215] Copyright 2021 Springer Nature.

3.1.3. Polymer–Metal Composite Dental Implant with Minimized Immune Reactions

One of the consequences of dental bacterial infection is the onset of immune responses that eventually disrupt bone remodeling and cause bone loss [185,186]. However, induced immune responses in the stomatognathic system cannot be completely prevented by simply incorporating antimicrobial functions to the dental implant. Nano-micro size wear particles can be generated during implant fabrication, implantoplasty, and cyclic occlusal force (i.e., biting) [217,218]. The impacts of different types of wear debris generated by dental implants have been discussed in detail: [99,100]. In brief, cells in the oral cavity generally elicit adverse effects when in contact with, or upon the uptake of the nano-micro size wear particles, including impaired osteoblast adhesion, proliferation, osteogenic differentiation and mineralization, elevated RANKL/OPG ratio in osteoblast, and secretion of proinflammatory cytokines from both osteoblast and activated macrophage, and collectively lead to osteolysis and peri-implantitis [219,220].

Dental implants mainly contain three compartments: the screw (insertion to the alveolar bone), the abutment (connector between the dental crown and implanted screw), and the dental crown (in contact with oral cavity and natural teeth). It is noteworthy that wear debris can be generated upon the loading of the abutment to the screw [221], which can be prevented using a protective film. Łępicka et al. [222] developed an anti-wear abutment screw using polysiloxane-TiO_2 nanoparticle composite film, which serves as a "locking coating" on the titanium abutment and screw. Compared to conventional protective films such as pure GPTMS/TEOS matrix, the nanoindentation results indicated that the polysiloxane film with TiO_2 NP in the polymeric backbone significantly reduced the hardness and elastic modulus, thereby rendering the film with anti-wear property [222]. Moreover, the wear resistance of Ti-6Al-4V alloy has been shown to be improved with a simple coating of PEEK due to its high wear resistance [223], which can be a generic approach to improve the wear resistance of dental implants. In the case of the dental crown, conventional dental crown materials include a resin-based composite, composed of organic fillers (e.g., zirconia), and organic monomers (e.g., triethylene glycol dimethacrylate (TEGDMA), bisphenol A-glycidyl methacrylate (Bis-GMA)). Early resin composites suffered from a high wear rate, presumably due to the larger filler particles. Recently, micro/nano-hybrid composites have been employed and the wear resistance significantly improved [224]. In contrast, the wear behavior of composite resins using metallic nanofillers such as TiO_2 NPs can be adjusted by the type of polymers and contact conditions. TiO_2 NPs can only be beneficial when they can be blended with other wear debris to form a strengthened transfer film (generated when sliding two materials together), thereby providing the adequate support required for other dislodged TiO_2 NPs to elicit a rolling effect, and thus anti-wear property [225]. Hence, it is important to firstly investigate the interactions between different tribo-fillers with well-designed contact conditions to mimic real clinical settings (biotribology model for oral cavity), and to design high wear resistant polymer metal composite materials for dental crowns.

3.2. Polymer–Metal Composite Materials for Cardiovascular Stent

Myocardial infarction (MI) is regarded as one of the most lethal cardiovascular diseases worldwide, presumably due to the narrowing of artery vessels, namely atherosclerosis [226,227]. Percutaneous coronary intervention (PCI) was first pioneered by Andreas Grüntzig in 1977 and became one of the most commonly used angioplasty surgeries used to treat atherosclerosis, with the help of the stainless bare-metal stent (BMS) to prevent artery contraction and therefore alleviate ischemia [228,229]. However, the PCI-related arterial wall injury triggers neointimal hyperplasia, which leads to the lethal restenosis within the first 12 months after the BA treatment (30~50%) [230]. The dual-antiplatelet therapy

(DAPT) was developed to inhibit platelet activation and vascular smooth muscle cell hyperproliferation, thereby preventing early stent-restenosis [231,232]. Nevertheless, a considerable group of patients still suffered from early stent-restenosis (20–30%) [233,234]. The effective inhibition of restenosis require proximal drug delivery to the iatrogenic injured vessel. A metallic drug eluting stent was developed, but with a limited amount of drugs, and the stent failed to release the drug molecules in a suitable time frame [235]. Polymer-based drug eluting stents, namely bioresorbable vascular stents (BVS), have recently been developed as a new class of cardiovascular stent, which aims to improve the atherosclerotic vessel healing by gradual bioresorption, thereby effacing the foreign implant over time [236]. However, the vessel healing using BVS could not meet the expected advantages and patients treated with BVS suffering from a higher risk of late stent thrombosis (LST), very late stent thrombosis (VLST), target lesion failure (TLF), and cardiac death, presumably due to the inherent properties of polymeric stent, such as limit stent expansion and weaker radial strength when compared with the metallic stent [237–240]. The BVS has to be made with thicker and wider strut to provide appropriate mechanical support, which disrupts the laminar blood flow, thus promoting platelet activation and subsequent thrombosis [241]. To date, the FDA approved cardiovascular stents are polymer–metal composite-based stents, mainly from two major classes: (1) first-generation drug-eluting stent using durable polymers, and (2) second-generation drug-eluting stent using biodegradable polymers.

3.2.1. Durable Polymer Metal Stent: First-Generation Drug Eluting Stent

The first major breakthrough of the PCI technology occured with the invention of the 1G-DES, a polymer-coated metal stent with antiproliferative drugs [27]. Current FDA approved 1G-DES released either an antiproliferative drug paclitaxel or an immunosuppressive drug sirolimus from a layer of polymer coating [242]. The FDA approved 1G-DES are coated with durable polymers such as poly(styrene-block-isobutylene-block-styrene) (SIBS), Poly(ethylene-co-vinyl acetate) (PEVA), and Poly(*n*-butyl methacrylate) (PBMA) [242]. The polymer coatings offer new functions to the cardiovascular stent: (1) serve as a reservoir to endow temporally controlled drug release from the polymer metal stent, to inhibit blood clotting, and to limit the overgrowth of tissues that triggered by PCI-related arterial wall injury; (2) provide protection to metallic stent from corrosion to maintain radical strength of the stent and to prevent stent fracture [243]. Moreover, 1G-DES creates much less burden for the patient in terms of in-stent restenosis, but with the cost of another problem, the development of LST, (between one month and one year after implantation) and VLST, (>1 year after implantation) [244,245]. The generally accepted underlying mechanism of such increased LST and VLST risk is due to the antiproliferative drugs in the 1G-DES delaying the re-endothelialization of blood vessels [244,245]. Hence, 1G-DES has been shown to present a considerably higher risk of developing VLST in comparison with BMS (adjusted risk ratio (RR) 1.87 (1.47–2.25)) [246]. Other studies have shown that the permanent polymer coatings (such as PEVA and PBMA) in 1G-DES contribute to impaired arterial healing [247]. These findings support that the permanent polymer coatings in 1G-DES hamper normal re-endothelialization. Moreover, the permanent polymer coating in 1G-DES is inevitably creating higher risk factors, such as accelerated neoatherosclerosis (NA) plaque growth and hypersensitivity reactions that will eventually develop into ST [247–249]. Indeed, the healing of atherosclerotic vessels into normal blood vessels requires long-term monitoring. At the early stage after the stent implantation, the drug-eluting should exert an antiproliferative effect in order to prevent restenosis, and the patients should receive the DAPT therapy for at least 12 months to prevent early thrombosis [250,251]. Proper blood vessel re-endothelialization after the PCI is pivotal to prevent LST and VLST.

3.2.2. Biodegradable Polymer Metal Stent: Second-Generation Drug Eluting Stent

With the lesson learnt from the 1G-DES, the second-generation drug eluting stent (2G-DES) aims to select the more biocompatible, biodegradable polymer to replace durable polymer as new coatings for drug eluting stents. The 2G-DES with a biodegradable coating

(e.g., CoCr-Everolimus with poly-L-lactide (PLLA) coating, CoCr-EES) mitigates polymer-associated chronic inflammation and hypersensitive reactions, thereby providing superior protection from LST and VLST (CoCr-EES vs. PES, a 1G-DES or vs. BMS, at median follow-up of 3.8 years) [230,252]. The 2G-DES also showed better clinical outcome than 1G-DES in terms of disease complications and mortality, such as reduced repeat revascularization in ST-segment elevation myocardial infarction (STEMI) patients [253]; lower rates in major adverse cardiovascular events (MACE), cardiac death, recurrent MI, as well as target or non-target lesion revascularization (TLR/non-TLR) in non-ST-segment elevation myocardial infarction (NSTEMI) patients [254,255]. This evidence places 2G-DESs as the current gold standard and benchmark comparator to ongoing trials [230,252].

3.2.3. The Advance of Cardiovascular Stent: Polymer–Metal Stents Engineered with Macroscopic and Microscopic Features

Recent advancements in stent technology have greatly reduced the risk of restenosis, stent thrombosis, and other clinical complications. The stent thrombosis remains a difficult task to solve due to its high mortality (45%) and high recurrence rate (15–20% at five years) [256,257]. There is a myriad of factors associated with the occurrence of thrombosis, such as the profile of patient, progress of lesion, and execution of the procedure, that have already been discussed in detail in other published reviews [258–260].

Compared to other implant biomaterials (e.g., dental implant, pacemaker, and joint replacement), the cardiovascular stent is placed in a bent vessel with continuous blood flow. The cardiovascular stent has to maintain structural integrity to prevent narrowing of the artery, and concurrently the stent should not exert too much circumferential stress on the artery that may lead to unnecessary trauma, subsequently leading to disease complications [261–263]. Therefore, the cardiovascular design requires the fine tuning of some extra macroscopic properties of the material, such as radial strength, elastic strength, and Poisson's ratio [264–266]. On the other hand, the haemodynamic nature of the blood vessel has been well known to be pivotal to proper vessel healing and tied to the occurrence of thrombosis. Laminar blood flow with high shear stress to artery is crucial to trigger atheroprotective effects that promote the survival of endothelial cells. Blood flow disturbances, such as turbulent flow/circulating flow, conversely, trigger both platelet activation and prevent endothelialization (Figure 11) [267–269].

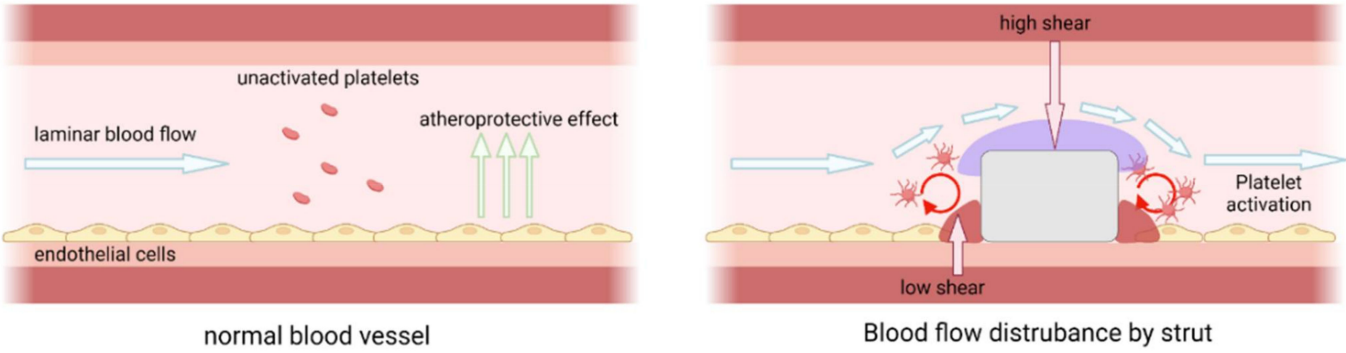

Figure 11. (**left**) The atheroprotective effect of laminar blood flow and (**right**) blood flow disturbance by a thick strut. Laminar blood flow creates high shear stress to artery and trigger the release of anticoagulant and antithrombotic molecules (e.g., NO, PGI2, TFPI, tPA, thrombomodulin) by endothelial cell, migration of leukocytes and monocytes, and proliferation of smooth muscle cells that collectively promote the survival of endothelial cells. Blood flow disturbance such as turbulent flow/circulating flow, conversely, trigger both platelet activation and prevent endothelialization.

The current design of cardiovascular stent aims to minimize turbulent flow via the development of different geometric stent models with minimal stent thickness (i.e., minimum polymer and metal) to avoid flow disturbance [270,271], without compromising their protective effects (e.g., optimal drug release kinetics, and stent radial strength). The effects

of polymer–metal stent macroscopic properties on the performance of cardiovascular stents and clinical performance are summarized in Table 1. Stent geometry (i.e., strut distance, strut width, stent shape) is one of the major parameters that affect the haemodynamic nature of arteries as discussed in other reviews [272–275]. On the other hand, thin stents are well known to minimize blood flow disturbance more than thick stents, thus benefiting their clinical performances (e.g., reduced the incidence of stent malapposition and evaginations) [271,276]. Therefore, the development of new alloys with better mechanical strength and radial strength [277], and thus new polymers with better drug loading and optimized drug release profile [278], can collectively contribute to the development of thinner stents.

Table 1. The effects of polymer–metal stent macroscopic properties on the performance of cardiovascular stents and clinical performance.

Parameters	Effects on the Performance of Cardiovascular Stents and Clinical Performance	Refs.
Stent Geometry		
Distance between strut	Further the distance elicit less blood flow disturbance	[258]
Strut width	Narrower the strut elicit less blood flow disturbance	[272]
Strut sizing (oversize/undersize)	Slightly oversize (10% than vessel diameter) is beneficial to reducing risk of ST and VLST	[273,274]
Properties of metal/alloy		
Metal/Alloy selection	Alloy with improved mechanical properties render thinner struts design possible CoCr, PtCr (81–91 μm) vs. 316 L stainless steel (141 μm)	[277]
Diameter/thickness of metal	Thin metal stent (<100 μm) → less blood flow distrubance that reduce the risk of stent malapposition and evaginations Thick metal stent (>100 μm) → generation of circulatory blood flow and promote platelet activation	[271,276]
Properties of polymer		
Selection of Amorphous/Semicrystalline/Crystalline polymer	Enhanced Polymer Crystallinity • Reduced Dispersion of drug in polymer coating • Increased Mechanical strength of polymer • Reduced of Moisture and gas permeability of polymer coating • (Biodegradable polymer) Reduced biodegradation rate	[236,243,278–280]
Polymer thickness	Increasing the thickness of the polymer coating • Increase the risk of the polymer deformity • Increase strut thickness thus create circulatory blood flow	[281–283]
Polymer degradation kinetics	No significant difference in target vessel revascularization (TVR), MI, ST, and VLST between fast (<6 months) and slow (>6 months) polymer degradation	[284]

3.2.4. Key Microscopic Features of Polymer—Metal Stent

Endothelialization (i.e., adhesion of endothelial cells) is a crucial step for arterial healing after the inevitable artery injury caused by PCI. Studies have indicated the critical role of the endothelium (i.e., layer of vascular endothelial cells) in preventing disease complications, such as vascular thrombosis, intimal hyperplasia, LST, and VLST [244,245,285]. A healthy endothelium is considered as an anticoagulative phenotype that secretes a high level of vasodilators (e.g., nitric oxide (NO), prostacyclin (PGI2)), and prevents the exposure of elastic lamina and SMCs that can release a pro-coagulant thromboplastin into the blood-

stream. Incomplete endothelialization or dysfunctional endothelium leads to a biological cascade that promotes SMCs proliferation and platelet activation, and thus blood coagulation, thereby causing thrombosis [286–289]. Therefore, it is of importance to promote early re-endothelialization after implantation of cardiovascular stents to prevent PCI associated complications. The advance of nanotechnology in biomaterials provides new tools for cell adhesion. Rapid re-endothelialization can be achieved via different nanotechnologies, such as the use of core-shell nano/micro particles as a multi-drug/bioactive molecules delivery system [290,291], creating different nanostructured stent surfaces (e.g., change of surface topography)[292,293], and by virtue of bioactive ligand-mediated cell adhesion [294].

One way to achieve early re-endothelialization is the implantation of a stent with drug and bioactive molecules that release in proximity to wounded arteries. Wang et al. [295] reported a hydrophobic core/hydrophilic shell nano/micro particles that was then coated as a drug eluting stent coating. The PLGA solution contains the antiproliferative drug and serves as the precursor of core coating, whereas the chitosan solution contains the platelet glycoprotein IIb/IIIa receptor monoclonal antibody SZ-21 for shell coating. These two solutions were injected from the coaxial nozzle and form the dual core/shell drug particles. Such a coating can inhibit platelet adhesion and activation, as well as SMCs proliferation and migration in vitro. In vivo data (porcine coronary artery model) have indicated that the SZ-21/DTX drug-loaded hydrophobic core/hydrophilic shell particle coating stents promotes re-endothelialization and inhibit neointimal hyperplasia.

Another way to achieve rapid re-endothelialization is to modulate artery microenvironment at the molecular level. Nitric oxide (NO) releasing materials have also been incorporated into a part of the polymer coating to elicit anti-thrombosis/restenosis functions, presumably due to their crucial role in vasodilation [296,297]. Pioneer research on NO-releasing/generating coatings involved either an NO supplier or catalyzer (e.g., N-diazeniumdiolate or ascorbic acid) that releases the therapeutic dosage of NO to restore endothelial cell functions [298–300]. On the other hand, there are various biomolecules/bioactive ligands that can promote the growth of endothelial cells, including heparin, hyaluronic acid, chondroitin sulfate, fucoidan, and gallic acid [301–305]. Combining the NO releasing coating with bioactive ligands can thereby promote re-endothelialization via biomimetic microenvironment. Zhao et al. [306] reported a stepwise copper-catechol-amine (MCA) surface coating approach on vascular stent. The amine groups of MCA were conjugated with heparin, and the CuII-DA/HD networks elicited a glutathione peroxidase (GPx) like activity similar to CuII, which triggered the decomposition of blood stream S-nitrosothiols (RSNO) into NO. The heparin moiety and NO release exhibited synergistic effects in terms of rapid re-endothelialization, enhanced antithrombogenicity, SMCs suppression, inhibition of intimal hyperplasia, and in-stent restenosis in the adult New Zealand white rabbit model. Wu et al. [307] reported a NO eluting hydrogel coated vascular stent that can suppress neointimal hyperplasia by virtue of GPx mimetic organoselenium generated NO. The hydrogel is composed of alginate and gelatin that are analogous to hyaluronic acid and collagen in the ECM. The hydrogel composition was optimized so that it is mechanically strong enough to withstand balloon angioplasty. The alginate backbone was modified with selenocysteine eliciting a GPx-3 like catalytic properties that were able to degrade RSNO into NO. The hydrogel coated vascular stent had shown the persistent suppression of neointimal hyperplasia in both the New Zealand white rabbit model and Bama miniature pig model.

Surface topography/nanotopography is an emerging technology to regulate cellular behaviors [308,309]. A change of surface topography can influence protein adhesion and even endow stent adhesive properties to a specific cell type. The design of surface topography primarily depends on the cell morphology and cell alignment of interest. In the case of endothelial cells, which possess an elongated morphology, studies have shown that substrates with a parallel grooved surface promote the migration of endothelial cells in comparison with the smooth counterpart [310]. Such groove patterns have shown the selective adhesion of endothelial cells and concurrent inhibition of SMCs adhesion [311].

The surface of the stent can also be modified by the addition of a nanostructure, such as TiO_2 nanotubes. Desai et al. [312,313] reported that the nanotubular titanium oxide surface promotes endothelial cell adhesion while inhibiting SMCs adhesion. Iglič et al. [314] reported the beneficial effects of an electrochemical oxidized TiO_2 nanotube array. This oxidized TiO_2 nanotube array (15 nm in diameter) elicited selective endothelial cell adhesion over the SMCs, and concurrently inhibited platelet adhesion, which is instrumental for antithrombotic metal stents.

4. Conclusions and Perspective

In the reviewed plasmonic biotechnology examples in Section 2.1, the unique optical features, such as fluorescence enhancement and high photothermal conversion efficiency, have been elicited in the interaction between plasmonic material and biomolecules. Such plasmonic–biomolecule interplay would be the basis of diagnostic strategy advancement. Furthermore, diagnostic approaches with simple procedures could be made commercially available to the public, e.g., as a lateral flow assay. Cost-effective and timely diagnosis could alleviate the pressure in diagnostic centers and facilitate the screening process in society. Particularly, in the outbreak of COVID-19, the development of high sensitivity biosensor platforms has become a significant research area [315–317]. Besides, nanomaterials could act as a biomolecule or drug carrier upon cellular uptake. Real time intracellular RNA detection would facilitate cell biology research and disease diagnosis through monitoring gene expression at the single cell level. The high photothermal conversion efficiency feature conferred its photothermal therapy application, which might be designed as a repeatable treatment. Furthermore, recent research has focused on the development of multifunctional nanocomposites, which could offer both diagnostic and therapeutic applications, such as the discussed RNA responsive nano-dimer reported by Kyriazi et al. [59]. Recently, Nam et al. [318] reported that chemo-photothermal therapy could activate antitumor immune response, which could suppress the non-treated second tumor. We believe the detailed interaction between such plasmonic particles assisted therapy and that the subsequent change in immunity would be of great research interest. We believe that the evaluation of engineered nanocomposite performance in vivo from the immunology aspect will become an essential path toward clinical translation.

In the reviewed examples of polymer–metal composite health devices under Section 3, polymer–metal composite materials are shown to play an indispensable role in optimizing the mechanical properties of implants. Titanium–PEEK composite dental implants have shown adjusted elastic modulus for better load transfer [160–162]. The metal implants were coated or composited with different functional polymers that improve the overall performance of implants, such as improved biointegration and biocompatibility [165,167,168], reduced risk of disease complications [215,230,242,252,275,278], and enhanced wound healing [291,292,294]. While the current development of polymer–metal composite dental implants focus on dental crowns, composite materials for dental screws and abutments remain largely unexplored. An uneven force distribution of the implant-abutment connection system can cause abutment screw fracture [319]. It is of importance to highlight that implant design often requires the aid of both analytical and computational support [320,321]. For example, the evaluation of the anti-wear performance of dental implants relies on a precise biotribology model (artificial saliva at the interface of the dental implant) for the dental implant, such that the dental implant can reproduce the same performance for surgical applications. Similarly, the development of cardiovascular implants requires multidisciplinary research, including material science, cardiology, computational studies on fluid mechanics, and large-scale network meta-analysis [322–326]. Recent findings on material cell interactions provide insights in developing novel cardiovascular stents. Barakat et al. [327] discovered the importance of microgroove depth in regulating the collective migration of vascular endothelial cells with intact cell–cell junctions, which can be utilized for rapid re-endothelialization and to restore endothelium functions after stent implantation. Moreover, new coating strategies can be instrumental for tailor made cardiovascular

stents. Studies have demonstrated the use of asymmetric surface coating (i.e., different coatings on the luminal and abluminal stent surface) to elicit excellent re-endothelialization as well as anti-inflammatory and anti-thrombotic effects, presumably due to the precise antiproliferative drug delivery to the bloodstream (abluminal layer) and avoidance of drug delivery to the artery (luminal layer) that inhibits re-endothelialization [328,329]. We believe such a strategy can be utilized in the existing polymer/polymeric nanoparticle coatings for developing next generation polymer–metal composite cardiovascular stents.

New polymer-based or metal-based materials can be the inspiration for developing new polymer–metal composite healthcare materials. Recently, amazing materials with intriguing features have been reported, including conformational change polymeric nanoparticles [330,331], photoactuating amphiphiles [332–334], mussel mimetic hydrogels [335,336], and chiral nanoparticles [337,338]. These new findings can contribute to the development of various polymer–metal composite healthcare materials, including personalized medications, high quality implants, and ultra-sensitive diagnostic kits.

Author Contributions: Writing—original draft preparation, W.-K.W., C.-H.L., W.-Y.C. and L.-H.T.; writing—review Sections 1, 2.1–2.3 and 4), W.-K.W.; (Sections 1, 2.4, 3 and 4), and C.-H.L.; editing, W.-K.W., C.-H.L. and W.-Y.C.; supervision, C.-C.C. and K.-C.L. All authors have read and agreed to the published version of the manuscript.

Funding: This research received no external funding.

Institutional Review Board Statement: Not applicable.

Data Availability Statement: Not applicable.

Acknowledgments: This work was partially supported the Croucher Foundation (Croucher Innovation Award-2021), and The Hong Kong Polytechnic University (W08A and P0034752). Figures 1, 8, and 11 were generated in Biorender (BioRender—biorender.com).

Conflicts of Interest: The authors declare no conflict of interest.

References

1. Gu, H.; Liu, C.; Zhu, J.; Gu, J.; Wujcik, E.K.; Shao, L.; Wang, N.; Wei, H.; Scaffaro, R.; Zhang, J.; et al. Introducing advanced composites and hybrid materials. *Adv. Compos. Hybrid Mater.* **2018**, *1*, 1–5. [CrossRef]
2. Faupel, F.; Zaporojtchenko, V.; Strunskus, T.; Elbahri, M. Metal-Polymer Nanocomposites for Functional Applications. *Adv. Eng. Mater.* **2010**, *12*, 1177–1190. [CrossRef]
3. Chouirfa, H.; Bouloussa, H.; Migonney, V.; Falentin-Daudre, C. Review of titanium surface modification techniques and coatings for antibacterial applications. *Acta Biomater.* **2019**, *83*, 37–54. [CrossRef] [PubMed]
4. Ko, E.H.; Kim, H.J.; Lee, S.M.; Kim, T.W.; Kim, H.K. Stretchable Ag electrodes with mechanically tunable optical transmittance on wavy-patterned PDMS substrates. *Sci. Rep.* **2017**, *7*, 46739. [CrossRef] [PubMed]
5. Jokerst, J.V.; Lobovkina, T.; Zare, R.N.; Gambhir, S.S. Nanoparticle PEGylation for imaging and therapy. *Nanomedicine* **2011**, *6*, 715–728. [CrossRef] [PubMed]
6. Pardo, A.; Gomez-Florit, M.; Barbosa, S.; Taboada, P.; Domingues, R.M.A.; Gomes, M.E. Magnetic Nanocomposite Hydrogels for Tissue Engineering: Design Concepts and Remote Actuation Strategies to Control Cell Fate. *ACS Nano* **2021**, *15*, 175–209. [CrossRef]
7. Ju, M.; Wu, B.; Sun, S.; Wu, P. Redox-Active Iron-Citrate Complex Regulated Robust Coating-Free Hydrogel Microfiber Net with High Environmental Tolerance and Sensitivity. *Adv. Funct. Mater.* **2020**, *30*, 1910387. [CrossRef]
8. Das, R.; Bhattacharjee, C. 16-Titanium-based nanocomposite materials for dental implant systems. In *Applications of Nanocomposite Materials in Dentistry*; Asiri, A.M., Inamuddin, M.A., Eds.; Woodhead Publishing: Sawston, UK; Cambridge, UK, 2019; pp. 271–284.
9. Qu, A.; Sun, M.; Kim, J.Y.; Xu, L.; Hao, C.; Ma, W.; Wu, X.; Liu, X.; Kuang, H.; Kotov, N.A.; et al. Stimulation of neural stem cell differentiation by circularly polarized light transduced by chiral nanoassemblies. *Nat. Biomed. Eng.* **2021**, *5*, 103–113. [CrossRef]
10. Khlebtsov, N.G.; Dykman, L.A. Optical properties and biomedical applications of plasmonic nanoparticles. *J. Quant. Spectrosc. Radiat. Transf.* **2010**, *111*, 1–35. [CrossRef]
11. Hutter, E.; Fendler, J.H. Exploitation of Localized Surface Plasmon Resonance. *Adv. Mater.* **2004**, *16*, 1685–1706. [CrossRef]
12. Piella, J.; Bastús, N.G.; Puntes, V. Size-Controlled Synthesis of Sub-10-nanometer Citrate-Stabilized Gold Nanoparticles and Related Optical Properties. *Chem. Mater.* **2016**, *28*, 1066–1075. [CrossRef]
13. Haiss, W.; Thanh, N.T.; Aveyard, J.; Fernig, D.G. Determination of size and concentration of gold nanoparticles from UV-vis spectra. *Anal. Chem.* **2007**, *79*, 4215–4221. [CrossRef] [PubMed]

14. Pölloth, B.; Röhrig, H.; Schwarzer, S. Why Is There a Red Line? A High School Experiment to Model the Role of Gold Nanoparticles in Lateral Flow Assays for COVID-19. *J. Chem. Educ.* **2022**, *99*, 2579–2587. [CrossRef]
15. Zhao, W.; Chiuman, W.; Brook, M.A.; Li, Y. Simple and rapid colorimetric biosensors based on DNA aptamer and noncrosslinking gold nanoparticle aggregation. *Chembiochem* **2007**, *8*, 727–731. [CrossRef] [PubMed]
16. Liu, J.; Lu, Y. Preparation of aptamer-linked gold nanoparticle purple aggregates for colorimetric sensing of analytes. *Nat. Protoc.* **2006**, *1*, 246–252. [CrossRef]
17. Pérez-Hernández, M.; del Pino, P.; Mitchell, S.G.; Moros, M.; Stepien, G.; Pelaz, B.; Parak, W.J.; Gálvez, E.M.; Pardo, J.; de la Fuente, J.M. Dissecting the Molecular Mechanism of Apoptosis during Photothermal Therapy Using Gold Nanoprisms. *ACS Nano* **2015**, *9*, 52–61. [CrossRef] [PubMed]
18. Barhoumi, A.; Wang, W.; Zurakowski, D.; Langer, R.S.; Kohane, D.S. Photothermally targeted thermosensitive polymer-masked nanoparticles. *Nano Lett.* **2014**, *14*, 3697–3701. [CrossRef]
19. Dubertret, B.; Calame, M.; Libchaber, A.J. Single-mismatch detection using gold-quenched fluorescent oligonucleotides. *Nat. Biotechnol.* **2001**, *19*, 365–370. [CrossRef]
20. Ramanathan, S.; Archunan, G.; Sivakumar, M.; Tamil Selvan, S.; Fred, A.L.; Kumar, S.; Gulyas, B.; Padmanabhan, P. Theranostic applications of nanoparticles in neurodegenerative disorders. *Int. J. Nanomed.* **2018**, *13*, 5561–5576. [CrossRef]
21. Mitra, S.K.; Hanson, D.A.; Schlaepfer, D.D. Focal adhesion kinase: In command and control of cell motility. *Nat. Rev. Mol. Cell Biol.* **2005**, *6*, 56–68. [CrossRef]
22. Rosso, F.; Giordano, A.; Barbarisi, M.; Barbarisi, A. From cell-ECM interactions to tissue engineering. *J. Cell Physiol.* **2004**, *199*, 174–180. [CrossRef] [PubMed]
23. Anderson, J.M.; Rodriguez, A.; Chang, D.T. Foreign body reaction to biomaterials. *Semin. Immunol.* **2008**, *20*, 86–100. [CrossRef] [PubMed]
24. Klopfleisch, R.; Jung, F. The pathology of the foreign body reaction against biomaterials. *J. Biomed. Mater. Res. A* **2017**, *105*, 927–940. [CrossRef] [PubMed]
25. Kim, M.S.; Dean, L.S. In-Stent Restenosis. *Cardiovasc. Ther.* **2011**, *29*, 190–198. [CrossRef]
26. Lowe, H.C.; Oesterle, S.N.; Khachigian, L.M. Coronary in-stent restenosis: Current status and future strategies. *J. Am. Coll. Cardiol.* **2002**, *39*, 183–193. [CrossRef]
27. Stone, G.W.; Ellis, S.G.; Cox, D.A.; Hermiller, J.; O'Shaughnessy, C.; Mann, J.T.; Turco, M.; Caputo, R.; Bergin, P.; Greenberg, J.; et al. One-year clinical results with the slow-release, polymer-based, paclitaxel-eluting TAXUS stent: The TAXUS-IV trial. *Circulation* **2004**, *109*, 1942–1947. [CrossRef]
28. Majetich, S.A.; Lim, J.; Tilton, R.D. Plasmonic magnetic nanoparticles for biomedicine. In Proceedings of the Annual International Conference of the IEEE Engineering in Medicine and Biology Society, Minneapolis, MN, USA, 3–6 September 2009; Volume 2009, pp. 4477–4478. [CrossRef]
29. Liu, J.; He, H.; Xiao, D.; Yin, S.; Ji, W.; Jiang, S.; Luo, D.; Wang, B.; Liu, Y. Recent Advances of Plasmonic Nanoparticles and their Applications. *Materials* **2018**, *11*, 1833. [CrossRef]
30. Behzadi, S.; Serpooshan, V.; Tao, W.; Hamaly, M.A.; Alkawareek, M.Y.; Dreaden, E.C.; Brown, D.; Alkilany, A.M.; Farokhzad, O.C.; Mahmoudi, M. Cellular uptake of nanoparticles: Journey inside the cell. *Chem. Soc. Rev.* **2017**, *46*, 4218–4244. [CrossRef]
31. Yameen, B.; Choi, W.I.; Vilos, C.; Swami, A.; Shi, J.; Farokhzad, O.C. Insight into nanoparticle cellular uptake and intracellular targeting. *J. Control. Release* **2014**, *190*, 485–499. [CrossRef]
32. Tabakman, S.M.; Lau, L.; Robinson, J.T.; Price, J.; Sherlock, S.P.; Wang, H.; Zhang, B.; Chen, Z.; Tangsombatvisit, S.; Jarrell, J.A.; et al. Plasmonic substrates for multiplexed protein microarrays with femtomolar sensitivity and broad dynamic range. *Nat. Commun.* **2011**, *2*, 466. [CrossRef]
33. Li, J.F.; Li, C.Y.; Aroca, R.F. Plasmon-enhanced fluorescence spectroscopy. *Chem. Soc. Rev.* **2017**, *46*, 3962–3979. [CrossRef] [PubMed]
34. Badshah, M.A.; Koh, N.Y.; Zia, A.W.; Abbas, N.; Zahra, Z.; Saleem, M.W. Recent Developments in Plasmonic Nanostructures for Metal Enhanced Fluorescence-Based Biosensing. *Nanomaterials* **2020**, *10*, 1749. [CrossRef] [PubMed]
35. Zhang, B.; Kumar, R.B.; Dai, H.; Feldman, B.J. A plasmonic chip for biomarker discovery and diagnosis of type 1 diabetes. *Nat. Med.* **2014**, *20*, 948–953. [CrossRef] [PubMed]
36. Xu, W.; Wang, L.; Zhang, R.; Sun, X.; Huang, L.; Su, H.; Wei, X.; Chen, C.C.; Lou, J.; Dai, H.; et al. Diagnosis and prognosis of myocardial infarction on a plasmonic chip. *Nat. Commun.* **2020**, *11*, 1654. [CrossRef]
37. Luan, J.; Seth, A.; Gupta, R.; Wang, Z.; Rathi, P.; Cao, S.; Gholami Derami, H.; Tang, R.; Xu, B.; Achilefu, S.; et al. Ultrabright fluorescent nanoscale labels for the femtomolar detection of analytes with standard bioassays. *Nat. Biomed. Eng.* **2020**, *4*, 518–530. [CrossRef]
38. Li, Y.; Srinivasan, B.; Jing, Y.; Yao, X.; Hugger, M.A.; Wang, J.P.; Xing, C. Nanomagnetic competition assay for low-abundance protein biomarker quantification in unprocessed human sera. *J. Am. Chem. Soc.* **2010**, *132*, 4388–4392. [CrossRef]
39. Moitra, P.; Alafeef, M.; Dighe, K.; Frieman, M.B.; Pan, D. Selective Naked-Eye Detection of SARS-CoV-2 Mediated by N Gene Targeted Antisense Oligonucleotide Capped Plasmonic Nanoparticles. *ACS Nano* **2020**, *14*, 7617–7627. [CrossRef]
40. Forootan, A.; Sjoback, R.; Bjorkman, J.; Sjogreen, B.; Linz, L.; Kubista, M. Methods to determine limit of detection and limit of quantification in quantitative real-time PCR (qPCR). *Biomol. Detect. Quantif.* **2017**, *12*, 1–6. [CrossRef]

41. Cheong, J.; Yu, H.; Lee, C.Y.; Lee, J.U.; Choi, H.J.; Lee, J.H.; Lee, H.; Cheon, J. Fast detection of SARS-CoV-2 RNA via the integration of plasmonic thermocycling and fluorescence detection in a portable device. *Nat. Biomed. Eng.* **2020**, *4*, 1159–1167. [CrossRef]
42. Bang, C.; Thum, T. Exosomes: New players in cell-cell communication. *Int. J. Biochem. Cell Biol.* **2012**, *44*, 2060–2064. [CrossRef]
43. Thongboonkerd, V. Roles for Exosome in Various Kidney Diseases and Disorders. *Front. Pharmacol.* **2019**, *10*, 1655. [CrossRef] [PubMed]
44. Zamani, P.; Fereydouni, N.; Butler, A.E.; Navashenaq, J.G.; Sahebkar, A. The therapeutic and diagnostic role of exosomes in cardiovascular diseases. *Trends Cardiovasc. Med.* **2019**, *29*, 313–323. [CrossRef] [PubMed]
45. Yin, B.; Ni, J.; Witherel, C.E.; Yang, M.; Burdick, J.A.; Wen, C.; Wong, S.H.D. Harnessing Tissue-derived Extracellular Vesicles for Osteoarthritis Theranostics. *Theranostics* **2022**, *12*, 207–231. [CrossRef]
46. Logozzi, M.; Mizzoni, D.; Di Raimo, R.; Fais, S. Exosomes: A Source for New and Old Biomarkers in Cancer. *Cancers* **2020**, *12*, 2566. [CrossRef] [PubMed]
47. Jiang, Y.; Shi, M.; Liu, Y.; Wan, S.; Cui, C.; Zhang, L.; Tan, W. Aptamer/AuNP Biosensor for Colorimetric Profiling of Exosomal Proteins. *Angew. Chem. Int. Ed. Engl.* **2017**, *56*, 11916–11920. [CrossRef] [PubMed]
48. Liang, K.; Liu, F.; Fan, J.; Sun, D.; Liu, C.; Lyon, C.J.; Bernard, D.W.; Li, Y.; Yokoi, K.; Katz, M.H.; et al. Nanoplasmonic Quantification of Tumor-derived Extracellular Vesicles in Plasma Microsamples for Diagnosis and Treatment Monitoring. *Nat. Biomed. Eng.* **2017**, *1*, 0021. [CrossRef]
49. Wu, X.; Zhao, H.; Natalia, A.; Lim, C.Z.J.; Ho, N.R.Y.; Ong, C.J.; Teo, M.C.C.; So, J.B.Y.; Shao, H. Exosome-templated nanoplasmonics for multiparametric molecular profiling. *Sci. Adv.* **2020**, *6*, eaba2556. [CrossRef]
50. Chen, C.; Hildebrandt, N. Resonance energy transfer to gold nanoparticles: NSET defeats FRET. *TrAC Trends Anal. Chem.* **2020**, *123*, 115748. [CrossRef]
51. Bhowmick, S.; Saini, S.; Shenoy, V.B.; Bagchi, B. Resonance energy transfer from a fluorescent dye to a metal nanoparticle. *J. Chem. Phys.* **2006**, *125*, 181102. [CrossRef]
52. Prigodich, A.E.; Randeria, P.S.; Briley, W.E.; Kim, N.J.; Daniel, W.L.; Giljohann, D.A.; Mirkin, C.A. Multiplexed Nanoflares: mRNA Detection in Live Cells. *Anal. Chem.* **2012**, *84*, 2062–2066. [CrossRef]
53. Seferos, D.S.; Giljohann, D.A.; Hill, H.D.; Prigodich, A.E.; Mirkin, C.A. Nano-Flares: Probes for Transfection and mRNA Detection in Living Cells. *J. Am. Chem. Soc.* **2007**, *129*, 15477–15479. [CrossRef] [PubMed]
54. Halo, T.L.; McMahon, K.M.; Angeloni, N.L.; Xu, Y.; Wang, W.; Chinen, A.B.; Malin, D.; Strekalova, E.; Cryns, V.L.; Cheng, C.; et al. NanoFlares for the detection, isolation, and culture of live tumor cells from human blood. *Proc. Natl. Acad. Sci. USA* **2014**, *111*, 17104–17109. [CrossRef] [PubMed]
55. Wiraja, C.; Mori, Y.; Ichimura, T.; Hwang, J.; Xu, C.; Bonventre, J.V. Nephrotoxicity Assessment with Human Kidney Tubuloids using Spherical Nucleic Acid-Based mRNA Nanoflares. *Nano Lett.* **2021**, *21*, 5850–5858. [CrossRef] [PubMed]
56. Zhao, J.; Liu, C.; Li, Y.; Ma, Y.; Deng, J.; Li, L.; Sun, J. Thermophoretic Detection of Exosomal microRNAs by Nanoflares. *J. Am. Chem. Soc.* **2020**, *142*, 4996–5001. [CrossRef]
57. Rosi, N.L.; Giljohann, D.A.; Thaxton, C.S.; Lytton-Jean, A.K.; Han, M.S.; Mirkin, C.A. Oligonucleotide-modified gold nanoparticles for intracellular gene regulation. *Science* **2006**, *312*, 1027–1030. [CrossRef]
58. Zhang, R.; Wang, Z.; Yang, Z.; Wang, L.; Wang, Z.; Chen, B.; Wang, Z.; Tian, J. RNA-silencing nanoprobes for effective activation and dynamic imaging of neural stem cell differentiation. *Theranostics* **2019**, *9*, 5386–5395. [CrossRef]
59. Kyriazi, M.E.; Giust, D.; El-Sagheer, A.H.; Lackie, P.M.; Muskens, O.L.; Brown, T.; Kanaras, A.G. Multiplexed mRNA Sensing and Combinatorial-Targeted Drug Delivery Using DNA-Gold Nanoparticle Dimers. *ACS Nano* **2018**, *12*, 3333–3340. [CrossRef]
60. Jayagopal, A.; Halfpenny, K.C.; Perez, J.W.; Wright, D.W. Hairpin DNA-functionalized gold colloids for the imaging of mRNA in live cells. *J. Am. Chem. Soc.* **2010**, *132*, 9789–9796. [CrossRef]
61. Lin, L.-S.; Cong, Z.-X.; Cao, J.-B.; Ke, K.-M.; Peng, Q.-L.; Gao, J.; Yang, H.-H.; Liu, G.; Chen, X. Multifunctional Fe_3O_4@Polydopamine Core–Shell Nanocomposites for Intracellular mRNA Detection and Imaging-Guided Photothermal Therapy. *ACS Nano* **2014**, *8*, 3876–3883. [CrossRef]
62. Choi, C.K.; Li, J.; Wei, K.; Xu, Y.J.; Ho, L.W.; Zhu, M.; To, K.K.; Choi, C.H.; Bian, L. A gold@polydopamine core-shell nanoprobe for long-term intracellular detection of microRNAs in differentiating stem cells. *J. Am. Chem. Soc.* **2015**, *137*, 7337–7346. [CrossRef]
63. Wong, W.K.; Wong, S.H.D.; Bian, L. Long-Term Detection of Oncogenic MicroRNA in Living Human Cancer Cells by Gold@ Polydopamine-Shell Nanoprobe. *ACS Biomater. Sci. Eng.* **2020**, *6*, 3778–3783. [CrossRef] [PubMed]
64. Pattani, V.P.; Shah, J.; Atalis, A.; Sharma, A.; Tunnell, J.W. Role of apoptosis and necrosis in cell death induced by nanoparticle-mediated photothermal therapy. *J. Nanoparticle Res.* **2015**, *17*, 20. [CrossRef]
65. Melamed, J.R.; Edelstein, R.S.; Day, E.S. Elucidating the Fundamental Mechanisms of Cell Death Triggered by Photothermal Therapy. *ACS Nano* **2015**, *9*, 6–11. [CrossRef] [PubMed]
66. Huang, X.; Jain, P.K.; El-Sayed, I.H.; El-Sayed, M.A. Plasmonic photothermal therapy (PPTT) using gold nanoparticles. *Lasers Med. Sci.* **2007**, *23*, 217. [CrossRef]
67. Estelrich, J.; Busquets, M.A. Iron Oxide Nanoparticles in Photothermal Therapy. *Molecules* **2018**, *23*, 1567. [CrossRef]
68. Li, Z.; Huang, P.; Zhang, X.; Lin, J.; Yang, S.; Liu, B.; Gao, F.; Xi, P.; Ren, Q.; Cui, D. RGD-conjugated dendrimer-modified gold nanorods for in vivo tumor targeting and photothermal therapy. *Mol. Pharm.* **2010**, *7*, 94–104. [CrossRef]

69. Zhang, L.; Su, H.; Cai, J.; Cheng, D.; Ma, Y.; Zhang, J.; Zhou, C.; Liu, S.; Shi, H.; Zhang, Y.; et al. A Multifunctional Platform for Tumor Angiogenesis-Targeted Chemo-Thermal Therapy Using Polydopamine-Coated Gold Nanorods. *ACS Nano* **2016**, *10*, 10404–10417. [CrossRef]
70. Huang, P.; Bao, L.; Zhang, C.; Lin, J.; Luo, T.; Yang, D.; He, M.; Li, Z.; Gao, G.; Gao, B.; et al. Folic acid-conjugated silica-modified gold nanorods for X-ray/CT imaging-guided dual-mode radiation and photo-thermal therapy. *Biomaterials* **2011**, *32*, 9796–9809. [CrossRef]
71. Wallace, D.C. Mitochondria and cancer. *Nat. Rev. Cancer* **2012**, *12*, 685–698. [CrossRef]
72. Tait, S.W.; Green, D.R. Mitochondria and cell signalling. *J. Cell Sci.* **2012**, *125*, 807–815. [CrossRef]
73. Shen, Y.; Liang, L.; Zhang, S.; Huang, D.; Deng, R.; Zhang, J.; Qu, H.; Xu, S.; Liang, C.; Xu, W. Organelle-Targeting Gold Nanorods for Macromolecular Profiling of Subcellular Organelles and Enhanced Cancer Cell Killing. *ACS Appl. Mater. Interfaces* **2018**, *10*, 7910–7918. [CrossRef] [PubMed]
74. Zeng, J.; Shi, D.; Gu, Y.; Kaneko, T.; Zhang, L.; Zhang, H.; Kaneko, D.; Chen, M. Injectable and Near-Infrared-Responsive Hydrogels Encapsulating Dopamine-Stabilized Gold Nanorods with Long Photothermal Activity Controlled for Tumor Therapy. *Biomacromolecules* **2019**, *20*, 3375–3384. [CrossRef] [PubMed]
75. Wang, C.; Wang, X.; Dong, K.; Luo, J.; Zhang, Q.; Cheng, Y. Injectable and responsively degradable hydrogel for personalized photothermal therapy. *Biomaterials* **2016**, *104*, 129–137. [CrossRef] [PubMed]
76. Xing, R.; Liu, K.; Jiao, T.; Zhang, N.; Ma, K.; Zhang, R.; Zou, Q.; Ma, G.; Yan, X. An Injectable Self-Assembling Collagen-Gold Hybrid Hydrogel for Combinatorial Antitumor Photothermal/Photodynamic Therapy. *Adv Mater* **2016**, *28*, 3669–3676. [CrossRef]
77. Liao, J.; Shi, K.; Jia, Y.; Wu, Y.; Qian, Z. Gold nanorods and nanohydroxyapatite hybrid hydrogel for preventing bone tumor recurrence via postoperative photothermal therapy and bone regeneration promotion. *Bioact. Mater.* **2021**, *6*, 2221–2230. [CrossRef]
78. Wang, J.; Zhu, G.; You, M.; Song, E.; Shukoor, M.I.; Zhang, K.; Altman, M.B.; Chen, Y.; Zhu, Z.; Huang, C.Z.; et al. Assembly of aptamer switch probes and photosensitizer on gold nanorods for targeted photothermal and photodynamic cancer therapy. *ACS Nano* **2012**, *6*, 5070–5077. [CrossRef]
79. Zong, S.; Wang, L.; Yang, Z.; Wang, H.; Wang, Z.; Cui, Y. Black Phosphorus-Based Drug Nanocarrier for Targeted and Synergetic Chemophotothermal Therapy of Acute Lymphoblastic Leukemia. *ACS Appl. Mater. Interfaces* **2019**, *11*, 5896–5902. [CrossRef]
80. Taghdisi, S.M.; Abnous, K.; Mosaffa, F.; Behravan, J. Targeted delivery of daunorubicin to T-cell acute lymphoblastic leukemia by aptamer. *J. Drug Target* **2010**, *18*, 277–281. [CrossRef]
81. Hou, Y.; Dan, X.; Babbar, M.; Wei, Y.; Hasselbalch, S.G.; Croteau, D.L.; Bohr, V.A. Ageing as a risk factor for neurodegenerative disease. *Nat. Rev. Neurol.* **2019**, *15*, 565–581. [CrossRef]
82. Huang, C.; Irwin, M.G.; Wong, G.T.C.; Chang, R.C.C. Evidence of the impact of systemic inflammation on neuroinflammation from a non-bacterial endotoxin animal model. *J. Neuroinflammation* **2018**, *15*, 147. [CrossRef]
83. Kline, S.A.; Mega, M.S. Stress-Induced Neurodegeneration: The Potential for Coping as Neuroprotective Therapy. *Am. J. Alzheimer's Dis. Other Dement.®* **2020**, *35*, 1533317520960873. [CrossRef] [PubMed]
84. Chin-Chan, M.; Navarro-Yepes, J.; Quintanilla-Vega, B. Environmental pollutants as risk factors for neurodegenerative disorders: Alzheimer and Parkinson diseases. *Front. Cell Neurosci.* **2015**, *9*, 124. [CrossRef] [PubMed]
85. Cheng, W.Y.; Ho, Y.S.; Chang, R.C. Linking circadian rhythms to microbiome-gut-brain axis in aging-associated neurodegenerative diseases. *Ageing Res. Rev.* **2022**, *78*, 101620. [CrossRef] [PubMed]
86. Dugger, B.N.; Dickson, D.W. Pathology of Neurodegenerative Diseases. *Cold Spring Harb. Perspect. Biol.* **2017**, *9*, a028035. [CrossRef] [PubMed]
87. Terstappen, G.C.; Meyer, A.H.; Bell, R.D.; Zhang, W. Strategies for delivering therapeutics across the blood-brain barrier. *Nat. Rev. Drug Discov.* **2021**, *20*, 362–383. [CrossRef]
88. Kamaly, N.; Yameen, B.; Wu, J.; Farokhzad, O.C. Degradable Controlled-Release Polymers and Polymeric Nanoparticles: Mechanisms of Controlling Drug Release. *Chem. Rev.* **2016**, *116*, 2602–2663. [CrossRef]
89. DeMarino, C.; Schwab, A.; Pleet, M.; Mathiesen, A.; Friedman, J.; El-Hage, N.; Kashanchi, F. Biodegradable Nanoparticles for Delivery of Therapeutics in CNS Infection. *J. Neuroimmune Pharmacol.* **2017**, *12*, 31–50. [CrossRef]
90. Fonseca-Santos, B.; Gremiao, M.P.; Chorilli, M. Nanotechnology-based drug delivery systems for the treatment of Alzheimer's disease. *Int. J. Nanomed.* **2015**, *10*, 4981–5003. [CrossRef]
91. DeTure, M.A.; Dickson, D.W. The neuropathological diagnosis of Alzheimer's disease. *Mol. Neurodegener.* **2019**, *14*, 32. [CrossRef]
92. Tosi, G.; Pederzoli, F.; Belletti, D.; Vandelli, M.A.; Forni, F.; Duskey, J.T.; Ruozi, B. Nanomedicine in Alzheimer's disease: Amyloid beta targeting strategy. *Prog. Brain Res.* **2019**, *245*, 57–88. [CrossRef]
93. Prades, R.; Guerrero, S.; Araya, E.; Molina, C.; Salas, E.; Zurita, E.; Selva, J.; Egea, G.; López-Iglesias, C.; Teixidó, M.; et al. Delivery of gold nanoparticles to the brain by conjugation with a peptide that recognizes the transferrin receptor. *Biomaterials* **2012**, *33*, 7194–7205. [CrossRef] [PubMed]
94. Kim, M.J.; Rehman, S.U.; Amin, F.U.; Kim, M.O. Enhanced neuroprotection of anthocyanin-loaded PEG-gold nanoparticles against Aβ1-42-induced neuroinflammation and neurodegeneration via the NF-KB /JNK/GSK3β signaling pathway. *Nanomed. Nanotechnol. Biol. Med.* **2017**, *13*, 2533–2544. [CrossRef] [PubMed]
95. Hertzog da Silva Leme, A.G.; Cardoso, B.R. Chapter 47-Selenium and Alzheimer's disease. In *Genetics, Neurology, Behavior, and Diet in Dementia*; Martin, C.R., Preedy, V.R., Eds.; Academic Press: Cambridge, MA, USA, 2020; pp. 739–748.

96. Zhang, J.; Zhou, X.; Yu, Q.; Yang, L.; Sun, D.; Zhou, Y.; Liu, J. Epigallocatechin-3-gallate (EGCG)-stabilized selenium nanoparticles coated with Tet-1 peptide to reduce amyloid-beta aggregation and cytotoxicity. *ACS Appl. Mater. Interfaces* **2014**, *6*, 8475–8487. [CrossRef]
97. Yang, L.; Sun, J.; Xie, W.; Liu, Y.; Liu, J. Dual-functional selenium nanoparticles bind to and inhibit amyloid beta fiber formation in Alzheimer's disease. *J. Mater. Chem. B* **2017**, *5*, 5954–5967. [CrossRef] [PubMed]
98. Huo, X.; Zhang, Y.; Jin, X.; Li, Y.; Zhang, L. A novel synthesis of selenium nanoparticles encapsulated PLGA nanospheres with curcumin molecules for the inhibition of amyloid beta aggregation in Alzheimer's disease. *J. Photochem. Photobiol. B* **2019**, *190*, 98–102. [CrossRef] [PubMed]
99. Kwon, H.J.; Cha, M.-Y.; Kim, D.; Kim, D.K.; Soh, M.; Shin, K.; Hyeon, T.; Mook-Jung, I. Mitochondria-Targeting Ceria Nanoparticles as Antioxidants for Alzheimer's Disease. *ACS Nano* **2016**, *10*, 2860–2870. [CrossRef]
100. Cline, E.N.; Bicca, M.A.; Viola, K.L.; Klein, W.L. The Amyloid-beta Oligomer Hypothesis: Beginning of the Third Decade. *J. Alzheimer's Dis.* **2018**, *64*, S567–S610. [CrossRef]
101. Mroczko, B.; Groblewska, M.; Litman-Zawadzka, A.; Kornhuber, J.; Lewczuk, P. Amyloid beta oligomers (AbetaOs) in Alzheimer's disease. *J. Neural Transm. (Vienna)* **2018**, *125*, 177–191. [CrossRef]
102. Lee, J.C.; Kim, S.J.; Hong, S.; Kim, Y. Diagnosis of Alzheimer's disease utilizing amyloid and tau as fluid biomarkers. *Exp. Mol. Med.* **2019**, *51*, 1–10. [CrossRef]
103. Bruggink, K.A.; Jongbloed, W.; Biemans, E.A.; Veerhuis, R.; Claassen, J.A.; Kuiperij, H.B.; Verbeek, M.M. Amyloid-beta oligomer detection by ELISA in cerebrospinal fluid and brain tissue. *Anal. Biochem.* **2013**, *433*, 112–120. [CrossRef]
104. Qin, J.; Cho, M.; Lee, Y. Ultrasensitive Detection of Amyloid-β Using Cellular Prion Protein on the Highly Conductive Au Nanoparticles–Poly(3,4-ethylene dioxythiophene)–Poly(thiophene-3-acetic acid) Composite Electrode. *Anal. Chem.* **2019**, *91*, 11259–11265. [CrossRef] [PubMed]
105. Lauren, J.; Gimbel, D.A.; Nygaard, H.B.; Gilbert, J.W.; Strittmatter, S.M. Cellular prion protein mediates impairment of synaptic plasticity by amyloid-beta oligomers. *Nature* **2009**, *457*, 1128–1132. [CrossRef] [PubMed]
106. Salerno, M.; Santo Domingo Porqueras, D. Alzheimer's disease: The use of contrast agents for magnetic resonance imaging to detect amyloid beta peptide inside the brain. *Coord. Chem. Rev.* **2016**, *327–328*, 27–34. [CrossRef]
107. Liu, X.-G.; Zhang, L.; Lu, S.; Liu, D.-Q.; Zhang, L.-X.; Yu, X.-L.; Liu, R.-T. Multifunctional Superparamagnetic Iron Oxide Nanoparticles Conjugated with Aβ Oligomer-Specific scFv Antibody and Class A Scavenger Receptor Activator Show Early Diagnostic Potentials for Alzheimer's Disease. *Int. J. Nanomed.* **2020**, *15*, 4919–4932. [CrossRef]
108. Wang, C.; Wang, X.; Chan, H.-N.; Liu, G.; Wang, Z.; Li, H.-W.; Wong, M.S. Amyloid-β Oligomer-Targeted Gadolinium-Based NIR/MR Dual-Modal Theranostic Nanoprobe for Alzheimer's Disease. *Adv. Funct. Mater.* **2020**, *30*, 1909529. [CrossRef]
109. Kouli, A.; Torsney, K.M.; Kuan, W.L. Parkinson's Disease: Etiology, Neuropathology, and Pathogenesis. In *Parkinson's Disease: Pathogenesis and Clinical Aspects, Stoker*; Stoker, T.B., Greenland, J.C., Eds.; Codon Publication: Brisbane, Australia, 2018.
110. Dickson, D.W. Parkinson's disease and parkinsonism: Neuropathology. *Cold Spring Harb. Perspect. Med.* **2012**, *2*, a009258. [CrossRef] [PubMed]
111. De Boer, E.M.J.; Orie, V.K.; Williams, T.; Baker, M.R.; De Oliveira, H.M.; Polvikoski, T.; Silsby, M.; Menon, P.; van den Bos, M.; Halliday, G.M.; et al. TDP-43 proteinopathies: A new wave of neurodegenerative diseases. *J. Neurol. Neurosurg. Psychiatry* **2020**, *92*, 86–95. [CrossRef]
112. Zhang, X.; Gao, F.; Wang, D.; Li, C.; Fu, Y.; He, W.; Zhang, J. Tau Pathology in Parkinson's Disease. *Front. Neurol.* **2018**, *9*, 809. [CrossRef]
113. Nemani, V.M.; Lu, W.; Berge, V.; Nakamura, K.; Onoa, B.; Lee, M.K.; Chaudhry, F.A.; Nicoll, R.A.; Edwards, R.H. Increased expression of alpha-synuclein reduces neurotransmitter release by inhibiting synaptic vesicle reclustering after endocytosis. *Neuron* **2010**, *65*, 66–79. [CrossRef]
114. Stefanis, L. alpha-Synuclein in Parkinson's disease. *Cold Spring Harb. Perspect. Med.* **2012**, *2*, a009399. [CrossRef]
115. Somayaji, M.; Cataldi, S.; Choi, S.J.; Edwards, R.H.; Mosharov, E.V.; Sulzer, D. A dual role for alpha-synuclein in facilitation and depression of dopamine release from substantia nigra neurons in vivo. *Proc. Natl. Acad. Sci. USA* **2020**, *117*, 32701–32710. [CrossRef] [PubMed]
116. Gandhi, K.R.; Saadabadi, A. Levodopa (L-Dopa). In *StatPearls*; StatPearls Publishing: Treasure Island, FL, USA, 2022.
117. Garcia-Pardo, J.; Novio, F.; Nador, F.; Cavaliere, I.; Suarez-Garcia, S.; Lope-Piedrafita, S.; Candiota, A.P.; Romero-Gimenez, J.; Rodriguez-Galvan, B.; Bove, J.; et al. Bioinspired Theranostic Coordination Polymer Nanoparticles for Intranasal Dopamine Replacement in Parkinson's Disease. *ACS Nano* **2021**, *15*, 8592–8609. [CrossRef] [PubMed]
118. Golpich, M.; Amini, E.; Mohamed, Z.; Azman Ali, R.; Mohamed Ibrahim, N.; Ahmadiani, A. Mitochondrial Dysfunction and Biogenesis in Neurodegenerative diseases: Pathogenesis and Treatment. *CNS Neurosci. Ther.* **2017**, *23*, 5–22. [CrossRef]
119. Liu, H.; Han, Y.; Wang, T.; Zhang, H.; Xu, Q.; Yuan, J.; Li, Z. Targeting Microglia for Therapy of Parkinson's Disease by Using Biomimetic Ultrasmall Nanoparticles. *J. Am. Chem. Soc.* **2020**, *142*, 21730–21742. [CrossRef] [PubMed]
120. Zhang, H.; Wang, T.; Qiu, W.; Han, Y.; Sun, Q.; Zeng, J.; Yan, F.; Zheng, H.; Li, Z.; Gao, M. Monitoring the Opening and Recovery of the Blood-Brain Barrier with Noninvasive Molecular Imaging by Biodegradable Ultrasmall Cu2- xSe Nanoparticles. *Nano Lett.* **2018**, *18*, 4985–4992. [CrossRef]

121. Peng, H.; Li, Y.; Ji, W.; Zhao, R.; Lu, Z.; Shen, J.; Wu, Y.; Wang, J.; Hao, Q.; Wang, J.; et al. Intranasal Administration of Self-Oriented Nanocarriers Based on Therapeutic Exosomes for Synergistic Treatment of Parkinson's Disease. *ACS Nano* **2022**, *16*, 869–884. [CrossRef]
122. Cryan, J.F.; O'Riordan, K.J.; Cowan, C.S.M.; Sandhu, K.V.; Bastiaanssen, T.F.S.; Boehme, M.; Codagnone, M.G.; Cussotto, S.; Fulling, C.; Golubeva, A.V.; et al. The Microbiota-Gut-Brain Axis. *Physiol. Rev.* **2019**, *99*, 1877–2013. [CrossRef]
123. Pan, H.; Sun, T.; Cui, M.; Ma, N.; Yang, C.; Liu, J.; Pang, G.; Liu, B.; Li, L.; Zhang, X.; et al. Light-Sensitive Lactococcus lactis for Microbe–Gut–Brain Axis Regulating via Upconversion Optogenetic Micro-Nano System. *ACS Nano* **2022**, *16*, 6049–6063. [CrossRef]
124. De Avila, E.D.; De Molon, R.S.; Palomari Spolidorio, D.M.; De Assis Mollo, F., Jr. Implications of Surface and Bulk Properties of Abutment Implants and Their Degradation in the Health of Periodontal Tissue. *Materials* **2013**, *6*, 5951–5966. [CrossRef]
125. Saini, M.; Singh, Y.; Arora, P.; Arora, V.; Jain, K. Implant biomaterials: A comprehensive review. *World J. Clin. Cases* **2015**, *3*, 52–57. [CrossRef]
126. O'Brien, F.J. Biomaterials & scaffolds for tissue engineering. *Mater. Today* **2011**, *14*, 88–95. [CrossRef]
127. Zechner, W.; Tangl, S.; Furst, G.; Tepper, G.; Thams, U.; Mailath, G.; Watzek, G. Osseous healing characteristics of three different implant types. *Clin. Oral Implants Res.* **2003**, *14*, 150–157. [CrossRef] [PubMed]
128. Wang, G.; Wan, Y.; Wang, T.; Liu, Z. Corrosion Behavior of Titanium Implant with different Surface Morphologies. *Procedia Manuf.* **2017**, *10*, 363–370. [CrossRef]
129. Shah, R.; Penmetsa, D.S.L.; Thomas, R.; Mehta, D.S. Titanium Corrosion: Implications for Dental Implants. *Eur. J. Prosthodont. Restor. Dent.* **2016**, *24*, 171–180. [CrossRef] [PubMed]
130. Jivraj, S.; Chee, W. Rationale for dental implants. *Br. Dent. J.* **2006**, *200*, 661–665. [CrossRef] [PubMed]
131. Gupta, R.; Gupta, N.; Weber, K.K.; Weber, K.K. Dental Implants. In *StatPearls*; StatPearls Publishing: Treasure Island, FL, USA, 2022.
132. Koc, D.; Dogan, A.; Bek, B. Bite force and influential factors on bite force measurements: A literature review. *Eur. J. Dent.* **2010**, *4*, 223–232. [CrossRef]
133. Robinson, D.; Aguilar, L.; Gatti, A.; Abduo, J.; Lee, P.V.S.; Ackland, D. Load response of the natural tooth and dental implant: A comparative biomechanics study. *J. Adv. Prosthodont.* **2019**, *11*, 169–178. [CrossRef]
134. Abe, I.; Milezewski, M.S.; Souza, M.A.; Kalinowski, H.J.; Machuca, O.F.; Marin, G.C.; Camargo, E.S. The force magnitude of a human bite measured at the molar intercuspidation using fiber Bragg gratings. *J. Microw. Optoelectron. Electromagn. Appl.* **2017**, *16*, 434–444. [CrossRef]
135. Souza, J.C.M.; Apaza-Bedoya, K.; Benfatti, C.A.M.; Silva, F.S.; Henriques, B. A Comprehensive Review on the Corrosion Pathways of Titanium Dental Implants and Their Biological Adverse Effects. *Metals* **2020**, *10*, 1272. [CrossRef]
136. Liu, X.; Chu, P.K.; Ding, C. Surface modification of titanium, titanium alloys, and related materials for biomedical applications. *Mater. Sci. Eng. R Rep.* **2004**, *47*, 49–121. [CrossRef]
137. Insua, A.; Monje, A.; Wang, H.L.; Miron, R.J. Basis of bone metabolism around dental implants during osseointegration and peri-implant bone loss. *J. Biomed. Mater. Res. Part A* **2017**, *105*, 2075–2089. [CrossRef] [PubMed]
138. Sumner, D.R.; Turner, T.M.; Igloria, R.; Urban, R.M.; Galante, J.O. Functional adaptation and ingrowth of bone vary as a function of hip implant stiffness. *J. Biomech.* **1998**, *31*, 909–917. [CrossRef]
139. Brizuela, A.; Herrero-Climent, M.; Rios-Carrasco, E.; Rios-Santos, J.V.; Pérez, R.A.; Manero, J.M.; Gil Mur, J. Influence of the Elastic Modulus on the Osseointegration of Dental Implants. *Materials* **2019**, *12*, 980. [CrossRef]
140. Knaus, J.; Schaffarczyk, D.; Cölfen, H. On the Future Design of Bio-Inspired Polyetheretherketone Dental Implants. *Macromol. Biosci.* **2020**, *20*, 1900239. [CrossRef] [PubMed]
141. Isidor, F. Loss of osseointegration caused by occlusal load of oral implants. A clinical and radiographic study in monkeys. *Clin. Oral Implant. Res.* **1996**, *7*, 143–152. [CrossRef]
142. Flanagan, D. Bite force and dental implant treatment: A short review. *Med. Devices (Auckl)* **2017**, *10*, 141–148. [CrossRef]
143. Albrektsson, T.A.-O.; Becker, W.A.-O.; Coli, P.; Jemt, T.A.-O.; Mölne, J.; Sennerby, L. Bone loss around oral and orthopedic implants: An immunologically based condition. *Clin. Implant. Dent. Relat. Res.* **2019**, *21*, 786–795. [CrossRef]
144. Albrektsson, T.A.-O.; Jemt, T.; Mölne, J.; Tengvall, P.; Wennerberg, A.A.-O. On inflammation-immunological balance theory-A critical apprehension of disease concepts around implants: Mucositis and marginal bone loss may represent normal conditions and not necessarily a state of disease. *Clin. Implant. Dent. Relat. Res.* **2019**, *21*, 183–189. [CrossRef]
145. Trindade, R.; Albrektsson, T.; Tengvall, P.; Wennerberg, A. Foreign Body Reaction to Biomaterials: On Mechanisms for Buildup and Breakdown of Osseointegration. *Clin. Implant. Dent. Relat. Res.* **2016**, *18*, 192–203. [CrossRef]
146. Trindade, R.; Albrektsson, T.; Galli, S.; Prgomet, Z.; Tengvall, P.; Wennerberg, A. Osseointegration and foreign body reaction: Titanium implants activate the immune system and suppress bone resorption during the first 4 weeks after implantation. *Clin. Implant. Dent. Relat. Res.* **2018**, *20*, 82–91. [CrossRef]
147. Hanke, M.L.; Angle, A.; Kielian, T.; Kielian, T. MyD88-dependent signaling influences fibrosis and alternative macrophage activation during Staphylococcus aureus biofilm infection. *PLoS ONE* **2012**, *7*, e42476. [CrossRef] [PubMed]
148. Trindade, R.A.-O.; Albrektsson, T.; Galli, S.A.-O.; Prgomet, Z.; Tengvall, P.; Wennerberg, A. Bone Immune Response to Materials, Part I: Titanium, PEEK and Copper in Comparison to Sham at 10 Days in Rabbit Tibia. *J. Clin. Med.* **2018**, *7*, 526. [CrossRef] [PubMed]
149. Schwarz, F.; Derks, J.; Monje, A.; Wang, H.-L. Peri-implantitis. *J. Periodontol.* **2018**, *89*, S267–S290. [CrossRef] [PubMed]

150. Parithimarkalaignan, S.; Padmanabhan, T.V. Osseointegration: An update. *J. Indian Prosthodont. Soc.* **2013**, *13*, 2–6. [CrossRef]
151. Irandoust, S.; Müftü, S. The interplay between bone healing and remodeling around dental implants. *Sci. Rep.* **2020**, *10*, 4335. [CrossRef]
152. Choi, J.-Y.; Sim, J.-H.; Yeo, I.-S.L. Characteristics of contact and distance osteogenesis around modified implant surfaces in rabbit tibiae. *J. Periodontal Implant Sci.* **2017**, *47*, 182–192. [CrossRef]
153. Toledano-Serrabona, J.; Sánchez-Garcés, M.Á.; Sánchez-Torres, A.; Sánchez-Torres, A.; Gay-Escoda, C.; Gay-Escoda, C. Alveolar distraction osteogenesis for dental implant treatments of the vertical bone atrophy: A systematic review. *Med. Oral Patol. Oral Y Cir. Bucal* **2019**, *24*, e70.
154. Marco, F.; Milena, F.; Gianluca, G.; Gianluca, G.; Vittoria, O.; Vittoria, O. Peri-implant osteogenesis in health and osteoporosis. *Micron* **2005**, *36*, 630–644. [CrossRef]
155. Villar, C.C.; Huynh-Ba, G.; Mills, M.P.; Cochran, D.L. Wound healing around dental implants. *Endod. Top.* **2011**, *25*, 44–62. [CrossRef]
156. Rokaya, D.; Srimaneepong, V.; Sapkota, J.; Qin, J.; Siraleartmukul, K.; Siriwongrungson, V. Polymeric materials and films in dentistry: An overview. *J. Adv. Res.* **2018**, *14*, 25–34. [CrossRef]
157. Al-Rabab'ah, M.; Hamadneh, W.; Alsalem, I.; Khraisat, A.; Abu Karaky, A. Use of High Performance Polymers as Dental Implant Abutments and Frameworks: A Case Series Report. *J. Prosthodont.* **2019**, *28*, 365–372. [CrossRef] [PubMed]
158. Schwitalla, A.D.; Abou-Emara, M.; Zimmermann, T.; Spintig, T.; Beuer, F.; Lackmann, J.; Müller, W.D. The applicability of PEEK-based abutment screws. *J. Mech. Behav. Biomed. Mater.* **2016**, *63*, 244–251. [CrossRef] [PubMed]
159. Sandler, J.; Werner, P.; Shaffer, M.S.P.; Demchuk, V.; Altstädt, V.; Windle, A.H. Carbon-nanofibre-reinforced poly(ether ether ketone) composites. *Compos. Part A Appl. Sci. Manuf.* **2002**, *33*, 1033–1039. [CrossRef]
160. Bathala, L.; Majeti, V.; Rachuri, N.; Singh, N.; Gedela, S. The Role of Polyether Ether Ketone (Peek) in Dentistry—A Review. *J. Med. Life* **2019**, *12*, 5–9. [CrossRef]
161. Kurtz, S.M.; Devine, J.N. PEEK biomaterials in trauma, orthopedic, and spinal implants. *Biomaterials* **2007**, *28*, 4845–4869. [CrossRef] [PubMed]
162. Stawarczyk, B.; Schmid, P.; Roos, M.; Eichberger, M.; Schmidlin, P.R. Spectrophotometric Evaluation of Polyetheretherketone (PEEK) as a Core Material and a Comparison with Gold Standard Core Materials. *Materials* **2016**, *9*, 491. [CrossRef] [PubMed]
163. Lee, W.T.; Koak, J.-Y.; Lim, Y.-J.; Kim, S.-K.; Kwon, H.-B.; Kim, M.-J. Stress shielding and fatigue limits of poly-ether-ether-ketone dental implants. *J. Biomed. Mater. Res. Part B Appl. Biomater.* **2012**, *100*, 1044–1052. [CrossRef]
164. Najeeb, S.; Bds, Z.K.; Bds, S.Z.; Bds, M.S. Bioactivity and Osseointegration of PEEK Are Inferior to Those of Titanium: A Systematic Review. *J. Oral Implantol.* **2016**, *42*, 512–516. [CrossRef]
165. Walsh, W.R.; Bertollo, N.; Christou, C.; Schaffner, D.; Mobbs, R.J. Plasma-sprayed titanium coating to polyetheretherketone improves the bone-implant interface. *Spine J.* **2015**, *15*, 1041–1049. [CrossRef]
166. Han, C.M.; Lee, E.J.; Kim, H.-E.; Koh, Y.-H.; Kim, K.N.; Ha, Y.; Kuh, S.-U. The electron beam deposition of titanium on polyetheretherketone (PEEK) and the resulting enhanced biological properties. *Biomaterials* **2010**, *31*, 3465–3470. [CrossRef]
167. Wu, X.; Liu, X.; Wei, J.; Ma, J.; Deng, F.; Wei, S. Nano-TiO2/PEEK bioactive composite as a bone substitute material: In vitro and in vivo studies. *Int. J. Nanomed.* **2012**, *7*, 1215.
168. Han, C.M.; Jang, T.S.; Kim, H.-E.; Koh, Y.-H. Creation of nanoporous TiO_2 surface onto polyetheretherketone for effective immobilization and delivery of bone morphogenetic protein. *J. Biomed. Mater. Res. Part A* **2014**, *102*, 793–800. [CrossRef] [PubMed]
169. Lu, T.; Liu, X.; Qian, S.; Cao, H.; Qiao, Y.; Mei, Y.; Chu, P.K.; Ding, C. Multilevel surface engineering of nanostructured TiO2 on carbon-fiber-reinforced polyetheretherketone. *Biomaterials* **2014**, *35*, 5731–5740. [CrossRef] [PubMed]
170. Sun, Y.; Liu, X.; Tan, J.; Lv, D.; Song, W.; Su, R.; Li, L.; Liu, X.; Ouyang, L.; Liao, Y. Strontium ranelate incorporated 3D porous sulfonated PEEK simulating MC3T3-E1 cell differentiation. *Regen. Biomater.* **2021**, *8*, rbaa043. [CrossRef] [PubMed]
171. Bianchi, M.; Degli Esposti, L.; Ballardini, A.; Liscio, F.; Berni, M.; Gambardella, A.; Leeuwenburgh, S.C.G.; Sprio, S.; Tampieri, A.; Iafisco, M. Strontium doped calcium phosphate coatings on poly(etheretherketone) (PEEK) by pulsed electron deposition. *Surf. Coat. Technol.* **2017**, *319*, 191–199. [CrossRef]
172. Najeeb, S.; Khurshid, Z.; Matinlinna, J.P.; Siddiqui, F.; Nassani, M.Z.; Baroudi, K. Nanomodified Peek Dental Implants: Bioactive Composites and Surface Modification—A Review. *Int. J. Dent.* **2015**, *2015*, 381759. [CrossRef]
173. Gu, X.; Sun, X.; Sun, Y.; Wang, J.; Liu, Y.; Yu, K.; Wang, Y.; Zhou, Y. Bioinspired Modifications of PEEK Implants for Bone Tissue Engineering. *Front. Bioeng. Biotechnol.* **2021**, *8*, 631616. [CrossRef]
174. Cook, S.D.; Rust-Dawicki, A.M. Preliminary evaluation of titanium-coated PEEK dental implants. *J. Oral Implantol.* **1995**, *21*, 176–181.
175. Delgado-Ruiz, R.; Romanos, G. Potential Causes of Titanium Particle and Ion Release in Implant Dentistry: A Systematic Review. *Int. J. Mol. Sci.* **2018**, *19*, 3585. [CrossRef]
176. Coelho, P.G.; Jimbo, R.; Tovar, N.; Bonfante, E.A. Osseointegration: Hierarchical designing encompassing the macrometer, micrometer, and nanometer length scales. *Dent. Mater.* **2015**, *31*, 37–52. [CrossRef]
177. Li, J.; Jansen, J.A.; Walboomers, X.F.; van den Beucken, J.J.J.P. Mechanical aspects of dental implants and osseointegration: A narrative review. *J. Mech. Behav. Biomed. Mater.* **2020**, *103*, 103574. [CrossRef] [PubMed]

178. Johansson, P.; Jimbo, R.; Kjellin, P.; Currie, F.; Chrcanovic, B.R.; Wennerberg, A. Biomechanical evaluation and surface characterization of a nano-modified surface on PEEK implants: A study in the rabbit tibia. *Int. J. Nanomed.* **2014**, *9*, 3903. [CrossRef] [PubMed]
179. Elawadly, T.; Radi, I.A.W.; El Khadem, A.; Osman, R.B. Can PEEK Be an Implant Material? Evaluation of Surface Topography and Wettability of Filled Versus Unfilled PEEK with Different Surface Roughness. *J. Oral Implantol.* **2017**, *43*, 456–461. [CrossRef] [PubMed]
180. Kubo, K.; Tsukimura, N.; Iwasa, F.; Ueno, T.; Saruwatari, L.; Aita, H.; Chiou, W.-A.; Ogawa, T. Cellular behavior on TiO_2 nanonodular structures in a micro-to-nanoscale hierarchy model. *Biomaterials* **2009**, *30*, 5319–5329. [CrossRef]
181. Brammer, K.S.; Oh, S.; Cobb, C.J.; Bjursten, L.M.; van der Heyde, H.; Jin, S. Improved bone-forming functionality on diameter-controlled TiO_2 nanotube surface. *Acta Biomater.* **2009**, *5*, 3215–3223. [CrossRef]
182. De Pablo, P.; Chapple, I.L.; Buckley, C.D.; Dietrich, T. Periodontitis in systemic rheumatic diseases. *Nat. Rev. Rheumatol.* **2009**, *5*, 218–224. [CrossRef]
183. Nair, S.; Faizuddin, M.; Dharmapalan, J. Role of autoimmune responses in periodontal disease. *Autoimmune Dis.* **2014**, *2014*, 596824. [CrossRef]
184. Moutsopoulos, N.M.; Konkel, J.E. Tissue-Specific Immunity at the Oral Mucosal Barrier. *Trends Immunol.* **2018**, *39*, 276–287. [CrossRef]
185. Hajishengallis, G.; Darveau, R.P.; Curtis, M.A. The keystone-pathogen hypothesis. *Nat. Rev. Microbiol.* **2012**, *10*, 717–725. [CrossRef]
186. Pan, W.; Wang, Q.; Chen, Q. The cytokine network involved in the host immune response to periodontitis. *Int. J. Oral Sci.* **2019**, *11*, 30. [CrossRef]
187. Tsukasaki, M.; Komatsu, N.; Nagashima, K.; Nitta, T.; Pluemsakunthai, W.; Shukunami, C.; Iwakura, Y.; Nakashima, T.; Okamoto, K.; Takayanagi, H. Host defense against oral microbiota by bone-damaging T cells. *Nat. Commun.* **2018**, *9*, 701. [CrossRef] [PubMed]
188. Prathapachandran, J.; Suresh, N. Management of peri-implantitis. *Dent. Res. J.* **2012**, *9*, 516–521. [CrossRef] [PubMed]
189. Ter Boo, G.J.; Grijpma, D.W.; Moriarty, T.F.; Richards, R.G.; Eglin, D. Antimicrobial delivery systems for local infection prophylaxis in orthopedic- and trauma surgery. *Biomaterials* **2015**, *52*, 113–125. [CrossRef] [PubMed]
190. Souza, J.G.S.; Bertolini, M.M.; Costa, R.C.; Nagay, B.E.; Dongari-Bagtzoglou, A.; Barão, V.A.R. Targeting implant-associated infections: Titanium surface loaded with antimicrobial. *IScience* **2021**, *24*, 102008. [CrossRef] [PubMed]
191. Lucke, M.; Schmidmaier, G.; Sadoni, S.; Wildemann, B.; Schiller, R.; Haas, N.P.; Raschke, M. Gentamicin coating of metallic implants reduces implant-related osteomyelitis in rats. *Bone* **2003**, *32*, 521–531. [CrossRef]
192. Lucke, M.; Wildemann, B.; Sadoni, S.; Surke, C.; Schiller, R.; Stemberger, A.; Raschke, M.; Haas, N.P.; Schmidmaier, G. Systemic versus local application of gentamicin in prophylaxis of implant-related osteomyelitis in a rat model. *Bone* **2005**, *36*, 770–778. [CrossRef]
193. Kälicke, T.; Schierholz, J.; Schlegel, U.; Frangen, T.M.; Köller, M.; Printzen, G.; Seybold, D.; Klöckner, S.; Muhr, G.; Arens, S. Effect on infection resistance of a local antiseptic and antibiotic coating on osteosynthesis implants: An in vitro and in vivo study. *J. Orthop. Res.* **2006**, *24*, 1622–1640. [CrossRef]
194. Zhang, B.; Braun, B.M.; Skelly, J.D.; Ayers, D.C.; Song, J. Significant Suppression of Staphylococcus aureus Colonization on Intramedullary Ti6Al4V Implants Surface-Grafted with Vancomycin-Bearing Polymer Brushes. *ACS Appl. Mater. Interfaces* **2019**, *11*, 28641–28647. [CrossRef]
195. Ghimire, A.; Skelly, J.D.; Song, J. Micrococcal-Nuclease-Triggered On-Demand Release of Vancomycin from Intramedullary Implant Coating Eradicates Staphylococcus aureus Infection in Mouse Femoral Canals. *ACS Cent. Sci.* **2019**, *5*, 1929–1936. [CrossRef]
196. Croes, M.; Bakhshandeh, S.; van Hengel, I.A.J.; Lietaert, K.; van Kessel, K.P.M.; Pouran, B.; van der Wal, B.C.H.; Vogely, H.C.; Van Hecke, W.; Fluit, A.C.; et al. Antibacterial and immunogenic behavior of silver coatings on additively manufactured porous titanium. *Acta Biomater.* **2018**, *81*, 315–327. [CrossRef]
197. Grohmann, S.; Menne, M.; Hesse, D.; Bischoff, S.; Schiffner, R.; Diefenbeck, M.; Liefeith, K. Biomimetic multilayer coatings deliver gentamicin and reduce implant-related osteomyelitis in rats. *Biomed. Eng. /Biomed. Tech.* **2019**, *64*, 383–395. [CrossRef] [PubMed]
198. Ma, K.; Cai, X.; Zhou, Y.; Wang, Y.; Jiang, T. In Vitro and In Vivo Evaluation of Tetracycline Loaded Chitosan-Gelatin Nanosphere Coatings for Titanium Surface Functionalization. *Macromol. Biosci.* **2017**, *17*, 1600130. [CrossRef] [PubMed]
199. Yang, L.; Li, L.; Li, H.; Wang, T.; Ren, X.; Cheng, Y.; Li, Y.; Huang, Q. Layer-by-Layer Assembled Smart Antibacterial Coatings via Mussel-Inspired Polymerization and Dynamic Covalent Chemistry. *Adv. Healthc. Mater.* **2022**, *11*, 2200112. [CrossRef] [PubMed]
200. Garg, U.; Chauhan, S.; Nagaich, U.; Jain, N. Current Advances in Chitosan Nanoparticles Based Drug Delivery and Targeting. *Adv. Pharm. Bull.* **2019**, *9*, 195–204. [CrossRef] [PubMed]
201. Stavrakis, A.I.; Zhu, S.; Hegde, V.; Loftin, A.H.; Ashbaugh, A.G.; Niska, J.A.; Miller, L.S.; Segura, T.; Bernthal, N.M. In Vivo Efficacy of a "Smart" Antimicrobial Implant Coating. *J. Bone Joint Surg. Am.* **2016**, *98*, 1183–1189. [CrossRef]
202. Stavrakis, A.I.; Zhu, S.; Loftin, A.H.; Weixian, X.; Niska, J.; Hegde, V.; Segura, T.; Bernthal, N.M. Controlled Release of Vancomycin and Tigecycline from an Orthopaedic Implant Coating Prevents Staphylococcus aureus Infection in an Open Fracture Animal Model. *Biomed. Res. Int.* **2019**, *2019*, 1638508. [CrossRef]

203. Lorenzetti, M.; Dogša, I.; Stošicki, T.; Stopar, D.; Kalin, M.; Kobe, S.; Novak, S. The Influence of Surface Modification on Bacterial Adhesion to Titanium-Based Substrates. *ACS Appl. Mater. Interfaces* **2015**, *7*, 1644–1651. [CrossRef]
204. Cao, Y.; Su, B.; Chinnaraj, S.; Jana, S.; Bowen, L.; Charlton, S.; Duan, P.; Jakubovics, N.S.; Chen, J. Nanostructured titanium surfaces exhibit recalcitrance towards Staphylococcus epidermidis biofilm formation. *Sci. Rep.* **2018**, *8*, 1071. [CrossRef]
205. Hizal, F.; Zhuk, I.; Sukhishvili, S.; Busscher, H.J.; van der Mei, H.C.; Choi, C.H. Impact of 3D Hierarchical Nanostructures on the Antibacterial Efficacy of a Bacteria-Triggered Self-Defensive Antibiotic Coating. *ACS Appl. Mater. Interfaces* **2015**, *7*, 20304–20313. [CrossRef]
206. Kong, M.; Chen, X.G.; Xing, K.; Park, H.J. Antimicrobial properties of chitosan and mode of action: A state of the art review. *Int. J. Food Microbiol.* **2010**, *144*, 51–63. [CrossRef]
207. Yuan, Y.; Chesnutt, B.M.; Haggard, W.O.; Bumgardner, J.D. Deacetylation of Chitosan: Material Characterization and in vitro Evaluation via Albumin Adsorption and Pre-Osteoblastic Cell Cultures. *Materials* **2011**, *4*, 1399–1416. [CrossRef] [PubMed]
208. Li, B.; Xia, X.; Guo, M.; Jiang, Y.; Li, Y.; Zhang, Z.; Liu, S.; Li, H.; Liang, C.; Wang, H. Biological and antibacterial properties of the micro-nanostructured hydroxyapatite/chitosan coating on titanium. *Sci. Rep.* **2019**, *9*, 14052. [CrossRef] [PubMed]
209. Park, S.; Kim, H.; Choi, K.S.; Ji, M.-K.; Kim, S.; Gwon, Y.; Park, C.; Kim, J.; Lim, H.-P. Graphene–Chitosan Hybrid Dental Implants with Enhanced Antibacterial and Cell-Proliferation Properties. *Appl. Sci.* **2020**, *10*, 4888. [CrossRef]
210. Hancock, R.E.; Sahl, H.G. Antimicrobial and host-defense peptides as new anti-infective therapeutic strategies. *Nat. Biotechnol.* **2006**, *24*, 1551–1557. [CrossRef] [PubMed]
211. Wisdom, C.; Chen, C.; Yuca, E.; Zhou, Y.; Tamerler, C.; Snead, M.L. Repeatedly Applied Peptide Film Kills Bacteria on Dental Implants. *JOM (1989)* **2019**, *71*, 1271–1280. [CrossRef]
212. Yazici, H.; O'Neill, M.B.; Kacar, T.; Wilson, B.R.; Oren, E.E.; Sarikaya, M.; Tamerler, C. Engineered Chimeric Peptides as Antimicrobial Surface Coating Agents toward Infection-Free Implants. *ACS Appl. Mater. Interfaces* **2016**, *8*, 5070–5081. [CrossRef]
213. Zhang, S.; Zhou, X.; Liu, T.; Huang, Y.; Li, J. The effects of Peptide Mel4-coated titanium plates on infection rabbits after internal fixation of open fractures. *Arch. Orthop. Trauma Surg.* **2022**, *142*, 729–734. [CrossRef]
214. Acosta, S.; Ibañez-Fonseca, A.; Aparicio, C.; Rodríguez-Cabello, J.C. Antibiofilm coatings based on protein-engineered polymers and antimicrobial peptides for preventing implant-associated infections. *Biomater. Sci.* **2020**, *8*, 2866–2877. [CrossRef]
215. Wu, S.; Xu, J.; Zou, L.; Luo, S.; Yao, R.; Zheng, B.; Liang, G.; Wu, D.; Li, Y. Long-lasting renewable antibacterial porous polymeric coatings enable titanium biomaterials to prevent and treat peri-implant infection. *Nat. Commun.* **2021**, *12*, 3303. [CrossRef]
216. Brånemark, P.I. Osseointegration and its experimental background. *J. Prosthet. Dent.* **1983**, *50*, 399–410. [CrossRef]
217. Barrak, F.N.; Li, S.; Muntane, A.M.; Jones, J.R. Particle release from implantoplasty of dental implants and impact on cells. *Int. J. Implant Dent.* **2020**, *6*, 50. [CrossRef] [PubMed]
218. Zhang, X.; Zhang, Y.; Jin, Z. A review of the bio-tribology of medical devices. *Friction* **2022**, *10*, 4–30. [CrossRef]
219. Messous, R.; Henriques, B.; Bousbaa, H.; Silva, F.S.; Teughels, W.; Souza, J.C.M. Cytotoxic effects of submicron- and nano-scale titanium debris released from dental implants: An integrative review. *Clin. Oral Investig.* **2021**, *25*, 1627–1640. [CrossRef] [PubMed]
220. Zhang, L.; Haddouti, E.M.; Welle, K.; Burger, C.; Wirtz, D.C.; Schildberg, F.A.; Kabir, K. The Effects of Biomaterial Implant Wear Debris on Osteoblasts. *Front. Cell Dev. Biol.* **2020**, *8*, 352. [CrossRef]
221. Sananez, A.; Lefebvre, C.; Looney, S.; Baker, P.; Mettenburg, D.; Rueggeberg, F.A. In vitro mechanical analysis of complete-arch mandibular implant-supported fixed prostheses abutment screws after cyclic loading. *J. Prosthet. Dent.* **2015**, *113*, 432–439. [CrossRef]
222. Łępicka, M.; Barros-Silva, S.; Licciardello, N.; Cortez, A.; Gobbo, P.; Sampaio, M.; Cortez, J.; Cortez, H.; Alves, F.; Lipowicz, P.; et al. Silane-based coating charged with TiO2 NPs for dental implant applications. *Surf. Coat. Technol.* **2021**, *413*, 127066. [CrossRef]
223. Kruk, A.; Zimowski, S.; Łukaszczyk, A.; Cieniek, Ł.; Moskalewicz, T. The influence of heat treatment on the microstructure, surface topography and selected properties of PEEK coatings electrophoretically deposited on the Ti-6Al-4V alloy. *Prog. Org. Coat.* **2019**, *133*, 180–190. [CrossRef]
224. Yadav, S.; Gangwar, S. A critical evaluation of tribological interaction for restorative materials in dentistry. *Int. J. Polym. Mater. Polym. Biomater.* **2019**, *68*, 1005–1019. [CrossRef]
225. Kan, W.H.; Chang, L. The mechanisms behind the tribological behaviour of polymer matrix composites reinforced with TiO2 nanoparticles. *Wear* **2021**, *474–475*, 203754. [CrossRef]
226. Thygesen, K.; Alpert, J.S.; Jaffe, A.S.; Chaitman, B.R.; Bax, J.J.; Morrow, D.A.; White, H.D.; Null, N. Fourth Universal Definition of Myocardial Infarction (2018). *Circulation* **2018**, *138*, e618–e651. [CrossRef]
227. Libby, P.; Buring, J.E.; Badimon, L.; Hansson, G.K.; Deanfield, J.; Bittencourt, M.S.; Tokgözoğlu, L.; Lewis, E.F. Atherosclerosis. *Nat. Rev. Dis. Primers* **2019**, *5*, 56. [CrossRef] [PubMed]
228. Gruntzig, A. Transluminal dilatation of coronary-artery stenosis. *Lancet* **1978**, *311*, 263. [CrossRef]
229. Sigwart, U.; Puel, J.; Mirkovitch, V.; Joffre, F.; Kappenberger, L. Intravascular stents to prevent occlusion and restenosis after transluminal angioplasty. *N. Engl. J. Med.* **1987**, *316*, 701–706. [CrossRef] [PubMed]
230. Torrado, J.; Buckley, L.; Durán, A.; Trujillo, P.; Toldo, S.; Valle Raleigh, J.; Abbate, A.; Biondi-Zoccai, G.; Guzmán, L.A. Restenosis, Stent Thrombosis, and Bleeding Complications: Navigating Between Scylla and Charybdis. *J. Am. Coll. Cardiol.* **2018**, *71*, 1676–1695. [CrossRef] [PubMed]

231. Tanner, F.C.; Yang, Z.Y.; Duckers, E.; Gordon, D.; Nabel, G.J.; Nabel, E.G. Expression of cyclin-dependent kinase inhibitors in vascular disease. *Circ. Res.* **1998**, *82*, 396–403. [CrossRef] [PubMed]
232. Acharya, G.; Park, K. Mechanisms of controlled drug release from drug-eluting stents. *Adv. Drug Deliv. Rev.* **2006**, *58*, 387–401. [CrossRef]
233. Dimitrova, G.; Tulman, D.B.; Bergese, S.D. Perioperative management of antiplatelet therapy in patients with drug-eluting stents. *HSR Proc. Intensive Care Cardiovasc. Anesth.* **2012**, *4*, 153–167.
234. Farooq, V.; Gogas, B.D.; Serruys, P.W. Restenosis. *Circ. Cardiovasc. Interv.* **2011**, *4*, 195–205. [CrossRef]
235. Kohn, J.; Zeltinger, J. Degradable, drug-eluting stents: A new frontier for the treatment of coronary artery disease. *Expert Rev. Med. Devices* **2005**, *2*, 667–671. [CrossRef]
236. Onuma, Y.; Serruys, P.W. Bioresorbable scaffold: The advent of a new era in percutaneous coronary and peripheral revascularization? *Circulation* **2011**, *123*, 779–797. [CrossRef]
237. Yamaji, K.; Ueki, Y.; Souteyrand, G.; Daemen, J.; Wiebe, J.; Nef, H.; Adriaenssens, T.; Loh, J.P.; Lattuca, B.; Wykrzykowska, J.J.; et al. Mechanisms of Very Late Bioresorbable Scaffold Thrombosis: The INVEST Registry. *J. Am. Coll. Cardiol.* **2017**, *70*, 2330–2344. [CrossRef]
238. Onuma, Y.; Serruys, P.W.; Muramatsu, T.; Nakatani, S.; van Geuns, R.J.; de Bruyne, B.; Dudek, D.; Christiansen, E.; Smits, P.C.; Chevalier, B.; et al. Incidence and imaging outcomes of acute scaffold disruption and late structural discontinuity after implantation of the absorb Everolimus-Eluting fully bioresorbable vascular scaffold: Optical coherence tomography assessment in the ABSORB cohort B Trial (A Clinical Evaluation of the Bioabsorbable Everolimus Eluting Coronary Stent System in the Treatment of Patients with De Novo Native Coronary Artery Lesions). *JACC Cardiovasc. Interv.* **2014**, *7*, 1400–1411. [CrossRef] [PubMed]
239. Montone, R.A.; Niccoli, G.; De Marco, F.; Minelli, S.; D'Ascenzo, F.; Testa, L.; Bedogni, F.; Crea, F. Temporal Trends in Adverse Events After Everolimus-Eluting Bioresorbable Vascular Scaffold Versus Everolimus-Eluting Metallic Stent Implantation: A Meta-Analysis of Randomized Controlled Trials. *Circulation* **2017**, *135*, 2145–2154. [CrossRef] [PubMed]
240. Ang, H.Y.; Huang, Y.Y.; Lim, S.T.; Wong, P.; Joner, M.; Foin, N. Mechanical behavior of polymer-based vs. metallic-based bioresorbable stents. *J. Thorac. Dis.* **2017**, *9*, S923–S934. [CrossRef] [PubMed]
241. Gori, T.; Weissner, M.; Gönner, S.; Wendling, F.; Ullrich, H.; Ellis, S.; Anadol, R.; Polimeni, A.; Münzel, T. Characteristics, Predictors, and Mechanisms of Thrombosis in Coronary Bioresorbable Scaffolds: Differences Between Early and Late Events. *JACC Cardiovasc. Interv.* **2017**, *10*, 2363–2371. [CrossRef] [PubMed]
242. Stefanini, G.G.; Holmes, D.R. Drug-Eluting Coronary-Artery Stents. *N. Engl. J. Med.* **2013**, *368*, 254–265. [CrossRef]
243. Rizas, K.D.; Mehilli, J. Stent Polymers: Do They Make a Difference? *Circ. Cardiovasc. Interv.* **2016**, *9*, e002943. [CrossRef]
244. Joner, M.; Finn, A.V.; Farb, A.; Mont, E.K.; Kolodgie, F.D.; Ladich, E.; Kutys, R.; Skorija, K.; Gold, H.K.; Virmani, R. Pathology of drug-eluting stents in humans: Delayed healing and late thrombotic risk. *J. Am. Coll. Cardiol.* **2006**, *48*, 193–202. [CrossRef]
245. Camenzind, E.; Steg, P.G.; Wijns, W. Stent thrombosis late after implantation of first-generation drug-eluting stents: A cause for concern. *Circulation* **2007**, *115*, 1440–1455, discussion 1455. [CrossRef]
246. Varenhorst, C.; Lindholm, M.; Sarno, G.; Olivecrona, G.; Jensen, U.; Nilsson, J.; Carlsson, J.; James, S.; Lagerqvist, B. Stent thrombosis rates the first year and beyond with new- and old-generation drug-eluting stents compared to bare metal stents. *Clin. Res. Cardiol.* **2018**, *107*, 816–823. [CrossRef]
247. Byrne, R.A.; Joner, M.; Kastrati, A. Polymer coatings and delayed arterial healing following drug-eluting stent implantation. *Minerva Cardioangiol.* **2009**, *57*, 567–584. [PubMed]
248. Yonetsu, T.; Kato, K.; Kim, S.-J.; Xing, L.; Jia, H.; McNulty, I.; Lee, H.; Zhang, S.; Uemura, S.; Jang, Y.; et al. Predictors for Neoatherosclerosis. *Circ. Cardiovasc. Imaging* **2012**, *5*, 660–666. [CrossRef] [PubMed]
249. Virmani, R.; Guagliumi, G.; Farb, A.; Musumeci, G.; Grieco, N.; Motta, T.; Mihalcsik, L.; Tespili, M.; Valsecchi, O.; Kolodgie, F.D. Localized hypersensitivity and late coronary thrombosis secondary to a sirolimus-eluting stent: Should we be cautious? *Circulation* **2004**, *109*, 701–705. [CrossRef] [PubMed]
250. Valgimigli, M.; Frigoli, E.; Heg, D.; Tijssen, J.; Jüni, P.; Vranckx, P.; Ozaki, Y.; Morice, M.-C.; Chevalier, B.; Onuma, Y.; et al. Dual Antiplatelet Therapy after PCI in Patients at High Bleeding Risk. *N. Engl. J. Med.* **2021**, *385*, 1643–1655. [CrossRef]
251. Rodriguez, F.; Harrington, R.A. Management of Antithrombotic Therapy after Acute Coronary Syndromes. *N. Engl. J. Med.* **2021**, *384*, 452–460. [CrossRef]
252. Palmerini, T.; Benedetto, U.; Biondi-Zoccai, G.; Della Riva, D.; Bacchi-Reggiani, L.; Smits, P.C.; Vlachojannis, G.J.; Jensen, L.O.; Christiansen, E.H.; Berencsi, K.; et al. Long-Term Safety of Drug-Eluting and Bare-Metal Stents: Evidence From a Comprehensive Network Meta-Analysis. *J. Am. Coll. Cardiol.* **2015**, *65*, 2496–2507. [CrossRef]
253. Kim, Y.H.; Her, A.Y.; Jeong, M.H.; Kim, B.K.; Hong, S.J.; Kim, S.; Ahn, C.M.; Kim, J.S.; Ko, Y.G.; Choi, D.; et al. Comparison of First- and Second-Generation Drug-Eluting Stents in Patients with ST-Segment Elevation Myocardial Infarction Based on Pre-Percutaneous Coronary Intervention Thrombolysis in Myocardial Infarction Flow Grade. *J. Clin. Med.* **2021**, *10*, 367. [CrossRef]
254. Kim, M.C.; Jeong, M.H.; Ahn, Y.; Kim, J.H.; Chae, S.C.; Kim, Y.J.; Hur, S.H.; Seong, I.W.; Hong, T.J.; Choi, D.H.; et al. What is optimal revascularization strategy in patients with multivessel coronary artery disease in non-ST-elevation myocardial infarction? Multivessel or culprit-only revascularization. *Int. J. Cardiol.* **2011**, *153*, 148–153. [CrossRef]
255. Hsieh, M.J.; Chen, C.C.; Lee, C.H.; Wang, C.Y.; Chang, S.H.; Chen, D.Y.; Yang, C.H.; Tsai, M.L.; Yeh, J.K.; Ho, M.Y.; et al. Complete and incomplete revascularization in non-ST segment myocardial infarction with multivessel disease: Long-term outcomes of first- and second-generation drug-eluting stents. *Heart Vessel.* **2019**, *34*, 251–258. [CrossRef]

256. Claessen, B.E.; Henriques, J.P.S.; Jaffer, F.A.; Mehran, R.; Piek, J.J.; Dangas, G.D. Stent Thrombosis. *JACC Cardiovasc. Interv.* **2014**, *7*, 1081–1092. [CrossRef]
257. Iakovou, I.; Schmidt, T.; Bonizzoni, E.; Ge, L.; Sangiorgi, G.M.; Stankovic, G.; Airoldi, F.; Chieffo, A.; Montorfano, M.; Carlino, M.; et al. Incidence, predictors, and outcome of thrombosis after successful implantation of drug-eluting stents. *JAMA* **2005**, *293*, 2126–2130. [CrossRef] [PubMed]
258. Gori, T.; Polimeni, A.; Indolfi, C.; Räber, L.; Adriaenssens, T.; Münzel, T. Predictors of stent thrombosis and their implications for clinical practice. *Nat. Rev. Cardiol.* **2019**, *16*, 243–256. [CrossRef] [PubMed]
259. Armstrong, E.J.; Waltenberger, J.; Rogers, J.H. Percutaneous coronary intervention in patients with diabetes: Current concepts and future directions. *J. Diabetes Sci. Technol.* **2014**, *8*, 581–589. [CrossRef] [PubMed]
260. Capodanno, D.; Bhatt, D.L.; Gibson, C.M.; James, S.; Kimura, T.; Mehran, R.; Rao, S.V.; Steg, P.G.; Urban, P.; Valgimigli, M.; et al. Bleeding avoidance strategies in percutaneous coronary intervention. *Nat. Rev. Cardiol.* **2022**, *19*, 117–132. [CrossRef] [PubMed]
261. Timmins, L.H.; Miller, M.W.; Clubb, F.J.; Moore, J.E. Increased artery wall stress post-stenting leads to greater intimal thickening. *Lab. Investig.* **2011**, *91*, 955–967. [CrossRef]
262. Xu, J.; Yang, J.; Huang, N.; Uhl, C.; Zhou, Y.; Liu, Y. Mechanical response of cardiovascular stents under vascular dynamic bending. *BioMed. Eng. OnLine* **2016**, *15*, 21. [CrossRef]
263. Conway, C.; Nezami, F.R.; Rogers, C.; Groothuis, A.; Squire, J.C.; Edelman, E.R. Acute Stent-Induced Endothelial Denudation: Biomechanical Predictors of Vascular Injury. *Front. Cardiovasc. Med.* **2021**, *8*, 1312. [CrossRef]
264. Rogers, C.; Edelman, E.R. Endovascular Stent Design Dictates Experimental Restenosis and Thrombosis. *Circulation* **1995**, *91*, 2995–3001. [CrossRef]
265. Rogers, C.; Tseng, D.Y.; Squire, J.C.; Edelman, E.R. Balloon-Artery Interactions During Stent Placement. *Circ. Res.* **1999**, *84*, 378–383. [CrossRef]
266. Han, Y.; Lu, W. Optimizing the deformation behavior of stent with nonuniform Poisson's ratio distribution for curved artery. *J. Mech. Behav. Biomed. Mater.* **2018**, *88*, 442–452. [CrossRef]
267. Traub, O.; Berk, B.C. Laminar Shear Stress. *Arterioscler. Thromb. Vasc. Biol.* **1998**, *18*, 677–685. [CrossRef] [PubMed]
268. Cooke, J.P. Flow, NO, and atherogenesis. *Proc. Natl. Acad. Sci. USA* **2003**, *100*, 768–770. [CrossRef] [PubMed]
269. Jimenez, J.M.; Davies, P.F. Hemodynamically driven stent strut design. *Ann. Biomed. Eng.* **2009**, *37*, 1483–1494. [CrossRef] [PubMed]
270. Wei, L.; Leo, H.L.; Chen, Q.; Li, Z. Structural and Hemodynamic Analyses of Different Stent Structures in Curved and Stenotic Coronary Artery. *Front. Bioeng. Biotechnol.* **2019**, *7*, 366. [CrossRef] [PubMed]
271. Kolandaivelu, K.; Swaminathan, R.; Gibson, W.J.; Kolachalama, V.B.; Nguyen-Ehrenreich, K.-L.; Giddings, V.L.; Coleman, L.; Wong, G.K.; Edelman, E.R. Stent Thrombogenicity Early in High-Risk Interventional Settings Is Driven by Stent Design and Deployment and Protected by Polymer-Drug Coatings. *Circulation* **2011**, *123*, 1400–1409. [CrossRef]
272. Nakatani, S.; Nishino, M.; Taniike, M.; Makino, N.; Kato, H.; Egami, Y.; Shutta, R.; Tanouchi, J.; Yamada, Y. Initial findings of impact of strut width on stent coverage and apposition of sirolimus-eluting stents assessed by optical coherence tomography. *Catheter. Cardiovasc. Interv.* **2013**, *81*, 776–781. [CrossRef]
273. Ellis, S.G.; Gori, T.; Serruys, P.W.; Nef, H.; Steffenino, G.; Brugaletta, S.; Munzel, T.; Feliz, C.; Schmidt, G.; Sabaté, M.; et al. Clinical, Angiographic, and Procedural Correlates of Very Late Absorb Scaffold Thrombosis: Multistudy Registry Results. *JACC Cardiovasc. Interv.* **2018**, *11*, 638–644. [CrossRef]
274. Kitahara, H.; Okada, K.; Kimura, T.; Yock, P.G.; Lansky, A.J.; Popma, J.J.; Yeung, A.C.; Fitzgerald, P.J.; Honda, Y. Impact of Stent Size Selection on Acute and Long-Term Outcomes After Drug-Eluting Stent Implantation in De Novo Coronary Lesions. *Circ. Cardiovasc. Interv.* **2017**, *10*, e004795. [CrossRef]
275. Foin, N.; Sen, S.; Allegria, E.; Petraco, R.; Nijjer, S.; Francis, D.P.; Di Mario, C.; Davies, J.E. Maximal expansion capacity with current DES platforms: A critical factor for stent selection in the treatment of left main bifurcations? *EuroIntervention* **2013**, *8*, 1315–1325. [CrossRef]
276. Abreu Filho, L.M.; Forte, A.A.; Sumita, M.K.; Favarato, D.; Meireles, G.C. Influence of metal alloy and the profile of coronary stents in patients with multivessel coronary disease. *Clinics (Sao Paulo)* **2011**, *66*, 985–989. [CrossRef]
277. Nikam, N.; Steinberg, T.B.; Steinberg, D.H. Advances in stent technologies and their effect on clinical efficacy and safety. *Med. Devices (Auckl)* **2014**, *7*, 165–178. [CrossRef] [PubMed]
278. Livingston, M.; Tan, A. Coating Techniques and Release Kinetics of Drug-Eluting Stents. *J. Med. Device* **2019**, *10*, 010801. [CrossRef] [PubMed]
279. Jain, R.A. The manufacturing techniques of various drug loaded biodegradable poly(lactide-co-glycolide) (PLGA) devices. *Biomaterials* **2000**, *21*, 2475–2490. [CrossRef]
280. Bao, L.; Dorgan, J.R.; Knauss, D.; Hait, S.; Oliveira, N.S.; Maruccho, I.M. Gas permeation properties of poly(lactic acid) revisited. *J. Membr. Sci.* **2006**, *285*, 166–172. [CrossRef]
281. Pinchuk, L.; Wilson, G.J.; Barry, J.J.; Schoephoerster, R.T.; Parel, J.-M.; Kennedy, J.P. Medical applications of poly(styrene-block-isobutylene-block-styrene) ("SIBS"). *Biomaterials* **2008**, *29*, 448–460. [CrossRef] [PubMed]
282. Hopkins, C.; Sweeney, C.A.; O'Connor, C.; McHugh, P.E.; McGarry, J.P. Webbing and Delamination of Drug Eluting Stent Coatings. *Ann. Biomed. Eng.* **2016**, *44*, 419–431. [CrossRef]

283. Basalus, M.W.Z.; Tandjung, K.; van Westen, T.; Sen, H.; van der Jagt, P.K.N.; Grijpma, D.W.; van Apeldoorn, A.A.; von Birgelen, C. Scanning electron microscopic assessment of coating irregularities and their precursors in unexpanded durable polymer-based drug-eluting stents. *Catheter. Cardiovasc. Interv.* **2012**, *79*, 644–653. [CrossRef]
284. McKittrick, C.M.; Cardona, M.J.; Black, R.A.; McCormick, C. Development of a Bioactive Polymeric Drug Eluting Coronary Stent Coating Using Electrospraying. *Ann. Biomed. Eng.* **2020**, *48*, 271–281. [CrossRef]
285. Van Belle, E.; Tio, F.O.; Couffinhal, T.; Maillard, L.; Passeri, J.; Isner, J.M. Stent endothelialization. Time course, impact of local catheter delivery, feasibility of recombinant protein administration, and response to cytokine expedition. *Circulation* **1997**, *95*, 438–448. [CrossRef]
286. Ishiwata, S.; Tukada, T.; Nakanishi, S.; Nishiyama, S.; Seki, A. Postangioplasty restenosis: Platelet activation and the coagulation-fibrinolysis system as possible factors in the pathogenesis of restenosis. *Am. Heart J.* **1997**, *133*, 387–392. [CrossRef]
287. Davies, M.G.; Hagen, P.O. Pathobiology of intimal hyperplasia. *Br. J. Surg.* **1994**, *81*, 1254–1269. [CrossRef] [PubMed]
288. Jana, S. Endothelialization of cardiovascular devices. *Acta Biomater.* **2019**, *99*, 53–71. [CrossRef] [PubMed]
289. Rajendran, P.; Rengarajan, T.; Thangavel, J.; Nishigaki, Y.; Sakthisekaran, D.; Sethi, G.; Nishigaki, I. The vascular endothelium and human diseases. *Int. J. Biol. Sci.* **2013**, *9*, 1057–1069. [CrossRef] [PubMed]
290. Lee, Y.H.; Mei, F.; Bai, M.Y.; Zhao, S.; Chen, D.R. Release profile characteristics of biodegradable-polymer-coated drug particles fabricated by dual-capillary electrospray. *J. Control. Release* **2010**, *145*, 58–65. [CrossRef]
291. Mitchell, M.J.; Billingsley, M.M.; Haley, R.M.; Wechsler, M.E.; Peppas, N.A.; Langer, R. Engineering precision nanoparticles for drug delivery. *Nat. Rev. Drug Discov.* **2021**, *20*, 101–124. [CrossRef]
292. Cherian, A.M.; Nair, S.V.; Maniyal, V.; Menon, D. Surface engineering at the nanoscale: A way forward to improve coronary stent efficacy. *APL Bioeng.* **2021**, *5*, 021508. [CrossRef]
293. Liang, C.; Tian, Y.; Zou, X.; Hu, Y.; Zhou, H.; Yang, L.; Wang, H. Improve endothelialization of metallic cardiovascular stent via femtosecond laser induced micro/nanostructure dependent cells proliferation and drug delivery control. *Colloids Surf. B Biointerfaces* **2022**, *212*, 112376. [CrossRef]
294. Bedair, T.M.; ElNaggar, M.A.; Joung, Y.K.; Han, D.K. Recent advances to accelerate re-endothelialization for vascular stents. *J. Tissue Eng.* **2017**, *8*, 2041731417731546. [CrossRef]
295. Du, R.; Wang, Y.; Huang, Y.; Zhao, Y.; Zhang, D.; Du, D.; Zhang, Y.; Li, Z.; McGinty, S.; Pontrelli, G.; et al. Design and testing of hydrophobic core/hydrophilic shell nano/micro particles for drug-eluting stent coating. *NPG Asia Mater.* **2018**, *10*, 642–658. [CrossRef]
296. Carpenter, A.W.; Schoenfisch, M.H. Nitric oxide release: Part II. Therapeutic applications. *Chem. Soc. Rev.* **2012**, *41*, 3742–3752. [CrossRef]
297. Rao, J.; Pan Bei, H.; Yang, Y.; Liu, Y.; Lin, H.; Zhao, X. Nitric Oxide-Producing Cardiovascular Stent Coatings for Prevention of Thrombosis and Restenosis. *Front. Bioeng. Biotechnol.* **2020**, *8*, 578. [CrossRef] [PubMed]
298. Yang, Z.; Yang, Y.; Zhang, L.; Xiong, K.; Li, X.; Zhang, F.; Wang, J.; Zhao, X.; Huang, N. Mussel-inspired catalytic selenocystamine-dopamine coatings for long-term generation of therapeutic gas on cardiovascular stents. *Biomaterials* **2018**, *178*, 1–10. [CrossRef] [PubMed]
299. Zhang, F.; Zhang, Q.; Li, X.; Huang, N.; Zhao, X.; Yang, Z. Mussel-inspired dopamine-Cu(II) coatings for sustained in situ generation of nitric oxide for prevention of stent thrombosis and restenosis. *Biomaterials* **2019**, *194*, 117–129. [CrossRef] [PubMed]
300. Tu, Q.; Shen, X.; Liu, Y.; Zhang, Q.; Zhao, X.; Maitz, M.F.; Liu, T.; Qiu, H.; Wang, J.; Huang, N.; et al. A facile metal–phenolic–amine strategy for dual-functionalization of blood-contacting devices with antibacterial and anticoagulant properties. *Mater. Chem. Front.* **2019**, *3*, 265–275. [CrossRef]
301. Ashikari-Hada, S.; Habuchi, H.; Kariya, Y.; Kimata, K. Heparin Regulates Vascular Endothelial Growth Factor$_{165}$-dependent Mitogenic Activity, Tube Formation, and Its Receptor Phosphorylation of Human Endothelial Cells. Comparison of the effects of heparin and modified heparins. *J. Biol. Chem.* **2005**, *280*, 31508–31515. [CrossRef]
302. Kastana, P.; Choleva, E.; Poimenidi, E.; Karamanos, N.; Sugahara, K.; Papadimitriou, E. Insight into the role of chondroitin sulfate E in angiogenesis. *Febs. J.* **2019**, *286*, 2921–2936. [CrossRef]
303. Zemani, F.; Benisvy, D.; Galy-Fauroux, I.; Lokajczyk, A.; Colliec-Jouault, S.; Uzan, G.; Fischer, A.M.; Boisson-Vidal, C. Low-molecular-weight fucoidan enhances the proangiogenic phenotype of endothelial progenitor cells. *Biochem. Pharmacol.* **2005**, *70*, 1167–1175. [CrossRef]
304. Genasetti, A.; Vigetti, D.; Viola, M.; Karousou, E.; Moretto, P.; Rizzi, M.; Bartolini, B.; Clerici, M.; Pallotti, F.; De Luca, G.; et al. Hyaluronan and human endothelial cell behavior. *Connect. Tissue Res.* **2008**, *49*, 120–123. [CrossRef]
305. Kam, A.; Li, K.M.; Razmovski-Naumovski, V.; Nammi, S.; Chan, K.; Li, G.Q. Gallic acid protects against endothelial injury by restoring the depletion of DNA methyltransferase 1 and inhibiting proteasome activities. *Int. J. Cardiol.* **2014**, *171*, 231–242. [CrossRef]
306. Yang, Y.; Gao, P.; Wang, J.; Tu, Q.; Bai, L.; Xiong, K.; Qiu, H.; Zhao, X.; Maitz, M.F.; Wang, H.; et al. Endothelium-Mimicking Multifunctional Coating Modified Cardiovascular Stents via a Stepwise Metal-Catechol-(Amine) Surface Engineering Strategy. *Research* **2020**, *2020*, 9203906. [CrossRef]
307. Chen, Y.; Gao, P.; Huang, L.; Tan, X.; Zhou, N.; Yang, T.; Qiu, H.; Dai, X.; Michael, S.; Tu, Q.; et al. A tough nitric oxide-eluting hydrogel coating suppresses neointimal hyperplasia on vascular stent. *Nat. Commun.* **2021**, *12*, 7079. [CrossRef] [PubMed]

308. Metavarayuth, K.; Sitasuwan, P.; Zhao, X.; Lin, Y.; Wang, Q. Influence of Surface Topographical Cues on the Differentiation of Mesenchymal Stem Cells in Vitro. *ACS Biomater. Sci. Eng.* **2016**, *2*, 142–151. [CrossRef] [PubMed]
309. Wang, S.; Li, J.; Zhou, Z.; Zhou, S.; Hu, Z. Micro-/Nano-Scales Direct Cell Behavior on Biomaterial Surfaces. *Molecules* **2018**, *24*, 75. [CrossRef]
310. Palmaz, J.C.; Benson, A.; Sprague, E.A. Influence of surface topography on endothelialization of intravascular metallic material. *J. Vasc. Interv. Radiol.* **1999**, *10*, 439–444. [CrossRef]
311. Ding, Y.; Yang, Z.; Bi, C.W.; Yang, M.; Xu, S.L.; Lu, X.; Huang, N.; Huang, P.; Leng, Y. Directing vascular cell selectivity and hemocompatibility on patterned platforms featuring variable topographic geometry and size. *ACS Appl. Mater. Interfaces* **2014**, *6*, 12062–12070. [CrossRef] [PubMed]
312. Peng, L.; Eltgroth, M.L.; LaTempa, T.J.; Grimes, C.A.; Desai, T.A. The effect of TiO2 nanotubes on endothelial function and smooth muscle proliferation. *Biomaterials* **2009**, *30*, 1268–1272. [CrossRef]
313. Cao, Y.; Desai, T.A. TiO2-Based Nanotopographical Cues Attenuate the Restenotic Phenotype in Primary Human Vascular Endothelial and Smooth Muscle Cells. *ACS Biomater. Sci. Eng.* **2020**, *6*, 923–932. [CrossRef]
314. Junkar, I.; Kulkarni, M.; Bencina, M.; Kovac, J.; Mrak-Poljsak, K.; Lakota, K.; Sodin-Semrl, S.; Mozetic, M.; Iglic, A. Titanium Dioxide Nanotube Arrays for Cardiovascular Stent Applications. *ACS Omega* **2020**, *5*, 7280–7289. [CrossRef]
315. Lam, C.Y.; Zhang, Q.; Yin, B.; Huang, Y.; Wang, H.; Yang, M.; Wong, S.H. Recent Advances in Two-Dimensional Transition Metal Dichalcogenide Nanocomposites Biosensors for Virus Detection before and during COVID-19 Outbreak. *J. Compos. Sci.* **2021**, *5*, 190. [CrossRef]
316. Yin, B.; Ho, W.K.H.; Zhang, Q.; Li, C.; Huang, Y.; Yan, J.; Yang, H.; Hao, J.; Wong, S.H.D.; Yang, M. Magnetic-Responsive Surface-Enhanced Raman Scattering Platform with Tunable Hot Spot for Ultrasensitive Virus Nucleic Acid Detection. *ACS Appl. Mater. Interfaces* **2022**, *14*, 4714–4724. [CrossRef]
317. Zhang, Q.; Yin, B.; Hao, J.; Ma, L.; Huang, Y.; Shao, X.; Li, C.; Chu, Z.; Yi, C.; Wong, S.H.D.; et al. An AIEgen/graphene oxide nanocomposite (AIEgen@GO)-based two-stage "turn-on" nucleic acid biosensor for rapid detection of SARS-CoV-2 viral sequence. *Aggregate* **2022**, e195. [CrossRef] [PubMed]
318. Nam, J.; Son, S.; Ochyl, L.J.; Kuai, R.; Schwendeman, A.; Moon, J.J. Chemo-photothermal therapy combination elicits anti-tumor immunity against advanced metastatic cancer. *Nat. Commun.* **2018**, *9*, 1074. [CrossRef] [PubMed]
319. Gupta, S.; Gupta, H.; Tandan, A. Technical complications of implant-causes and management: A comprehensive review. *Natl. J. Maxillofac. Surg.* **2015**, *6*, 3–8. [CrossRef] [PubMed]
320. Zhou, Z.R.; Jin, Z.M. Biotribology: Recent progresses and future perspectives. *Biosurface Biotribology* **2015**, *1*, 3–24. [CrossRef]
321. Dini, C.; Costa, R.C.; Sukotjo, C.; Takoudis, C.G.; Mathew, M.T.; Barão, V.A.R. Progression of Bio-Tribocorrosion in Implant Dentistry. *Front. Mech. Eng.* **2020**, *6*, 1. [CrossRef]
322. Serruys, P.W.; Kutryk, M.J.B.; Ong, A.T.L. Coronary-Artery Stents. *N. Engl. J. Med.* **2006**, *354*, 483–495. [CrossRef]
323. Gundert, T.J.; Marsden, A.L.; Yang, W.; LaDisa, J.F., Jr. Optimization of Cardiovascular Stent Design Using Computational Fluid Dynamics. *J. Biomech. Eng.* **2012**, *134*, 011002. [CrossRef]
324. De Vries, E.E.; Meershoek, A.J.A.; Vonken, E.J.; den Ruijter, H.M.; van den Berg, J.C.; de Borst, G.J.; Group, E.S. A meta-analysis of the effect of stent design on clinical and radiologic outcomes of carotid artery stenting. *J. Vasc. Surg.* **2019**, *69*, 1952–1961.e1. [CrossRef]
325. Piccolo, R.; Bonaa, K.H.; Efthimiou, O.; Varenne, O.; Baldo, A.; Urban, P.; Kaiser, C.; Remkes, W.; Raber, L.; de Belder, A.; et al. Drug-eluting or bare-metal stents for percutaneous coronary intervention: A systematic review and individual patient data meta-analysis of randomised clinical trials. *Lancet* **2019**, *393*, 2503–2510. [CrossRef]
326. Samant, S.; Wu, W.; Zhao, S.; Khan, B.; Sharzehee, M.; Panagopoulos, A.; Makadia, J.; Mickley, T.; Bicek, A.; Boismier, D.; et al. Computational and experimental mechanical performance of a new everolimus-eluting stent purpose-built for left main interventions. *Sci. Rep.* **2021**, *11*, 8728. [CrossRef]
327. Leclech, C.; Gonzalez-Rodriguez, D.; Villedieu, A.; Lok, T.; Deplanche, A.M.; Barakat, A.I. Topography-induced large-scale antiparallel collective migration in vascular endothelium. *Nat. Commun.* **2022**, *13*, 2797. [CrossRef] [PubMed]
328. Jeong, D.W.; Park, W.; Bedair, T.M.; Kang, E.Y.; Kim, I.H.; Park, D.S.; Sim, D.S.; Hong, Y.J.; Koh, W.G.; Jeong, M.H.; et al. Augmented re-endothelialization and anti-inflammation of coronary drug-eluting stent by abluminal coating with magnesium hydroxide. *Biomater Sci* **2019**, *7*, 2499–2510. [CrossRef] [PubMed]
329. Kang, M.-H.; Cheon, K.-H.; Jo, K.-I.; Ahn, J.-H.; Kim, H.-E.; Jung, H.-D.; Jang, T.-S. An asymmetric surface coating strategy for improved corrosion resistance and vascular compatibility of magnesium alloy stents. *Mater. Des.* **2020**, *196*, 109182. [CrossRef]
330. Chen, X.; Li, R.; Wong, S.H.D.; Wei, K.; Cui, M.; Chen, H.; Jiang, Y.; Yang, B.; Zhao, P.; Xu, J.; et al. Conformational manipulation of scale-up prepared single-chain polymeric nanogels for multiscale regulation of cells. *Nat. Commun.* **2019**, *10*, 2705. [CrossRef]
331. Chen, X.; Lai, N.C.; Wei, K.; Li, R.; Cui, M.; Yang, B.; Wong, S.H.D.; Deng, Y.; Li, J.; Shuai, X.; et al. Biomimetic Presentation of Cryptic Ligands via Single-Chain Nanogels for Synergistic Regulation of Stem Cells. *ACS Nano* **2020**, *14*, 4027–4035. [CrossRef]
332. Chen, S.; Yang, L.; Leung, F.K.; Kajitani, T.; Stuart, M.C.A.; Fukushima, T.; van Rijn, P.; Feringa, B.L. Photoactuating Artificial Muscles of Motor Amphiphiles as an Extracellular Matrix Mimetic Scaffold for Mesenchymal Stem Cells. *J. Am. Chem. Soc.* **2022**, *144*, 3543–3553. [CrossRef]
333. Chen, S.; Costil, R.; Leung, F.K.; Feringa, B.L. Self-Assembly of Photoresponsive Molecular Amphiphiles in Aqueous Media. *Angew. Chem. Int. Ed. Engl.* **2021**, *60*, 11604–11627. [CrossRef]

334. Shi, Q.; Liu, H.; Tang, D.; Li, Y.; Li, X.; Xu, F. Bioactuators based on stimulus-responsive hydrogels and their emerging biomedical applications. *NPG Asia Mater.* **2019**, *11*, 64. [CrossRef]
335. Kim, B.J.; Oh, D.X.; Kim, S.; Seo, J.H.; Hwang, D.S.; Masic, A.; Han, D.K.; Cha, H.J. Mussel-mimetic protein-based adhesive hydrogel. *Biomacromolecules* **2014**, *15*, 1579–1585. [CrossRef]
336. Zhao, P.; Yin, C.; Zhang, Y.; Chen, X.; Yang, B.; Xia, J.; Bian, L. Mussel cuticle-mimetic ultra-tough, self-healing elastomers with double-locked nanodomains exhibit fast stimuli-responsive shape transformation. *J. Mater. Chem. A* **2020**, *8*, 12463–12471. [CrossRef]
337. Lee, H.E.; Ahn, H.Y.; Mun, J.; Lee, Y.Y.; Kim, M.; Cho, N.H.; Chang, K.; Kim, W.S.; Rho, J.; Nam, K.T. Amino-acid- and peptide-directed synthesis of chiral plasmonic gold nanoparticles. *Nature* **2018**, *556*, 360–365. [CrossRef] [PubMed]
338. Xu, L.; Wang, X.; Wang, W.; Sun, M.; Choi, W.J.; Kim, J.Y.; Hao, C.; Li, S.; Qu, A.; Lu, M.; et al. Enantiomer-dependent immunological response to chiral nanoparticles. *Nature* **2022**, *601*, 366–373. [CrossRef] [PubMed]